Ph.D. Thesis

Secluded dark matter with a massive mediator

(重い媒介粒子を伴う隔離的暗黒物質)

Shohei Okawa

Department of Physics, Graduate School of Science
Nagoya University, Japan

Submitted: December 1, 2017
Revised: February 18, 2018

Abstract

Dark matter (DM) may be hidden from us at some degrees, taking into account failure of all experimental efforts to search for DM candidates sizably coupled to the standard model (SM). In this thesis, we study DM scenarios in which DM particles have only small or tiny couplings to the SM, while the cosmological abundance can correctly be produced by some novel mechanisms. In particular, we focus on thermal relic scenarios. We study a secluded scenario that a DM particle annihilates into intermediate particles (mediator) subsequently decaying into the SM, while DM has no sizable couplings with the SM. In the case, if the mediator is adequately lighter than the DM particle, the DM abundance is controllable solely by a pair annihilation of DM into the mediator particles. We also point out that the seclusion mechanism is fully operative even in a setup of degenerate DM-mediator, though the mediator lifetime has an impact on determination of the DM abundance. Of interest is that the DM density can exhibit a delayed freeze-out behavior in the thermal history of the universe. In addition, we propose a UV complete model that realizes the degenerate setup in a renormalizable manner. In the model, DM and mediator particles are unified in an approximate symmetry multiplet as dark pions that appear in a new strongly coupled sector. All of the required features for delayed freeze-out are explained in a natural manner.

Contents

Chapter 1

Introduction

Dark matter (DM) is one of the most long-standing unsolved mysteries in nature. Many cosmological and astrophysical observations have demonstrated that there is about five times larger energy density of DM than that of visible matter in the universe [1–5]. These observations, especially cosmic microwave background (CMB) observations, are conducted so precisely that the presence of DM can be established in the standard model of cosmology. However, all the solid evidences are only through the gravitational interaction, and only a few are known about the nature of DM, except for the cosmological abundance.

In particle physics, DM can be explained by introducing some particle. If this is the case, the particle has to be stable or long-lived enough at a cosmological time scale to survive until now without decreasing the abundance. In addition, it must not have electromagnetic charge. There is another restriction on the motion; DM should be non-relativistically moving in space in order to successfully form the large scale structure of the universe. One of the quests in particle physics is to elucidate true characters of a DM particle with these properties.

It is well-known, however, that there is no good DM candidate in the standard model (SM) of particle physics. It has turned out that the light neutrinos cannot be DM because of the failure in the structure formation. Further, the SM has no other massive, neutral and stable particles. Therefore, we have to demand alternative particles in new physics beyond the SM (BSM). Some BSM models often predict new massive particles that weakly interact with the SM. Such new particles are generally called Weakly Interacting Massive Particles (WIMPs), among which the stable and neutral ones can be good DM candidates. A lot of WIMP DM models have been proposed so far. For review, see Refs. [6–9].

Whatever BSM models are, it is necessary to answer how DM was produced in the early universe. A major scenario is that DM was produced in a thermal bath (thermal

relic scenario) [10]. In the scenario, the DM abundance is determined by the DM annihilation cross section, as we will see in Sec. 3.1. If the main process is assumed to be a DM pair annihilation into the SM particles, such as $2\,\mathrm{DM} \to 2\,\mathrm{SM}$ process, the produced abundance is expressed solely by DM mass and DM couplings to the SM. Interestingly, when we further assume the DM mass to be around the electroweak scale ($\sim 100\,\mathrm{GeV}$), the observed abundance predicts the coupling strength of order of the electroweak coupling strength. This marvelous coincidence is dubbed as *WIMP miracle*. Moreover, the thermal relic scenario of WIMP DM suggests that the DM particle can be detected through the DM-to-SM couplings that are relevant for the DM production. That has encouraged experimentalists to directly or indirectly search for DM at colliders [11], at underground detectors [12–15], with space telescopes [16–20] and so on. Unfortunately, however, all the experimental efforts to discover the DM candidates have failed so far, and many WIMP DM models come under strong pressures from these negative results.

The current disappointing experimental results in the DM searches can simply be interpreted by considering DM is hidden more than expected. In the WIMP DM scenario, the DM annihilation is assumed to be dominated by the pair annihilations into the SM. This leads to sizable DM-SM scatterings and the DM particle easily shows up at the DM search experiments. Then, if the DM annihilation is dominated by other processes, the strong direct search bounds can be evaded while keeping the relic abundance. Based on this consideration, novel scenarios for thermal relic DM have recently been proposed, in which DM candidates have only small or possibly tiny interactions with the SM, while the observed abundance can correctly be produced. About ten years ago, for example, in order to explain cosmic ray excesses consistently with the severe direct detection bounds, a secluded DM scenario was proposed [21]. In the secluded scenario, DM predominantly annihilates into light intermediate particles (mediator), and the annihilation cross section can determine the DM relic abundance based on the thermal relic scenario. The mediator weakly couples to the SM particles and can decay into them later. Since the DM particle itself does not necessarily couple to the SM in the secluded scenario, it can escape from the stringent bounds at the direct searches. Note that in the original proposal of the secluded DM, the mediator particle is assumed to be much lighter than the DM particle.

There is another proposal for novel mechanisms of DM thermal production, that is called Strongly Interacting Massive Particle (SIMP) DM scenario [22]. In the SIMP scenario, the observed DM abundance can be explained by a thermal relic produced through self-annihilation processes (e.g. $3\,\mathrm{DM} \to 2\,\mathrm{DM}$ or $4\,\mathrm{DM} \to 2\,\mathrm{DM}$ processes), unlike the DM pair annihilation processes into the SM in the WIMP DM scenario. The successful production requires DM mass of $\mathcal{O}(100\,\mathrm{MeV})$ and a coupling of order

unity. This requirement may automatically lead to a size of DM self-scattering that is compatible with the small scale structure problem [23–25]. A simple realization of the SIMP DM scenario using dark pions has carefully been studied in some papers [22, 26, 27].

In the above works, it is assumed that the SM sector and the hidden sector are not sizably coupled, but have small couplings such that the kinetic equilibrium was maintained at the freeze-out epoch. If the assumption is spoiled, on the other hand, a hidden sector is able to have its own temperature different from the SM, so that the thermal history of the universe will considerably be changed. In Ref. [28], the authors consider a highly decoupled sector whose temperature differs from the SM one. The hidden sector involves a large particle content, among which a stable particle can be DM. In this case, if a hidden particle has a large self-annihilation like $3 \to 2$ in the non-relativistic regime, the hidden sector can experience a characteristic thermal era (*cannibal era*), in which the hidden sector has an exponentially higher temperature than the SM one. During the cannibal era, the thermal environment surrounding DM is considerably altered, so that unique phenomena much different from the WIMP DM can be predicted (cannibal DM). Besides, Ref. [29] considers another application of highly decoupled hidden sectors. The authors point out that a late-time decay of a mediator particle dilutes the DM abundance after the thermal freeze-out and thus allows DM to have PeV-scale mass, which is much heavier than an upper bound on thermal relic DM [30].

In this thesis, I study a novel possibility of the secluded DM scenario that DM and mediator particles have close mass with each other [31]. I especially stress that the seclusion mechanism works well even in the case that the DM and mediator particles are completely degenerate in mass. Using a toy model, I first show that the DM number density can exhibit a characteristic behavior like a "terrace" in the thermal history of the universe, while the observed abundance can correctly be achieved. I also examine impacts of the mass difference of the DM and mediator on the relic abundance. It is found that only if the mass difference is within 50 %, we can see the difference with the original secluded scenario. After the study using the toy model, we can consider a DM model building that DM and mediator are unified in an approximate symmetry multiplet. I propose a renormalizable model that realizes such a unified description of DM and mediator in a natural way. In the model, DM and mediator particles show up as dark pions that are pseudo-Nambu-Goldstone bosons associated with dark chiral symmetry breaking in a new strong sector.

This thesis is organized as follows. In Sec. 2, we summarize theoretical foundation of the SM and the standard cosmology. Particle contents and data of the SM are also collected in this section. The evolution of the universe is affected by the contents

involved in particle physics models, so that these informations will be essential to study DM physics. Section 3 is a brief review of the WIMP DM paradigm based on a thermal freeze-out scenario. First, we introduce a basic equation, Boltzmann equation, that governs time evolution of number densities of interacting particles in the expanding universe. Then, we approximately solve the Boltzmann equation and study the freezing process of the DM density. After that, we will be able to find that WIMPs provide one natural solution to the DM problem. To concretely study WIMP DM, we often need to fix the basic properties, such as spin, gauge quantum number and interactions with the SM. In Sec. 3.3, we simply show some major examples of WIMP DM and discuss the current status of such candidates. In Sec. 4, we study secluded DM scenarios. This section is a main part of this thesis. We first introduce, in Sec. 4.1, a secluded DM scenario with a light mediator along with discussion in the original paper. Then, we present our work in Sec. 4.2, where the secluded scenario is extended to the one with a massive mediator. A renomalizable model for our setup is also proposed there. Section 5 is devoted to summary and conclusion. In Appendix, we collect some supplemental materials to support our understanding.

Chapter 2

Foundation

Study of particle cosmology is built on a gravitational theory that governs dynamics of universe and a particle theory that describes interactions between particles. In many cases, the former is given by a cosmological model based on general relativity (GR) and the latter by a particle model based on quantum field theory. Further, since it has been confirmed that our universe is homogeneous and isotropic at a large enough scale, one often considers the Friedmann-Robertson-Walker (FRW) spacetime that reflects the large-scale property of the universe. Assuming the SM in the particle physics sector, the cosmological description based on GR in the FRW spacetime is in good agreement with observations. This success becomes an anchor in study of modern particle cosmology. In this chapter, we give theoretical foundations of the SM and the standard cosmology, and collect particle data of the SM.

2.1 Standard Model in Particle Physics

As unified description of three fundamental forces (electromagnetic, weak and strong forces) in nature, the standard model (SM) of particle physics makes great success in explaining plenty of experimental and observational results below the electroweak (EW) scale. In this section, we give a brief review of the SM, mainly focused on the gauge groups, the matter contents and the mass spectrum.

Gauge Sector The SM is a gauge theory consisting of three symmetry groups: $SU(3)_C \times SU(2)_L \times U(1)_Y$. The quantum numbers of these gauge groups are called *color*, *weak isospin* and *hypercharge*, respectively. All the SM fields have non-trivial charges under the groups without exception. See Table 2.1.

The gauge theory based on $SU(3)_C$ is named quantum chromodynamics (QCD). The gauge boson associated with the group, termed *gluon*, plays a crucial role as a car-

rier of the so-called strong force. Because of the strong interaction, dynamics of colored particles is very complicated and causes many interesting phenomena. For instance, the quarks and gluon cannot be picked up alone: *color confinement*. Further, light or moderately heavy quarks form composite bound states, called mesons or baryons. In the framework of QCD, the proton and neutron can be understood as baryons, and the pions as mesons.

A gauge kinetic term of the gluon field is simply written by

$$\mathcal{L}_{SU(3)_C} = -\frac{1}{2c_G}\mathrm{tr}[G_{\mu\nu}G^{\mu\nu}], \tag{2.1.1}$$

where $G_{\mu\nu}$ denotes the field strength tensor of the gluon field, G_μ,

$$G_{\mu\nu} = \partial_\mu G_\nu - \partial_\nu G_\mu + ig_s[G_\mu, G_\nu], \tag{2.1.2}$$

with c_G and g_s being a normalization constant and the QCD gauge coupling, respectively. The gauge transformation is

$$G_\mu \to U_\theta G_\mu U_\theta^\dagger + \frac{i}{g_s}U_\theta \partial_\mu U_\theta^\dagger, \tag{2.1.3}$$

for the gluon field. Here, the transformation matrix is defined by $U_\theta = \exp(i\theta^\alpha T_r^\alpha)$ with T_r^α ($\alpha = 1, 2, \cdots, 8$) being $SU(3)$ generators in a representation r, which satisfy an orthogonal condition, $\mathrm{tr}[T_r^\alpha T_r^\beta] = c_G\delta^{\alpha\beta}/2$. The field strength tensor transforms under Eq.(2.1.3) as

$$G_{\mu\nu} \to U_\theta G_{\mu\nu} U_\theta^\dagger. \tag{2.1.4}$$

We can easily see that Eq.(2.1.1) is invariant under the gauge transformation. It is often useful to rewrite Eq.(2.1.1) in terms of a component field ($G_\mu \equiv G_\mu^\alpha T_r^\alpha$),

$$G_{\mu\nu} \equiv G_{\mu\nu}^\alpha T_r^\alpha, \quad G_{\mu\nu}^\alpha = \partial_\mu G_\nu^\alpha - \partial_\nu G_\mu^\alpha + g_s f^{\alpha\beta\gamma} G_\mu^\beta G_\nu^\gamma, \tag{2.1.5}$$

with $f^{\alpha\beta\gamma}$ being the structure constant of the $SU(3)$ group. For the component field, the kinetic term is translated into

$$\mathcal{L}_{SU(3)_C} = -\frac{1}{4}G_{\mu\nu}^\alpha G^{\alpha\mu\nu}, \tag{2.1.6}$$

and, especially for the infinitesimal θ^α, the gauge transformation indicates

$$G_\mu^\alpha \to G_\mu^\alpha + \frac{1}{g_s}\partial_\mu\theta^\alpha + f^{\alpha\beta\gamma}G_\mu^\beta\theta^\gamma. \tag{2.1.7}$$

Note that the gauge invariance forbids a gluon mass term like $m_G^2 G_\mu^\alpha G^{\alpha\mu}$.

Fields	spin	$SU(3)_C$	$SU(2)_L$	$U(1)_Y$
Q_L^i	1/2	**3**	**2**	1/6
u_R^i	1/2	**3**	**1**	2/3
d_R^i	1/2	**3**	**1**	−1/3
L_L^i	1/2	**1**	**2**	−1/2
e_R^i	1/2	**1**	**1**	−1
ϕ	0	**1**	**2**	1/2

Table 2.1. The fermions and the Higgs field in the SM.

We can also write down another gauge invariant, but P-odd and T-odd term, what is called a θ-term,

$$\mathcal{L} \supset \theta \frac{g_s^2}{64\pi^2} G^\alpha_{\mu\nu} G^\alpha_{\rho\sigma} \epsilon^{\mu\nu\rho\sigma}. \tag{2.1.8}$$

This term can be rewritten by a total derivative and does not contribute to the equation of motion. However, it is known that this P- and T-violating term makes non-vanishing phenomenological effects in fact. A famous effect of the θ-term is to generate an electric dipole moment (EDM) of the neutron. If we have a non-vanishing θ, it generates the neutron EDM of order of $d_e \sim \theta \times 10^{-15}\,[e\,\mathrm{cm}]$. According to the experiments, θ is found to be tiny: $\theta \lesssim 10^{-11}$ [32]. This unnatural smallness of the θ-parameter is known as the strong-CP problem. A dynamical solution to the problem predicts a light particle, named *axion* [33], which is one of the promising DM candidates, but the topic is beyond the scope of this thesis.

The gauge theory based on $SU(2)_L$ and $U(1)_Y$ describes the remaining two forces, electromagnetic and weak forces, in a unified manner, and therefore it is called the electroweak (EW) theory. The weak force associated with the EW theory is only one to violate P-invariance, and causes the β-decay of isotopes as well. The kinetic term for the EW gauge fields is given by analogy of QCD:

$$\mathcal{L}_{SU(2)_L \times U(1)_Y} = -\frac{1}{4} W^a_{\mu\nu} W^{a\mu\nu} - \frac{1}{4} B_{\mu\nu} B^{\mu\nu}, \tag{2.1.9}$$

with $a = 1, 2, 3$. Needless to say, but note again that the gauge invariance forbids the weak gauge bosons to have mass terms. The total Lagrangian in the gauge sector is given by simple summation of Eq.(2.1.6) and Eq.(2.1.9).

Higgs Sector Spontaneous breaking of symmetries is an essential feature in modern physics [34, 35]. The concept is extensively studied and applied in broad disciplines of

theoretical physics. In particle physics, it plays crucial roles in generating our mass. Our body is composed of molecules and atoms, whose mass is contributed nearly by that of nucleons, except for a small electron mass and tiny binding energies. The nucleons acquire most of their mass due to a quark-antiquark pair condensate in vacuum, that is caused by strong dynamics in QCD. Of importance is that the condensation is accompanied by spontaneous breaking of a chiral symmetry of quarks at the same time [34]. It is about 99 % of the nucleon mass that the QCD dynamics can explain in total.

The rest of the mass, that is only 1 %, comes from mass of quarks that constitute the nucleons. Though the quarks are massless in the SM Lagrangian, they become massive due to spontaneous breaking of the EW symmetry, as we will see in the next part. The breakdown also makes three weak gauge bosons massive. In the SM, one scalar particle, say a Higgs particle, is predicted as a by-product of the symmetry breaking, and it was finally discovered at LHC in 2012. Here, we will briefly see the key particle and the mass generation mechanism, namely Higgs mechanism [36].

The SM has one $SU(2)_L$-doublet Higgs field with a half hypercharge and no color. The Lagrangian in the Higgs sector is given by

$$\mathcal{L}_{\text{higgs}} = (D_\mu \phi)^\dagger (D^\mu \phi) - V(\phi), \tag{2.1.10}$$

with the covariant derivative defined by

$$D_\mu \phi \equiv (\partial_\mu - igW_\mu^a T^a - ig' Y B_\mu)\phi. \tag{2.1.11}$$

The scalar potential $V(\phi)$ is

$$V(\phi) = \mu^2 (\phi^\dagger \phi) + \frac{\lambda}{2}(\phi^\dagger \phi)^2, \tag{2.1.12}$$

with $\lambda > 0$ because of the vacuum stability. For $\mu^2 < 0$, an extreme minimum of the potential appears at a non-zero field value, $\phi \neq 0$. The field value at the potential minimum is referred to as a vacuum expectation value (VEV) of the Higgs field. We can find that the VEV can always be expressed in the form of

$$\langle \phi \rangle = \frac{1}{\sqrt{2}} \begin{pmatrix} 0 \\ v \end{pmatrix}, \tag{2.1.13}$$

thanks to $SU(2)$ and $U(1)$ symmetries. The VEV is related to λ and μ through the stationary condition: $v = \sqrt{2\mu^2/\lambda}$. One can easily see that this vacuum is not invariant under the general $SU(2)_L \times U(1)_Y$ transformation, but is invariant under a $U(1)$ component: that is, the EW symmetry is broken down to the $U(1)$ in the vacuum

state. We call this phenomena *electroweak symmetry breaking (EWSB)* and identify the unbroken $U(1)$ part as the electromagnetic group.

As seen in the previous part, the gauge invariance forces the gauge bosons to be massless. After the EWSB, however, three gauge bosons become massive and the mass eigenstates are

$$W_\mu^\pm = \frac{W_\mu^1 \mp iW_\mu^2}{\sqrt{2}}, \quad Z_\mu = \cos\theta_W W_\mu^3 - \sin\theta_W B_\mu, \tag{2.1.14}$$

with the Weinberg angle, $\sin\theta_W = g'/\sqrt{g^2+g'^2}$, and the masses,

$$m_W = \frac{gv}{2}, \quad m_Z = \frac{\sqrt{g^2+g'^2}v}{2}. \tag{2.1.15}$$

The remaining one gauge boson remains massless, and can be identified as photon:

$$A_\mu = \sin\theta_W W_\mu^3 + \cos\theta_W B_\mu. \tag{2.1.16}$$

In the mass basis, we can express the covariant derivative of a field with SM gauge charges as

$$D_\mu = \partial_\mu + i\frac{g}{\sqrt{2}}(W_\mu^+ T^+ + W_\mu^- T^-) - ig_Z\left(T^3 - Q\sin^2\theta_W\right)Z_\mu - ieQA_\mu, \tag{2.1.17}$$

with $T^\pm \equiv T^1 \pm iT^2$ and the couplings,

$$g_Z = \sqrt{g^2+g'^2}, \quad e = \frac{gg'}{\sqrt{g^2+g'^2}}, \tag{2.1.18}$$

and the electromagnetic charge operator,

$$Q = T^3 + Y. \tag{2.1.19}$$

This expression is rather useful sometimes.

Fermion and Yukawa Sectors Quantum mechanics predicts particles with half-integer spin, namely fermions. The fermions are fundamental particles in nature, and all the elementary particles that have been discovered so far are fermions except for the gauge bosons and the Higgs boson. The SM involves both colored and colorless fermions: quarks and leptons, respectively. There are three generations and six species in both the fermion sectors. See Table 2.1.

We first write down the kinetic terms,

$$\mathcal{L}_{\text{fermion}} = \overline{Q_L^i} i\not{D} Q_L^i + \overline{u_R^i} i\not{D} u_R^i + \overline{d_R^i} i\not{D} d_R^i + \overline{L_L^i} i\not{D} L_L^i + \overline{e_R^i} i\not{D} e_R^i, \tag{2.1.20}$$

with $i = 1, 2, 3$ being a family index for each fermion. Covariant derivatives for the fermions are defined similarly to the Higgs field. The fermions can couple to the Higgs field through the Yukawa interaction. The yukawa terms are collected into the form,

$$-\mathcal{L}_{\text{yukawa}} = Y_u^{ij}\overline{Q_L^i}\widetilde{\phi}u_R^j + Y_d^{ij}\overline{Q_L^i}\phi d_R^j + Y_e^{ij}\overline{L_L^i}\phi e_R^j + h.c., \tag{2.1.21}$$

with $\widetilde{\phi} \equiv i\sigma_2\phi^*$ and Y_u, Y_d and Y_e being 3×3 complex matrices. After the EWSB, mass terms show up from the yukawa terms with the mass matrices,

$$\mathcal{M}_f^{ij} = \frac{Y_f^{ij}v}{\sqrt{2}}, \tag{2.1.22}$$

with $f = u, d, e$. To move to the mass basis, we perform appropriate unitary transformations against the fermions,

$$u_{L,R}^i \to U_{L,R}^{ij}u_{L,R}^j, \quad d_{L,R}^i \to D_{L,R}^{ij}d_{L,R}^j, \quad e_{L,R} \to E_{L,R}^{ij}e_{L,R}^j, \tag{2.1.23}$$

where they satisfy the relations,

$$U_L\mathcal{M}_u U_R^\dagger = \text{diag}(m_u, m_c, m_t), \tag{2.1.24}$$

$$D_L\mathcal{M}_d D_R^\dagger = \text{diag}(m_d, m_s, m_b), \tag{2.1.25}$$

$$E_L\mathcal{M}_e E_R^\dagger = \text{diag}(m_e, m_\mu, m_\tau). \tag{2.1.26}$$

After the unitary transformations, let us redefine the Q_L^i and L_L^i fields by

$$Q_L^i = (u_L^i, V_{CKM}^{ij}d_L^j)^T, \quad L_L^i = (\tilde{\nu}_L^i, e_L^i)^T, \tag{2.1.27}$$

where $f_{L,R}$ ($f = u, d, e$) denote the fermions in the mass basis, and $V_{CKM} \equiv U_L D_L^\dagger$ the Cabibbo-Kobayashi-Maskawa (CKM) matrix. What we show in Table 2.1 follows this notation. Note that in fact the light neutrinos have mass and a non-trivial mixing structure, so that it is standard to take $\tilde{\nu}_L^i \equiv V_{PMNS}^{ij}\nu_L^j$ with the Pontecorvo-Maki-Nakagawa-Sakata (PMNS) matrix, V_{PMNS}, similarly to the quarks. Though, we can always take the mixing into account by the above replacement.

In this basis, the gauge current interactions are given by

$$\mathcal{L}_{CC} = \frac{g}{\sqrt{2}}V_{CKM}^{ij}W_\mu^+\overline{u_L^i}\gamma^\mu d_L^j + \frac{g}{\sqrt{2}}W_\mu^+\overline{\tilde{\nu}_L^i}\gamma^\mu e_L^i + h.c. \tag{2.1.28}$$

$$\mathcal{L}_{NC} = g_Z Z_\mu \sum_{i,f}\overline{f^i}\gamma^\mu(C_V^f - C_A^f\gamma_5)f^i + h.c. \tag{2.1.29}$$

with $C_V^f = T_f^3 - 2Q_f\sin^2\theta_W$ and $C_A^f = T_f^3$. Further, in the unitary gauge, $\phi = (0, (v+h)/\sqrt{2})^T$, the yukawa terms reduce to

$$-\mathcal{L}_{\text{yukawa}} = \sum_{i,f} m_f^i\left(1 + \frac{h}{v}\right)\overline{f_L^i}f_R^i + h.c., \tag{2.1.30}$$

Particles	Mass	Particles	Mass
h	$125.09 \pm 0.24\,\text{GeV}$	e	$511.000\,\text{keV}$
W	$80.385 \pm 0.015\,\text{GeV}$	μ	$105.658\,\text{MeV}$
Z	$91.1876 \pm 0.0021\,\text{GeV}$	τ	$1.777\,\text{GeV}$
		ν	$< 2\,\text{eV}$ (tritium decay)
			$\sum_i m_{\nu_i} < 0.17\,\text{eV}$ (CMB) [5]
u	$2.2^{+0.6}_{-0.4}\,\text{MeV}$	d	$4.4^{+0.5}_{-0.4}\,\text{MeV}$
c	$1.27 \pm 0.03\,\text{GeV}$ ($\overline{\text{MS}}$)	s	$96^{+8}_{-4}\,\text{MeV}$
t	$173.21 \pm 0.51 \pm 0.71\,\text{GeV}$ (MC)	b	$4.18^{+0.04}_{-0.03}\,\text{GeV}$ ($\overline{\text{MS}}$)
	$160^{+5}_{-4}\,\text{GeV}$ ($\overline{\text{MS}}$)		$4.66^{+0.04}_{-0.03}\,\text{GeV}$ (1S)
	$174.2 \pm 1.4\,\text{GeV}$ (Pole)		

Table 2.2. Mass spectrum of the SM particles [37].

with the yukawa couplings to the Higgs particle h,

$$y_f^i = \frac{m_f^i}{v}. \tag{2.1.31}$$

One can see that effects of the flavor mixing appears only through the charged current (CC) interaction.

Mass spectrum The total Lagrangian of the SM is the collection of all the above parts,

$$\mathcal{L}_{SM} = \mathcal{L}_{\text{gauge}} + \mathcal{L}_{\text{higgs}} + \mathcal{L}_{\text{fermion}} + \mathcal{L}_{\text{yukawa}}. \tag{2.1.32}$$

The quantum numbers of the SM fields are summarized in Table 2.1. In summary of this section, we show the mass spectrum of the SM particles in Table 2.2, that will be significant to study thermal history of the universe.

2.2 Standard Cosmology

Our universe is not static, but dynamical: the universe is expanding. The expansion is a basis nature of gravitational theories that describe the dynamics of the universe.

In general relativity, it is caused by a brilliant interplay between the gravitational field and the other existing fields.

It has been widely confirmed that our universe is almost homogeneous and isotropic, seen at a large enough scale. To reflect the spacetime feature, the standard cosmology is based on general relativity with the Friedmann-Robertson-Walker (FRW) metric,

$$ds^2 = dt^2 - a^2(t)\left(\frac{dr^2}{1-Kr^2} + r^2 d\theta^2 + r^2 \sin^2\theta d\phi^2\right), \tag{2.2.1}$$

where K denotes spatial curvature of the spacetime and the possible choice is either $+1$, -1, or 0. We will consider the flat space, i.e. $K = 0$, without a special notice. The scale factor, $a(t)$, is only unknown quantity in this cosmological model, and characterizes the size of the universe. In this section, we overview the expansion of the FRW universe.

2.2.1 Evolution of the Universe

A basic equation in general relativity is the Einstein equation,

$$R_{\mu\nu} - \frac{1}{2}\mathcal{R}g_{\mu\nu} = 8\pi G T_{\mu\nu}, \tag{2.2.2}$$

where the left-hand-side is the Einstein tensor, and G denotes the Newton constant and $T_{\mu\nu}$ the energy-momentum tensor for all the fields that involves the so-called cosmological constant in our notation. This equation means that the spacetime is disturbed wherever the fields are and the disturbance affects the dynamical motion of the fields.

In the FRW spacetime, $T_{\mu\nu}$ has to obey the homogeneity and isotropy, and is characterized in terms of the energy density, ρ, and pressure, p:

$$T_{\mu\nu} = \mathrm{diag}(\rho, -p, -p, -p). \tag{2.2.3}$$

The energy-momentum tensor is also a conserved current associated with the spatial translations, so that there is a corresponding continuous equation: $T^{\mu\nu}{}_{;\nu} = 0$. For the $\mu = 0$ component, we can see

$$d(\rho a^3) = -p d(a^3), \tag{2.2.4}$$

which is the same as the 1st law of thermodynamics for an adiabatic process. The relation of ρ and p is determined by an equation of state (EOS) of a particle concerned, and can generally be expressed in the form of

$$p = w\rho. \tag{2.2.5}$$

Then, we can also interpret Eq.(2.2.4) as the equation that provides scale factor dependence of the energy density, ρ. For a practical purpose, we show what we often consider in the following,

$$\begin{aligned} w = 1/3 &: \text{ radiation} \\ w = 0 \quad &: \text{ matter} \qquad\qquad , \\ w = -1 &: \text{ vacuum energy} \end{aligned} \tag{2.2.6}$$

which will appear many times in the thesis.

Let us back to the Einstein equation. In the FRW spacetime, this equation reduces to a basic equation, called the Friedmann equation,

$$\left(\frac{\dot{a}}{a}\right)^2 = \frac{8\pi G}{3}\rho, \tag{2.2.7}$$

with $\dot{a} \equiv da/dt$. We also define the Hubble parameter, $H \equiv \dot{a}/a$, that indicates the expansion rate of the universe. Using the Hubble parameter, the Friedmann equation is expressed as

$$H^2 = \frac{8\pi G}{3}\rho. \tag{2.2.8}$$

Below, we will see how the expansion depends on what dominates over the universe.

Radiation dominated universe Our universe is considered to be dominated by relativistic particles until $z \sim 3300$. In the radiation dominated (RD) universe, the energy density obeys

$$\rho_R \propto a^{-4}, \tag{2.2.9}$$

because of the EOS,

$$p_R = \frac{1}{3}\rho_R. \tag{2.2.10}$$

Then, the Friedmann equation leads

$$\left(\frac{\dot{a}}{a_0}\right)^2 = \frac{8\pi G}{3}\rho_{R0}\left(\frac{a_0}{a}\right)^2, \tag{2.2.11}$$

with a_0 being a scale factor at a reference time, t_0. It is easy to solve this equation and obtain the solution,

$$a(t) \propto t^{1/2}. \tag{2.2.12}$$

Matter dominated universe After $z \sim 3300$, the matter component is superior to that of radiation. In contrast to radiation, the EOS of matter is

$$p_M = 0, \tag{2.2.13}$$

so that the energy density depends on the scale factor as

$$\rho_M \propto a^{-3}. \tag{2.2.14}$$

In this case, the Friedmann equation turns to

$$\left(\frac{\dot{a}}{a_0}\right)^2 = \frac{8\pi G}{3}\rho_{M0}\left(\frac{a_0}{a}\right), \tag{2.2.15}$$

whose solution is

$$a(t) \propto t^{2/3}. \tag{2.2.16}$$

We can see the evolution of the universe is obviously different from the RD case.

Vacuum energy dominant universe In both the RD and MD cases, the universe expands with evolving time, but the expansion is decelerating: $\ddot{a}(t) < 0$. The observation implies, however, that our universe is acceleratedly expanding at present. This means in our universe there exists another source that causes the acceleration. We call it *dark energy*. Fortunately, GR allows us to introduce dark energy as the so-called cosmological constant into the Einstein equation in a simple way. The cosmological constant term formally corresponds to the following energy-momentum tensor,

$$T^{\Lambda}_{\mu\nu} = \frac{\Lambda}{8\pi G} g_{\mu\nu}, \tag{2.2.17}$$

in the right-hand-side of Eq.(2.2.2). That indicates the EOS of the cosmological constant equals to the vacuum energy,

$$p_\Lambda = -\rho_\Lambda. \tag{2.2.18}$$

Combining Eq.(2.2.4) and Eq.(2.2.18), we find the Λ-dominated universe indicates an exponential expansion,

$$a(t) \propto e^{Ht}, \tag{2.2.19}$$

with the constant rate, $H = \text{Const}$. It can easily be seen that the expansion of the universe is accelerating: $\ddot{a}(t) > 0$. Surprisingly, the dark energy occupies about 70 % of the energy density in the present universe, while the remaining 30 % is dominated by pressureless matter and radiation has only a slight fraction of $\mathcal{O}(10^{-5}\,\%)$ [37].

2.2.2 Thermodynamics

In the previous subsection, it has been found that the expansion is a generic feature of the FRW universe. Then, we can imagine that as going back in time, the size of the universe was much smaller than at present and particles would exist very closely with each other. If a particle reaction frequently occurs during a cosmological time scale, we can consider the particles were in an equilibrium. In this case, the phase-space distribution of these particle species can be regarded as thermal one, and some quantities, such as number density, energy density and pressure, can be parametrized in terms of temperature and some particle data. In fact, a theory of nucleosynthesis based on this consideration predicts a correct primordial abundance of light elements [38], and CMB observations [4, 5] also provide a solid evidence that the universe was in thermal equilibrium in the past.

Note that in a precise sense, it is not possible for the FRW universe to have experienced the thermal equilibrium because the universe is ceaselessly expanding: in a mathematical sense, this is because there is no time-like Killing vector in the cosmological model. At a practical level, however, it is much valid to consider the interacting particles were nearly in thermal equilibrium at an early time. There is a standard to simply judge whether a reaction is efficient enough for particles to achieve the equilibrium. That is known as Gamov criterion, and is stated in a very simple form: when a reaction rate of a process via particle interactions satisfies the inequality,

$$\Gamma \gtrsim H, \tag{2.2.20}$$

then the particles concerned with the process achieve the equilibrium; otherwise, the particles are considered to decouple. In other words, this criterion means that the reaction should occur at least once during a time interval comparable to the age of the universe at that time. In fact, unless we solve an equation describing the equilibration, we cannot see whether interacting particles are decoupled or not, but the Gamov criterion is justifiable in many cases.

Let us study thermodynamics, assuming a particle species i with mass m_i is in equilibrium with a thermal bath with a temperature, T. In this case, a phase-space distribution of the particle species equals to the thermal one,

$$f_i(\vec{p}, T) = \frac{1}{e^{(E-\mu_i)/T} \mp 1}, \tag{2.2.21}$$

where in the denominator, minus $(-)$ is for bosons and plus $(+)$ for fermions. This is nothing but the Bose-Einstein and the Fermi-Dirac distributions, respectively. The number density, energy density and pressure are given by integrating the distribution function over the particle momentum, $\vec{p}$. We show only results here and the further

details are given in Appendix A. For a relativistic particle ($m_i \ll T$), for $\mu_i \ll T$,

$$
\begin{aligned}
n_i &\simeq \begin{cases} (\zeta(3)/\pi^2) g_i T^3 & \text{(Boson)} \\ (\zeta(3)/\pi^2)(3/4) g_i T^3 & \text{(Fermion)} \end{cases}, \\
\rho_i &\simeq \begin{cases} (\pi^2/30) g_i T^4 & \text{(Boson)} \\ (\pi^2/30)(7/8) g_i T^4 & \text{(Fermion)} \end{cases}, \\
p_i &\simeq \frac{1}{3}\rho_i,
\end{aligned}
\tag{2.2.22}
$$

and for $\mu_i \gg T$ (a degenerate fermion),

$$
\begin{aligned}
n_i &\simeq \frac{1}{6\pi^2} g_i \mu_i^3, \\
\rho_i &\simeq \frac{1}{8\pi^2} g_i \mu_i^4, \\
p_i &\simeq \frac{1}{3}\rho_i.
\end{aligned}
\tag{2.2.23}
$$

Here, g_i denotes the internal degrees of freedom for the particle and $\zeta(3)$ the Riemann zeta function of 3: $\zeta(3) \simeq 1.202$. For a non-relativistic particle ($m_i \gg T$), on the other hand, we have

$$
\begin{aligned}
n_i &\simeq g_i \left(\frac{m_i T}{2\pi}\right)^{3/2} e^{-(m_i-\mu_i)/T}, \\
\rho_i &\simeq (m_i + \frac{3}{2}T) n_i, \\
p_i &\simeq T n_i,
\end{aligned}
\tag{2.2.24}
$$

which are common to both bosons and fermions. It can be seen that a non-relativistic particle species hardly has sizable contributions to the thermodynamical quantities, so that it is much convenient to introduce a measure of the number of relativistic degrees of freedom. We parametrize the total energy density in terms of the thermal bath temperature,

$$
\rho = \frac{\pi^2}{30} g_* T^4, \tag{2.2.25}
$$

with the effective relativistic degrees of freedom,

$$
g_* = \sum_{i=\text{bosons}} g_i \left(\frac{T_i}{T}\right)^4 + \sum_{i=\text{fermions}} \frac{7}{8} g_i \left(\frac{T_i}{T}\right)^4, \tag{2.2.26}
$$

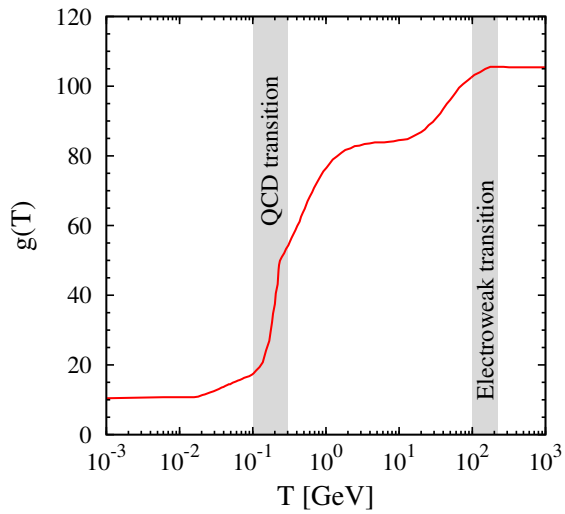

Figure 2.1. The temperature dependence of the effective relativistic degrees of freedom for the energy density, $g_*(T)$ [39]. It is monotonically decreasing as temperature decreases. The degrees of freedom drastically reduce before and after the QCD phase transition, though there is a large theoretical uncertainty near the transition. The counterpart for the entropy density, $g_{*s}(T)$, basically has the same behavior before the e^+e^- annihilation.

where we take into account a temperature deviation from the thermal bath temperature by T_i. The introduced $g_*(T)$ measures how many relativistic degrees of freedom there are in the thermodynamical system. In Fig. 2.1, we show the temperature dependence of $g_*(T)$, assuming the SM in the particle sector [39]. We find $g_*(T)$ to monotonically decrease as temperature decreases.

Since the total energy in a comoving volume is not a conserved quantity as seen in Eq.(2.2.4), it will be more useful if we can introduce a conserved quantity in the expanding universe. For a thermal system, that is entropy in a comoving volume, defined by

$$S \equiv sa^3 = \left(\frac{\rho + p - \mu n}{T}\right) a^3, \tag{2.2.27}$$

with s being the entropy density. Similarly to other thermodynamical quantities, the entropy density is mainly contributed to by the relativistic particles, so that we also define the entropic effective degrees of freedom through

$$\begin{aligned} s &= \frac{2\pi^2}{45} g_{*s} T^3, \\ g_{*s} &= \sum_{i=\text{bosons}} g_i \left(\frac{T_i}{T}\right)^3 + \sum_{i=\text{fermions}} \frac{7}{8} g_i \left(\frac{T_i}{T}\right)^3. \end{aligned} \tag{2.2.28}$$

The temperature dependence of $g_{*s}(T)$ is similar to $g_*(T)$ before the e^+e^- annihilation.

Next, we clarify a relation of the time variable and the temperature, and study the time evolution of the temperature. Since the entropy in a comoving volume is conserved in the thermal system, we find

$$s \propto a^{-3}. \tag{2.2.29}$$

Using Eq.(2.2.28), we can easily see the temperature is evolving as

$$T \propto g_{*s}^{-1/3} a^{-1}. \tag{2.2.30}$$

With the constant g_{*s}, the temperature of the thermal bath is getting cold as

$$T \propto \begin{cases} t^{-1/2} & \text{(RD)} \\ t^{-2/3} & \text{(MD)} \end{cases}. \tag{2.2.31}$$

Note that Eq.(2.2.30) indicates the energy in radiation is redshifting, but there is a slight deviation from this observation. That is due to an entropy transfer from non-relativistic particles to relativistic particles in the thermal bath. According to the entropy conservation law, the bulk of the entropy that the non-relativistic particles possessed flows into the relativistic particles. As a result, the latter particles have to be responsible for more entropy than before, and thus the temperature decease is made slower.

A particle species decoupled from the thermal bath can no longer participate in the entropy sharing. Thus, such a decoupled particle does not get the benefit of the entropy transfer, even if it is relativistic. This leads to a fact that the particle distribution is frozen and only affected by redshift after the decoupling. We will see the consequences below. First, we note that the particle momentum is redshifted by the expansion of the universe as

$$\frac{|\vec{p}|}{|\vec{p}_D|} = \frac{a_D}{a}, \tag{2.2.32}$$

where $|\vec{p}_D|$ and a_D denote the magnitude of the momentum and the scale factor at the decoupling time, respectively. For a decoupled relativistic particle, $E \simeq |\vec{p}|$, so that the energy of each particle in the distribution is just redshifted. Then, the distribution keeps its form,

$$f(\vec{p}, T) = f(\vec{p}_D, T_D), \tag{2.2.33}$$

with an *apparent* temperature,

$$\frac{T}{T_D} = \frac{a_D}{a}, \tag{2.2.34}$$

that is equal to the one in the thermal equilibrium, Eq.(2.2.30), with a constant g_{*s}. Thus, the thermodynamical quantities for this particle species receive only the effects of the redshifting, Eq.(2.2.34).

If the decoupled particle is non-relativistic at that time, on the other hand, the temperature decreases more rapidly. In the non-relativistic limit, the energy is divided into the rest energy, m, and the kinetic energy, $E_{\rm kin} = |\vec{p}|^2/2m$. Then, by using the momentum redshift, Eq.(2.2.32), we find the temperature decrease for the case,

$$\frac{T}{T_D} = \left(\frac{a_D}{a}\right)^2, \tag{2.2.35}$$

with the chemical potential,

$$\mu = m + (\mu_D - m)\frac{T}{T_D}, \tag{2.2.36}$$

to maintain the proper formula of the adiabatic expansion: $n \propto a^{-3}$.

Finally, we shall mention a special case, what is called *cannibalism* [24, 28]. If a decoupled massive particle keeps sizable self-annihilation reactions, the chemical potential is vanishing: $\mu = 0$. This leads to an unusual scale factor dependence of the temperature. Now, since the number density is

$$n = \left(\frac{mT}{2\pi}\right)^{3/2} e^{-m/T}, \tag{2.2.37}$$

the temperature has to logarithmically be dumping with increasing scale factor, at a good approximation,

$$T \propto \frac{m}{\ln(a/a_0)^3}, \tag{2.2.38}$$

in order to maintain $n \propto a^{-3}$. This means that the temperature of the cannibal sector is exponentially higher than that of radiation [24, 28].

Chapter 3

WIMP DM paradigm

The SM in particle physics was established in 2012 by the discovery of the 125 GeV Higgs particle. However, the discovery gives rise to an unanswered problem concerned with a sort of naturalness [40]. In order to solve the problem, BSM physics often introduces massive new particles around the TeV scale that weakly interact with the SM particles. These particles are generically called Weakly Interacting Massive Particles (WIMPs). Among these, the lightest particle can often be stable thanks to a newly introduced symmetry in the BSM models, so that it can be a DM candidate. Interestingly, when we try to evaluate the relic abundance of such a DM candidate based on a thermal freeze-out scenario, we obtain the abundance comparable with the observed one [10]. What we have learned from the WIMP DM have extensively been applied to many BSM models and has built one of the standard DM paradigms. Since then, we have pursued the WIMP DM for several decades.

In this chapter, we give a short review of the standard WIMP DM paradigm and take a quick look at some concrete examples of WIMP DM and their experimental status. We first study particle reactions in a thermal background in the expanding universe in Sec. 3.1. It is found that a massive relic particle is decoupled from the thermal plasma at an early time, and a freeze-out phenomenon of the number density subsequently occurs. We also give an approximate solution of the relic abundance for a clear understanding of the DM scenario. Then, WIMPs are introduced as a natural solution that can provide the correct abundance. We also mention a theoretical limit on thermal relic DM from partial-wave unitarity.

An intriguing prediction of the standard thermal WIMP scenario is that DM has sizable interactions with the SM particles, so that we are able to directly or indirectly search for the DM particles. In Sec 3.2, we simply introduce major strategies of WIMP DM searches; direct detection, indirect detection and collider searches. Some examples of thermal WIMP DM and their current status are collected in Sec. 3.3.

3.1 Thermal freeze-out scenario

In the FRW universe involving interacting particles, a number density of a particle species is evolving, influenced in two ways: one is the expansion of the universe, another is particle interactions that change the particle number before and after reactions. The expansion dilutes the number density just following the adiabatic law ($n \propto a^{-3}$), while the particle interactions can both increase and decrease the number density. As mentioned in Sec. 2.2, if the particle reaction occurs frequently enough, the particles participating in the reaction fall into the equilibrium. Once the equilibrium is achieved, the phase-space distribution is very close to the thermal one, as far as the reaction continues to rapidly occur. However, as the universe is expanding, the particle reaction scarcely become able to occur, and will finally be stopped. That is the decoupling phenomenon of the interacting particles. In this section, we observe in more detail how particle interactions are decoupling and a stable particle meets a freeze-out phenomenon in the expanding universe.

3.1.1 Decoupling and Freeze-out

In this subsection, we shall briefly outline essential phenomena, *decoupling* and *freeze-out*, to understand thermal relic WIMP DM. A simplified, but generic discussion will be developed here. There are some traditional references concerning this subject. For example, see Refs. [41–43] for sophisticated treatments and delicate issues that we do not touch here. For a precise calculation, please refer to the recent literature [39].

Let us consider a particle species with a phase-space distribution. The distribution is probably complicated in general, but if we assume it was in equilibrium with a thermal plasma in the past, then it is reasonable to think it close to the thermal one. Further, as far as the particle density is dilute, we can consider the Maxwell-Boltzmann distribution,

$$f(\vec{p}, T) = e^{-(E-\mu)/T}, \tag{3.1.1}$$

with a thermal bath temperature, T. Here, μ stands for a *chemical potential* of the particle species that is determined as a result of particle interactions and the expansion of the universe.

Suppose that the particle is stable due to a Z_2 symmetry, pair annihilations are main processes changing the particle number. Further, it is also assumed that all the final state particles are the SM ones and in the thermal bath. This assumption is quit reasonable for WIMP DM in many BSM models. In this case, time evolution of the

particle number through the annihilations is governed by the Boltzmann equation[1],

$$\frac{1}{a^3}\frac{d(na^3)}{dt} = -\langle\sigma_{\rm ann}v_{\rm rel}\rangle\left[n^2 - n_{\rm eq}^2\right], \tag{3.1.2}$$

where we define the number density and its equilibrium one by

$$n = g\int\frac{d^3\vec{p}}{(2\pi)^3}\,e^{-(E-\mu)/T}, \tag{3.1.3}$$

$$n_{\rm eq} = g\int\frac{d^3\vec{p}}{(2\pi)^3}\,e^{-E/T}. \tag{3.1.4}$$

In the above equation, we also introduce the total annihilation cross section averaged over the thermal distribution, $\langle\sigma_{\rm ann}v_{\rm rel}\rangle$. Eq.(3.1.2) means the particle number in a comoving volume alters only because of the annihilations.

Now, we try to guesstimate the solution of the Boltzmann equation (3.1.2), based on the Gamov criterion and a sudden freeze-out approximation [10]. We first rewrite the equation in the following,

$$\frac{1}{N_{\rm eq}}\frac{dN}{d(\ln a)} = -\frac{\Gamma}{H}\left[\left(\frac{N}{N_{\rm eq}}\right)^2 - 1\right], \tag{3.1.5}$$

with $N_{\rm (eq)} \equiv n_{\rm (eq)}a^3$ and $\Gamma \equiv \langle\sigma_{\rm ann}v_{\rm rel}\rangle\, n_{\rm eq}$. From this equation, we can see that as far as $\Gamma \gg H$, the particle number in a comoving volume is balanced with the equilibrium one, i.e. $N \simeq N_{\rm eq}$, because the creation and annihilation reactions occur frequently enough at a small time interval. In other words, when $\Gamma \simeq H$, the reactions can no longer keep the equilibrium and change the particle number. Thus, we simply argue that the particle number is fixed when $\Gamma = H$ is fulfilled (sudden freeze-out approximation). Then, the number density at the freeze-out is approximated to

$$n_{\rm fo} \sim \frac{H(T_{\rm fo})}{\langle\sigma_{\rm ann}v_{\rm rel}\rangle_{\rm fo}}. \tag{3.1.6}$$

After the freeze-out, the particle number in a comoving volume does not change, so that the present density is simply written by

$$n_0 = n_{\rm fo}\left(\frac{a_{\rm fo}}{a_0}\right)^3. \tag{3.1.7}$$

On the other hand, as far as entropy of the universe is conserved after the freeze-out, the entropy density also obeys

$$s_0 = s_{\rm fo}\left(\frac{a_{\rm fo}}{a_0}\right)^3. \tag{3.1.8}$$

[1]The derivation of the equation is given in Appendix A.

Combining Eqs.(3.1.7)-(3.1.8), we find

$$n_0 = n_{\rm fo}\left(\frac{s_0}{s_{\rm fo}}\right). \tag{3.1.9}$$

From Eq.(3.1.9) and $\Omega \equiv \rho/\rho_c$, the present abundance is estimated by

$$\Omega h^2 \sim \frac{1.07\times 10^9\, x_{\rm fo}}{(g_{*s}/g_*^{1/2})M_{\rm pl}\cdot {\rm GeV}\,\langle\sigma_{\rm ann}v_{\rm rel}\rangle_{\rm fo}}, \tag{3.1.10}$$

where $x \equiv m/T$ and we use [37]

$$s_0 = 2970\,{\rm cm}^{-3}, \tag{3.1.11}$$

$$\rho_{c,0} = \frac{3H_0^2}{8\pi G} = 1.05\times 10^{-5}\, h^2\,[{\rm GeV}\cdot {\rm m}^{-3}]. \tag{3.1.12}$$

The freeze-out temperature is obtained by the Gamov criteion, $\Gamma_{\rm fo} = H(T_{\rm fo})$,

$$x_{\rm fo} \sim \ln\left[\sqrt{45/32\pi^6}(g/g_*^{1/2})M_{\rm pl}m\,\langle\sigma_{\rm ann}v_{\rm rel}\rangle_{\rm fo}\right], \tag{3.1.13}$$

with g being the internal degrees of freedom for the relic particle. Now, let us scale the annihilation cross section as

$$\langle\sigma_{\rm ann}v_{\rm rel}\rangle \equiv \frac{\alpha_{\rm eff}^2}{m^2}, \tag{3.1.14}$$

with $\alpha_{\rm eff}$ being an effective coupling of the annihilation process. When we take $\alpha_{\rm eff} = 1/137$ and $m = 100\,{\rm GeV}$ which leads to $\langle\sigma_{\rm ann}v_{\rm rel}\rangle \simeq 2\times 10^{-26}\,{\rm cm}^3/{\rm s}$, Eq.(3.1.10) predicts the DM abundance,

$$\Omega h^2 \sim 0.1, \tag{3.1.15}$$

that is close to the observed value: $\Omega_{\rm CDM}h^2 = 0.1188 \pm 0.0010$ [37]. This is the famous WIMP miracle. In Fig. 3.1, we show the behavior of the yield ($Y \equiv n/s$), that is obtained by numerically solving the Boltzmann equation in fact. If the relic particle would continue to keep in equilibrium with the thermal bath, the evolution on the solid line would be predicted. On the other hand, the decoupling phenomenon changes the behaviors like the dashed lines. One can see that the larger cross section results in the fewer abundance. The figure supports our knowledge of the approximate formula.

Note that more careful treatment provides a useful formula for the abundance [43],

$$\Omega h^2 \simeq \frac{1.07\times 10^9 (n+1)x_{\rm fo}}{(g_{*s}/g_*^{1/2})M_{\rm pl}\cdot {\rm GeV}\,\langle\sigma_{\rm ann}v_{\rm rel}\rangle_{\rm fo}}, \tag{3.1.16}$$

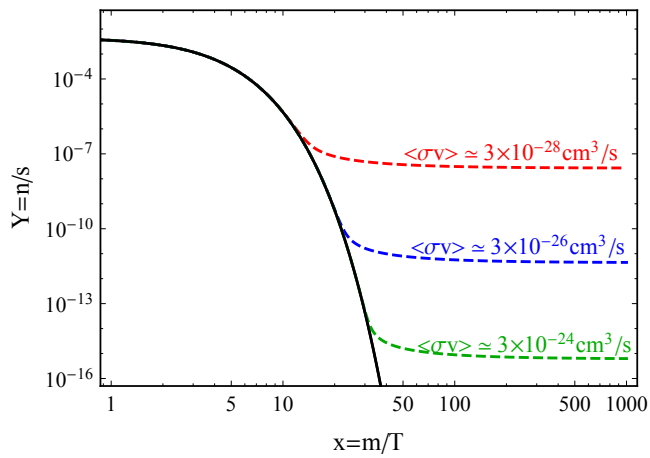

Figure 3.1. Rough sketch of the thermal freeze-out phenomenon. The holizontal axis is the inverse temperature normalized by the relic particle mass considered: $x \equiv m/T$. The vertical axis is the produced yield of the stable particle, that is the number density divided by the entropy density: $Y \equiv n/s$. The thermal equilibrium predicts the behavior of the yield on solid line. The dashed lines show a typical decoupling behavior for various sizes of annihilation cross section. It is seen that the larger cross section predicts the fewer abundance.

with the freeze-out temperature,

$$x_{\rm fo} \simeq \ln\left[0.038(n+1)(g/g_*^{1/2})M_{\rm pl}m\sigma_0\right]. \tag{3.1.17}$$

Here, σ_0 is defined through the thermal averaged cross section in the low velocity limit, that is characterized as

$$\langle\sigma_{\rm ann}v_{\rm rel}\rangle \simeq \sigma_0\, x^{-n}. \tag{3.1.18}$$

Substituting a canonical value ($\sigma_0 = 3\times10^{-26}\,\mathrm{cm}^3/\mathrm{s}$) into Eq.(3.1.17), the freeze-out temperature reads the value,

$$x_{\rm fo} \simeq 20\text{-}30, \tag{3.1.19}$$

that is insensitive to the precise value of σ_0. Intriguingly, Eq.(3.1.10) is a good approximation, though our discussion is very crude.

3.1.2 A unitarity bound on thermal WIMP DM

Before going on to DM searches, we make a mention of a theoretical limit on thermal relic WIMP DM. In the previous subsection, we have studied thermal abundance of the WIMP DM and seen that the (thermal averaged) annihilation cross section is crucial

to fix the abundance. The dependence of the DM abundance on the cross section is inversely proportional, and then the larger annihilation predicts the fewer abundance. This means that as the DM mass increases, we have to arrange a suitably large coupling. Therefore, there is an upper bound on WIMP DM mass in order not to spoil unitarity of theories. Here, we show there is a generic bound on thermal relic DM mass from the partial wave unitarity [30].

Consider a scattering process, $a + b \to c + d$. The S-matrix of the process is

$$\langle f|S|i\rangle = \langle f|i\rangle + i(2\pi)^4\delta^{(4)}(P_i - P_f)\langle f|T|i\rangle, \tag{3.1.20}$$

with $P_i^\mu \equiv (p_a + p_b)^\mu$ and $P_f^\mu \equiv (p_c + p_d)^\mu$. The T-matrix is expanded in terms of the partial waves using the helicity formalism:

$$\langle \lambda_c\lambda_d|T(s,\theta,\phi)|\lambda_a\lambda_b\rangle = 8\pi s^{1/2}e^{i\phi(\lambda-\lambda')}\sum_J (2J+1)d^J_{\lambda\lambda'}(\theta)\langle\lambda_c\lambda_d|T_J(s)|\lambda_a\lambda_b\rangle, \tag{3.1.21}$$

where s denotes the Mandelstam variable, (θ, ϕ) the scattering angle in the center of mass frame, and $d^J_{\lambda\lambda'}(\theta)$ the Wigner functions. We also define $\lambda \equiv \lambda_a - \lambda_b$ and $\lambda' \equiv \lambda_c - \lambda_d$. Using the matrix notation, $\langle\lambda_c\lambda_d|T_J|\lambda_a\lambda_b\rangle \equiv T_{if,J}$, and the partial wave unitarity of the S-matrix, we obtain the unpolarized cross section for the scattering process,

$$\sigma = \sum_J \sigma_J, \tag{3.1.22}$$

in terms of summation of the partial wave cross sections,

$$\sigma_J = \frac{4\pi(2J+1)}{(2s_a+1)(2s_b+1)}\sum_\lambda\sum_f \frac{|\vec{p}_f|}{|\vec{p}_i|}|T_{if,J}|^2. \tag{3.1.23}$$

The inelastic part is written by using an inelastic factor, η_J $(0 \le \eta_J \le 1)$, as

$$|T_{i\neq f,J}|^2 = \frac{1-\eta_J^2}{4|\vec{p}_i||\vec{p}_f|}, \tag{3.1.24}$$

so that we find an inelastic cross section $(i \neq f)$ to be

$$\sigma_{\text{inel},J} = \frac{\pi(2J+1)(1-\eta_J^2)}{|\vec{p}_i|^2}. \tag{3.1.25}$$

This equation means there is a maximum cross section for an inelastic process [30],

$$(\sigma_{\text{inel},J})_{\max} = \frac{\pi(2J+1)}{|\vec{p}_i|^2}. \tag{3.1.26}$$

Now, we study the interpretation of the result, Eq.(3.1.31), in the early universe. Suppose that the scattering process is a pair annihilation of DM. Since the DM particle was non-relativistic at the freeze-out, the initial state momentum is expressed in terms of the mass and the relative velocity,

$$|\vec{p}_i|^2 = \frac{m_{DM}^2 v_{\rm rel}^2}{4(1 - v_{\rm rel}^2/4)} \simeq \frac{m_{DM}^2 v_{\rm rel}^2}{4}, \tag{3.1.27}$$

in the low velocity limit. Then, the maximum partial-wave cross section is

$$(\sigma_J)_{\rm max} v_{\rm rel} \simeq \frac{4\pi(2J+1)}{m_{DM}^2 v_{\rm rel}}. \tag{3.1.28}$$

Averaging it over the thermal distribution, then we obtain

$$\langle (\sigma_J)_{\rm max} v_{\rm rel} \rangle \simeq \frac{4\pi(2J+1)}{m_{DM}^2} \sqrt{\frac{x}{\pi}}\,, \tag{3.1.29}$$

with $x = m_{DM}/T$. Using the approximate formula of the thermal relic abundance, Eq.(3.1.16), we find

$$\Omega h^2 \gtrsim 0.12 \times \left(\frac{m_{DM}}{300\,{\rm TeV}}\right)^2 \left(\frac{106.75}{g_*}\right)^{1/2} \left(\frac{x_{\rm fo}}{25}\right)^{1/2}, \tag{3.1.30}$$

where $g_*(T_{\rm fo}) \simeq g_{*s}(T_{\rm fo})$ is assumed. We can see there is an upper bound on the DM mass,

$$m_{DM} \lesssim 300\,{\rm TeV}, \tag{3.1.31}$$

which is consistent with the literature [30].

Finally, we would like to emphasize that the unitarity bound is put on the cross section rather than DM mass, so that the mass limit, Eq.(3.1.31), can be evaded if DM has a sizable geometrical cross section, without any conflict with the unitarity [44]. Further, if there is a huge entropy production after the freeze-out, the DM abundance is diluted and the mass bound can be escaped as well [29].

3.2 DM searches

We have found that a thermal relic WIMP can be produced in the early universe with the correct abundance. An important feature of such a particle is that it has moderate or sizable interactions with the SM and thus may leave some measurable signatures. That has encouraged us to search for WIMP DM somehow. The major strategy of the searches is to watch DM scattering off nuclei, directly produce it from the SM particle's collisions, or look for some signatures in cosmic rays. In this section, we briefly summarize these DM searches.

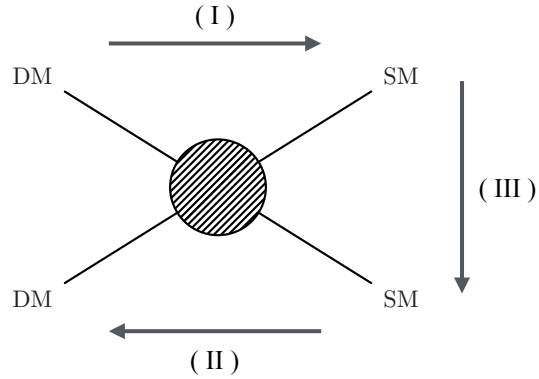

Figure 3.2. Significant processes in WIMP DM scenarios. Crossing processes are expected to be correlated with each other at some degrees. (I) DM annihilations, which not only determine the thermal relic abundance at the early universe, but also provide extra cosmic ray fluxes at present. (II) Direct productions of DM, which we aim to conduct at collider experiments. (III) Elastic scattering of DM with the SM particles, which can induce the measurable nuclear recoils at direct detections.

3.2.1 Direct detection

WIMP DM can interact with the quarks or vector bosons directly or through some quantum effects. Then, their interactions induce scatterings of DM with nucleons, or equivalently with nuclei, although the rate will be very small. The idea to directly detect DM particles through the scattering is old and goes back to the 80's [45]. At present, the direct detections are a major strategy of the WIMP DM searches, and most of them have been conducted at underground [12–15] to reduce backgrounds.

To address the direct detections from a theoretical side, we have to evaluate the elastic scattering with nuclei and predict the event rate. To do this, we first calculate effective interactions of DM with nucleons in each DM model in the limit of the low velocity and the low energy transfer. After that, we translate the interactions into the DM-nuclei scattering cross section. In this subsection, we present a theoretical procedure to predict the cross section.

Let us consider a case of Majorana fermion DM. We will show other candidates later. In the non-relativistic limit, the effective interactions relevant for the elastic scattering are written by

$$\mathcal{L}_{\text{eff}} = \sum_{N=p,n} \left[f_N \overline{\chi}\chi\overline{N}N + a_N(\overline{\chi}\gamma^\mu\gamma_5\chi)(\overline{N}\gamma_\mu\gamma_5 N) \right] , \tag{3.2.1}$$

where χ and N denotes the DM fermion and the nucleon. The former is spin-independent (SI) interaction, and the latter is spin-dependent (SD) interaction. The other combinations of the four-fermi operators are vanishing in the low velocity limit or by the

Mojarana condition of χ. The coefficients, f_N and a_N, are model dependent and should be calculated in each DM model. Using these coefficients, we can evaluate the DM-nuclei scattering cross section. The DM particle can scatter off nucleons in a target nucleus $\mathcal{A}$. For the SI process, the scattering is coherently summed up over the nucleons, so that the cross section with the nucleus is evaluated as

$$\sigma_{SI} = \frac{4\mu^2}{\pi}\left[f_p Z + (A-Z) f_n\right]^2, \tag{3.2.2}$$

where Z and A are the atomic charge and the total number of the nucleons in the nucleus, and $\mu = m_\chi m_\mathcal{A}/(m_\chi + m_\mathcal{A})$ is the reduced mass. Note that when we use a nucleus with a large atomic number as a target, the cross section, or equivalently the event rate, can benefit from the largeness of the number. In particular, in the limit of $f_p = f_n$, we find the gain is proportional to A^2.

For the SD process, we can evaluate the cross section, similarly to the SI case, but the procedure of summing over the nucleons leads some cancellation. As a result, we find the cross section to be

$$\sigma_{SD} = \frac{16\mu^2}{\pi}\frac{J_\mathcal{A}+1}{J_\mathcal{A}}\left[a_p S_p^\mathcal{A} + a_n S_n^\mathcal{A}\right]^2, \tag{3.2.3}$$

with $J^\mathcal{A}$ being the angular momentum for the nucleus. The quantities, $S_p^\mathcal{A}$ and $S_n^\mathcal{A}$, are the expectation values of the spin content of the nucleons in the nucleus, and are estimated by nuclear calculations or by nuclear models. The values are approximated to 0.5 for a nucleus with an odd number of proton or neutron and 0 with an even number. It can be seen that there is no gain due to the large atomic number.

Next, we briefly outline calculations for other DM candidates. The procedure is totally same as before. For Dirac DM, the number of the effective operators is larger than Majorana DM, and we have

$$\begin{aligned}\mathcal{L}_{\text{Dirac}} = \sum_{N=p,n} &[f_{N,e}\overline{\chi}\chi\overline{N}N + f_{N,o}(\overline{\chi}\gamma_\mu\chi)(\overline{N}\gamma^\mu N) \\ &+ a_{N,e}(\overline{\chi}\gamma_\mu\gamma_5\chi)(\overline{N}\gamma^\mu\gamma_5 N) - \frac{1}{2}a_{N,o}(\overline{\chi}\sigma_{\mu\nu}\chi)(\overline{N}\sigma^{\mu\nu}N)],\end{aligned} \tag{3.2.4}$$

in the non-relativistic limit. The evaluated cross sections take the same forms as Eqs.(3.2.2) and (3.2.3) if we define

$$f_N \equiv \frac{f_{N,e} \pm f_{N,o}}{2}, \quad a_N \equiv \frac{a_{N,e} \pm a_{N,o}}{2}, \tag{3.2.5}$$

where the plus sign (+) is for DM and the minus (−) for anti-DM. For scalar and vector DM, the effective Lagrangians are

$$\mathcal{L}_{\text{scalar}} = \sum_{N=p,n} 2 f_{N,e} m_X X^* X \overline{N}N + f_{N,o}(X^* i\overleftrightarrow{\partial_\mu} X)(\overline{N}\gamma^\mu N), \tag{3.2.6}$$

and

$$\mathcal{L}_{\text{vector}} = \sum_{N=p,n} 2f_{N,e} m_V V^*_\mu V^\mu \overline{N} N + f_{N,o}(V^*_\nu i \overleftrightarrow{\partial_\mu} V^\nu)(\overline{N}\gamma^\mu N) \\ + \sqrt{6} a_{N,e}(V^*_\nu \overleftrightarrow{\partial}_\mu V_\rho)\epsilon^{\mu\nu\rho\sigma}\overline{N}\gamma_\sigma\gamma_5 N - i\frac{\sqrt{3}}{2} a_{N,o}(V^*_\mu V_\nu - V^*_\nu V_\mu)\overline{N}\sigma^{\mu\nu} N. \tag{3.2.7}$$

For arbitrary two fields, φ_1 and φ_2, we define $\varphi_2 \overleftrightarrow{\partial_\mu} \varphi_1 \equiv \varphi_2 \partial_\mu \varphi_1 - \partial_\mu \varphi_2 \varphi_1$. For the scalar DM, there is no spin-dependent term, of course. Similarly to the fermionic DM, the cross section is obtained in the form of Eqs.(3.2.2) and (3.2.3) with the definition of Eq.(3.2.5). For a case of self-conjugate DM, i.e., a real scalar or vector, we have to take $f_{N,o} = 0$ and $a_{N,o} = 0$. We would like to note again that the coefficients, f_N and a_N, are model dependent and all the informations of DM models are included in them. The procedure to calculate the coefficients in each model is demonstrated in Appendix B.

In Figs. 3.3 and 3.4, we show the recent and projected bounds on the elastically scattering of DM with nuclei. The left panel shows the SI cross section and the right panel the SD one. The region above the solid lines are excluded (or will be probed at XENON1T). For the SI case, the limit is translated into the cross section with the nucleon, assuming $f_p = f_n$. The bound is approaching to $\mathcal{O}(10^{-47}\,\text{cm}^2)$. Some DM candidates have already been or will be excluded by these constraints, as we will see in Sec 3.3. For the SD case, the limits are obtained by assuming the proton-only or the neutron-only interactions. The solid lines represent the direct detection bounds, while the dashed lines are limits from the other experiments, e.g., collider searches and indirect detection measurements. The bounds are still weaker than the SI case, and in some cases the collider seaches and indirect detections are stronger.

3.2.2 Indirect detection

The standard thermal relic DM scenario predicts the annihilation of $\mathcal{O}(10^{-26})[\text{cm}^3/\text{s}]$ at freeze-out. Since DM undoubtedly exists in the present universe, the annihilation occurs somewhere also today. The products of the annihilation are usually the SM particles that are stable or subsequently decay into the stable particles, such as photon, electron, neutrinos, proton and their antiparticles. Further, if the produced particles are electromagnetically charged, they can emit gamma rays through the bremsstrahlung due to the interstellar magnetic field while traveling in space. Therefore, the DM annihilation at the present universe can be an extra source of cosmic rays. In particular, it is strategical and hopeful to observe cosmic rays from DM rich objects, e.g., galactic center, (dwarf spheroidal) galaxies, clusters of galaxies and so on [16–20]. Further, the sun can also be a good source of cosmic ray neutrinos for WIMP DM [46].

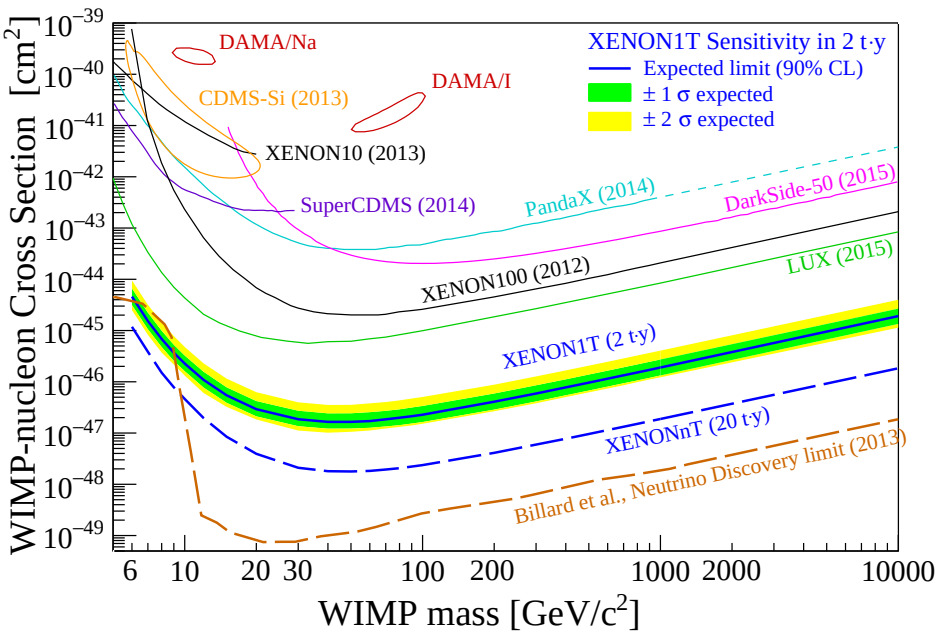

Figure 3.3. Recent bounds (XENON100 [47], LUX [12] and PandaX [48]) and the future sensitivity prospects of XENON [15] on the SI cross section of DM with the nucleon at the direct detection experiments. The bounds are obtained by assuming $f_p = f_n$.

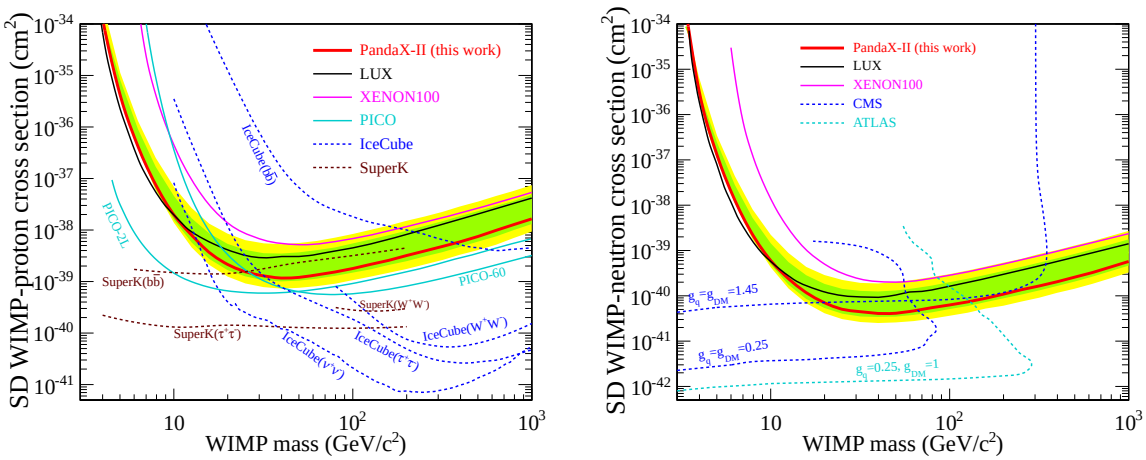

Figure 3.4. The latest bounds on the SD cross section of DM with the proton (left) and the neutron (right) by the PandaX-II [13]. The solid lines represent the direct detection bounds, while the dashed lines are limits from the LHC and the indirect detections.

The production rate of a particle species, i, from DM annihilations at a point, $\vec{x}$, is expressed by

$$R_i(\vec{x}, E) = \frac{1}{2}(\sigma v)\frac{\rho_{DM}(\vec{x})^2}{m_{DM}^2}\frac{dN_i}{dE}, \tag{3.2.8}$$

where dN_i/dE denotes the energy spectrum of the particle per one annihilation[2]. It can be seen that the rate is proportional to the annihilation cross section times the square of the DM number density: $R_i \propto (\sigma v)n_{DM}^2 = (\sigma v)\rho_{DM}^2/m_{DM}^2$. The flux of the cosmic rays at detectors, however, considerably differs from Eq.(3.2.8) because of various effects during the travel in space. For instance, if the cosmic-ray particle is not neutral, the magnetic field in space bends the motion and diffuses the energy spectrum on the way to detectors. Since the effects are complicated, the precise calculation of the flux is very difficult in fact. Thus, the bounds from indirect detections will suffer from large astrophysical uncertainties, though they are vey stringent in some cases [16, 19, 49]. The evaluation of the flux we observe is performed by solving a propagation equation [50].

For gamma rays, we can predict the flux to some extent because the gamma rays straightly travel to detectors after the production. Then, the flux is given by

$$\frac{d\Phi_i}{d\Omega dE} = \frac{\langle \sigma v \rangle}{8\pi m_{DM}^2}\frac{dN_i}{dE} \times \int_{\text{l.o.s}} dl\ \left[\rho(\vec{x}(l, \Omega)\right]^2. \tag{3.2.9}$$

The contributions can be divided into two parts. The former factor is calculated in particle physics and the latter integration comes from astrophysical informations, that is often called J-factor. In Fig. 3.5, we show the current bounds on DM annihilations from cosmic-ray photon observations. The analysis combines the Fermi and MAGIC observations [16, 17]. The bounds depend on the dominant annihilation channels, and $m_{DM} \lesssim 100\,\text{GeV}$ is disfavored for $b\bar{b}, W^+W^-, \tau\bar{\tau}$ channels for the canonical cross section in the thermal relic scenario. For $\mu\bar{\mu}$ channel, the bound is still very weaker. For other channels, the bounds are similar to either of the shown channels.

3.2.3 Collider search

All the DM annihilations have the backward processes, typically with the same size. Then, we can directly produce the DM particles if it couples to the familiar particles for us. In addition, DM may appear in a decay product of SM particles, if it is light. In any case, since DM particles hardly interact with detectors, we will recognize the

[2]It is assumed that DM is not its own anti-particle. If DM is self-conjugate, Eq.(3.2.8) should be multiplied by a factor 2.

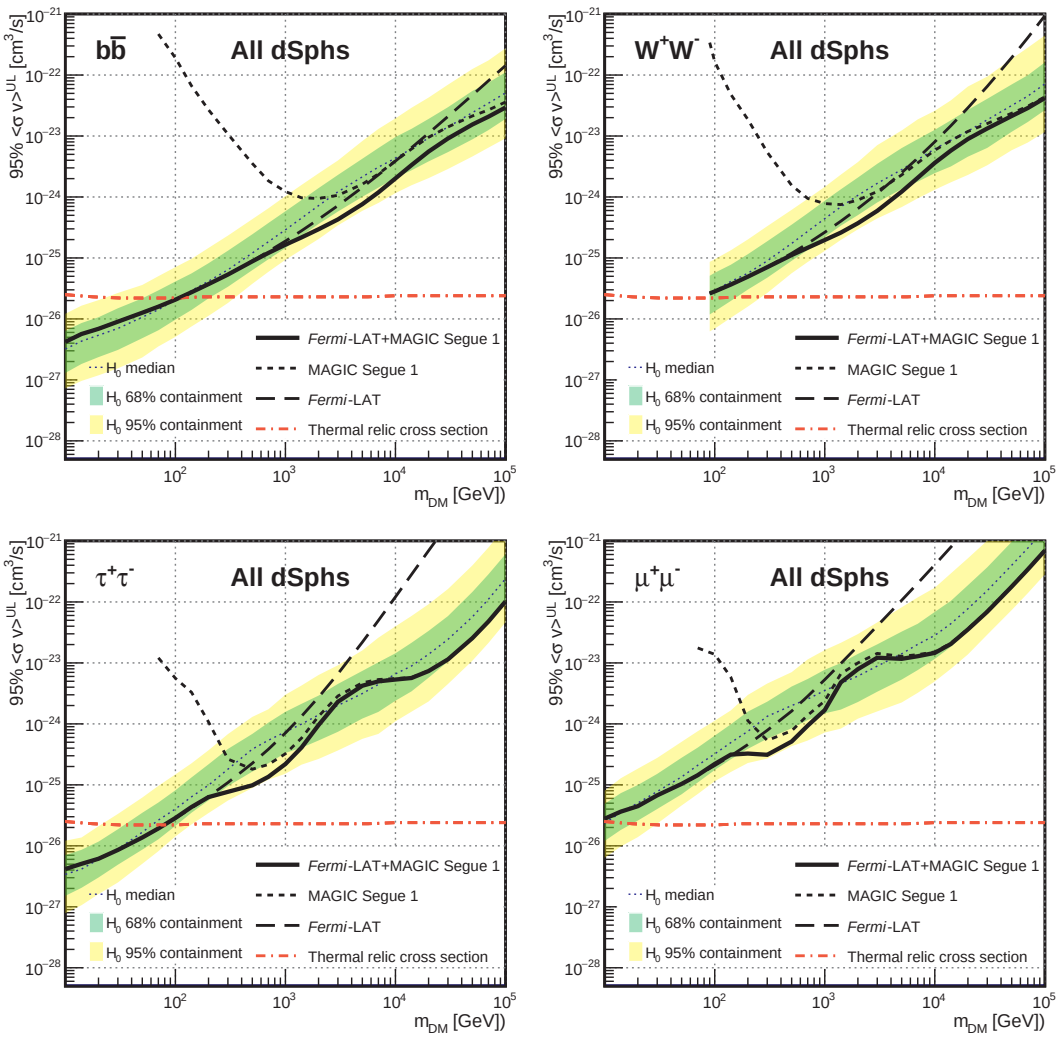

Figure 3.5. Bounds on DM annihilation cross sections from cosmic ray photon observations [16, 17]. The canonical cross section for the thermal relic abundance is also shown by the red lines. The limits are different by the annihilation channels.

productions as energy loss in reactions. At collider experiments, large efforts have been devoted to discover such missing events [11], as well as direct detection and indirect detection.

If a DM pair annihilation process is completely reversed, the final state is totally invisible. However, since we can produce the DM particles associated with a light SM particle in the final state, the searches are possible in fact. See the left diagram in Fig. 3.6, for example. The major search design is known as mono-jet search or mono-photon searches [51].

Light DM candidates may appear in decay products of the SM particles. The decay into the DM particles increases the invisible branching ratio, so that the precise observations enable us to find some evidences of DM. Assuming DM and the related new physics do not significantly change the SM prediction, the invisible branching ratio for a SM particle X is given by

$$\mathrm{Br}(X \to \mathrm{inv}) = \frac{\Gamma_{X\to DM+DM}}{\Gamma_{X\to DM+DM} + \Gamma_X^{SM}}, \tag{3.2.10}$$

with Γ_X^{SM} being the prediction in the SM. For the Z boson and the Higgs boson, the measurements of the decay width have been carried out at a good precision and can put bounds on some light DM regimes [37, 52–54].

In coannihilation scenarios [55], it is often easier to produce other new particles decaying into DM and the SM particles, rather than to directly produce the DM particles. In most cases, the heavy particles and DM carry a common charge under a global symmetry that guarantees the DM stability, while the SM particles have no charge. The expected process is a pair production of the heavy new particles whose subsequent decay produces the SM particles and a pair of DM. Then, we can look for the DM particles by searching for events with the jets or the leptons and the large missing energy. These event topologies are applied to jets $+\not{E}_T$ search or leptons$+\not{E}_T$ search as shown in the right diagram of Fig. 3.6, and are the major search designs [56].

3.3 Experimental Status

Direct detection, indirect detection and collider search experiments provide us with ample opportunities to discover WIMP DM, and the sensitivities have been improved again and again. In this section, we exemplify simple WIMP DM candidates and their experimental bounds.

To study WIMP DM models, we have to specify some properties of the DM candidates, such as spin, quantum number and self-conjugation. They can be fixed when we introduce concrete BSM theories and choose the parameter values, or just by hand in

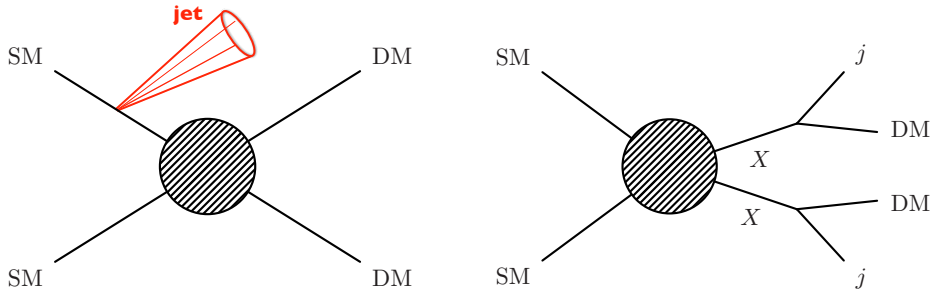

Figure 3.6. Major event topologies for DM searches at colliders. Produced DM particles can pass through the detectors without any signals. The left diagram exemplifies a mono-jet $+\not{E}_T$ event. The right diagram shows an example of multi-jet $+\not{E}_T$ events, originated from decays of intermediate heavy particles, X.

bottom-up ways. A simple, but reasonable assumption we can make on WIMP DM is that DM is singlet under the SM gauge groups. In the case, the interaction with the SM is given through non-renormalizable operators in a minimal manner, or is mediated by another particle in a renormalizable manner. Such simplified setups have been studied many times in the literature, and thus are suitable for the purpose in this section.

3.3.1 Higgs portal dark matter

First, we consider a minimal setup in which DM dominantly couples to the Higgs boson. Such a DM candidate is called Higgs portal DM. The notion of Higgs portal was first proposed by Silveira and Zee in the context of DM [57], and after that, it has extensively been studied as a benchmark model of DM [58–62]. The model setup is rather phenomenological and is studied from a bottom-up point of view in many cases, but it is also low energy effective models for some UV theories. The Higgs portal models have only a few free parameters, DM mass and couplings of DM and the SM Higgs field, so that the models are quite predictive. Here, we present minimal Higgs portal DM models up to the spin-1 candidates.

The Higgs portal models are classified according to the spin and the self-conjugation property of the DM particles. The simplest version of the models is given by the interaction Lagrangian,

$$\mathcal{L}_S \supset a\lambda_{hS} S^* S(\phi^\dagger\phi - v^2/2), \tag{3.3.1}$$

$$\mathcal{L}_F \supset a\left[\frac{1}{\Lambda_s}\overline{\chi}\chi + \frac{1}{\Lambda_p}\overline{\chi}i\gamma_5\chi\right](\phi^\dagger\phi - v^2/2), \tag{3.3.2}$$

$$\mathcal{L}_V \supset a\lambda_{hV} V_\mu^* V^\mu(\phi^\dagger\phi - v^2/2), \tag{3.3.3}$$

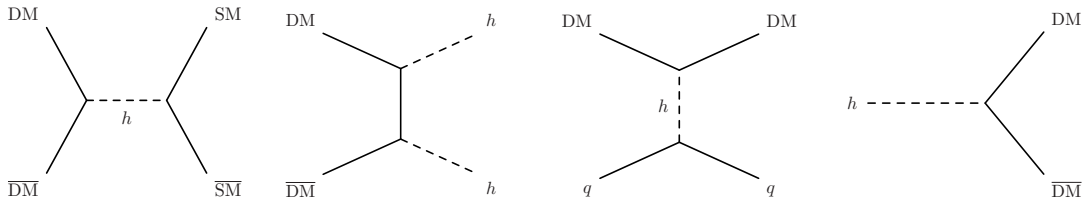

Figure 3.7. Relevant processes for significant DM observables in the Higgs portal models. Time goes from left to right in the diagrams. The left two diagrams are the main annihilation processes of DM into the SM particles. The third diagram induces the elastic scattering of DM with the nuclei. The right diagram contributes to the invisible decay width of the Higgs boson.

up to kinetic terms and self-interaction terms[3]. Here, $a = 1\,(1/2)$ for a complex (real) DM candidate. The stability of the DM particles is guaranteed by a discrete symmetry,

$$(S, \chi, V) \to -(S, \chi, V). \tag{3.3.4}$$

We find there are only two or three free parameters in each model. Relevant processes for DM physics induced by the Higgs portal couplings are DM pair annihilation and creation, the elastic scattering with nuclei and the Higgs decay into DM, as shown in Fig. 3.7. Below, we show the experimental bounds on these DM models one by one. The observables are evaluated by employing micrOMEGAs_4.3.5 [63], a public code to calculate DM observables.

Scalar DM First, we see the case of the scalar DM given by Eq.(3.3.1). DM annihilations into the SM particles proceeds through the Higgs boson exchanging as shown in the left two diagrams of Fig. 3.7. Since the Higgs couplings to the SM particles are known, the Higgs portal coupling, λ_{hS}, and DM mass are free parameters.

In the region of $m_S < m_h/2$, the Higgs boson can decay into a pair of DM and anti-DM. The decay width is given by

$$\Gamma(h \to SS^*) = \frac{av^2\lambda_{hS}^2}{16\pi m_h}\sqrt{1 - \frac{4m_S^2}{m_h^2}}, \tag{3.3.5}$$

which contributes to the Higgs invisible decay width [53].

[3]If one would like to have DM possess a sizable self-scattering, motivated by the small scale problems of the universe [23, 25], then one can introduce self-interaction terms, independently of the thermal relic abundance. Here, we are not interested in such a possibility.

The portal coupling also induces the elastic scattering of the DM particle off nuclei. The cross section is

$$\sigma_{SI} = \frac{\mu^2}{\pi m_h^4} \frac{m_N^2}{m_S^2} \lambda_{hS}^2 \left[Z \bar{f}_p + (A - Z) \bar{f}_n \right]^2 , \tag{3.3.6}$$

where μ is the reduced mass and $\bar{f}_p$ and $\bar{f}_n$ are given by

$$\bar{f}_N = \sum_{q=u,d,s} f_q^N + \frac{2}{9} f_g^N \quad (N = p, n) \tag{3.3.7}$$

at the leading order with the nucleon matrix element of the quarks and gluon,

$$m_N f_q^N \equiv \langle N | m_q \bar{q} q | N \rangle, \quad f_g^N = 1 - \sum_{q=u,d,s} f_q^N . \tag{3.3.8}$$

We use the micrOMEGAs default values [63],

$$\begin{aligned} f_u^p &= 0.0153, \quad f_d^p = 0.0191, \quad f_s^p = 0.0447, \\ f_u^n &= 0.0110, \quad f_d^n = 0.0273, \quad f_s^n = 0.0447. \end{aligned} \tag{3.3.9}$$

in this thesis.

The constraints on the model are summarized in Fig. 3.8. The correct abundance can be explained on the black (dashed) line for the complex (real) scalar DM candidate. The red region is excluded by the invisible Higgs decay [53]. The direct detection experiments are also considered. The LUX [12] and the PandaX-II [13] experiments give constraints on DM mass, and the complex (real) scalar candidate is excluded for $m_S \lesssim 840\,(400)$ GeV, if it is assumed to be dominant component of the observed DM. We also show the future prospect of the XENON1T experiment [15] and the sensitivity limit at direct detections (neutrino floor) with purple and green lines, respectively. It can be seen that the XENON1T experiment will be able to cover up to 10 TeV after the complete exposure. If we could conduct experiments with a high sensitivity comparable to the neutrino floor, even the resonance region can be probed. In addition, the lighter region ($m_S < m_h/2$) is strongly constrained by the invisible Higgs decay as well, and there is no allowed region.

Fermion DM Next, we study the fermionic DM, whose relevant interaction is given by Eq.(3.3.2). We have three free parameters in the model, DM mass and scalar and pseudo-scalar couplings. Note that the difference of the couplings is crucial to direct detections as we will see below.

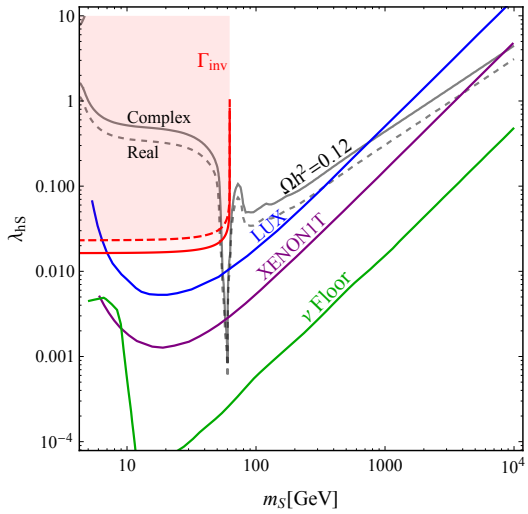

Figure 3.8. The observed DM abundance and experimental bounds for the Higgs portal scalar DM [62]. In the heavy mass region ($m_S > m_h/2$), the model is excluded by the direct detection experiments in $m_S \lesssim 840\,(400)$ GeV for the complex (real) candidate. The light region ($m_S < m_h/2$), the invisible Higgs decay [53] also gives a strong constraint on the model.

In the region of $m_\chi < m_h/2$, the model is constrained by the Higgs decay again. The decay width is

$$\Gamma(h \to \chi\bar{\chi}) = \frac{a m_h}{8\pi}\left[\left(\frac{v}{\Lambda_s}\right)^2\left(1-\frac{4m_\chi^2}{m_h^2}\right)+\left(\frac{v}{\Lambda_p}\right)^2\right]\sqrt{1-\frac{4m_\chi^2}{m_h^2}}. \tag{3.3.10}$$

In the limit of $m_\chi \ll m_h$, the scalar and pseudo-scalar couplings provide the same contributions to the decay width. On the other hand, the contributions to the elastic scattering cross section are quit different:

$$\sigma_{SI} = \frac{\mu^2}{\pi m_h^4}\frac{m_N^2}{v^2}\left[Z\bar{f}_p + (A-Z)\bar{f}_n\right]^2\left[\left(\frac{v}{\Lambda_s}\right)^2+\left(\frac{v}{\Lambda_p}\right)^2\frac{q^2}{4m_\chi^2}\right], \tag{3.3.11}$$

where q denotes the transfer momentum of the scattering process, and $q/2m_\chi = \mathcal{O}(10^{-3})$ for typical scattering events. Emphasize that for $1/\Lambda_s = 0$, the direct detection bound will be very weak.

We summarize the constraints in Fig. 3.9. For the fermionic DM, there two couplings, so that we assume either of them is vanishing in each panel. The left (right) panel is the plot for the case with the scalar (pseudoscalar) coupling. In both cases, the light mass region is constrained by the measurements of the Higgs decay as the scalar DM. Further, for the scalar coupling (left panel), it seems that the direct detection

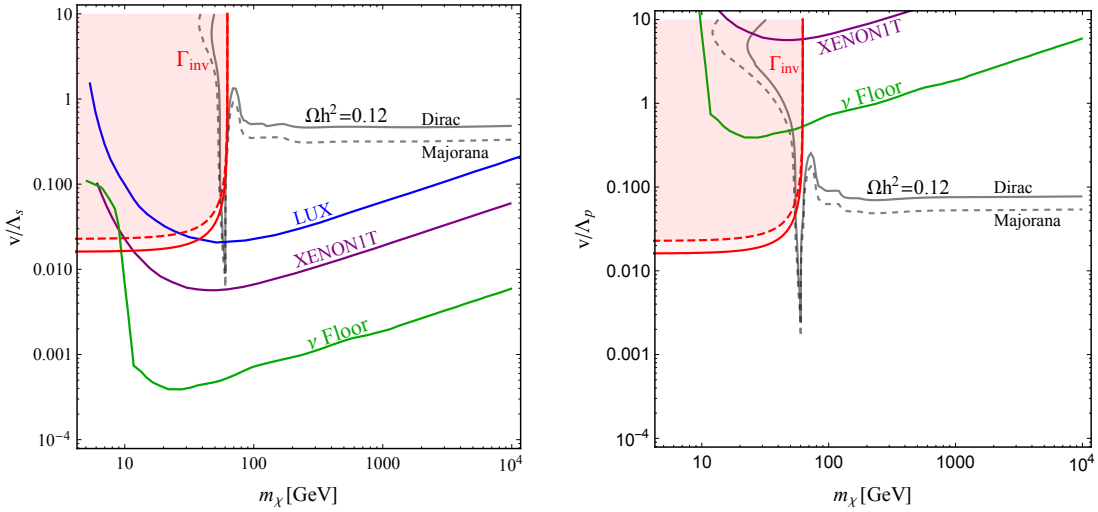

Figure 3.9. The observed DM abundance and experimental bounds for the Higgs portal fermionic DM [62]. The case of the scalar (pseudoscalar) coupling is shown in the left (right) panel. The light region ($m_\chi < m_h/2$) is mainly excluded by the invisible Higgs decay as the scalar DM. In the heavy mass region ($m_\chi > m_h/2$), the direct detection experiments put strong limits on DM mass lighter than 10 TeV for the case of the scalar coupling. On the other hand, the setup only with the pseudo-scalar coupling has no constraints from them.

bound is very strong and the XENON1T is sufficient to probe the resonance region. For the pseudo-scalar coupling (right panel), even the neutrino floor sensitivity cannot probe the whole region.

Note that the fermion model is obviously non-renormalizable, so that renormalizable improvements may help to evade the strong constraints. For instance, let us introduce a new scalar particle coupled to both DM and the Higgs field in a renomalizable way. In the case, another scalar can also mediate the elastic scattering off the nucleus. Of interest is that the contribution is destructive to that of the Higgs boson [64], so that the interference effect may relax the bounds at some degree. Another remark is that the pseudo-scalar coupling make it possible to evade the strong direct detection bound, but this coupling violates the CP-invariance. Then, the coupling may have an impact on CP-violating observables, such as electric dipole moments (EDMs). A complementarity of the direct detection and EDM measurement has been discussed in Ref. [65] in a singlet-doublet model.

Vector DM Now, we move on the vector DM. The phenomena induced by the portal coupling are basically same as the above two cases. The Higgs invisible decay width

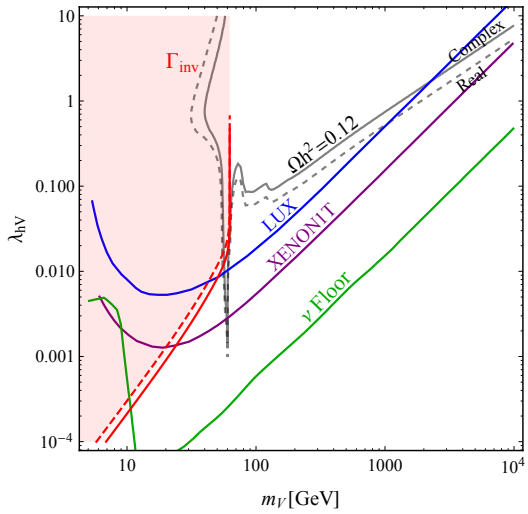

Figure 3.10. The observed DM abundance and experimental bounds for the Higgs portal vector DM [62]. The bounds are close to the scalar candidates. In the heavy mass region ($m_V > m_h/2$), this DM model is excluded by the direct detection experiments for $m_V \lesssim 1160\,(1000)$ GeV for the complex (real) candidate. In the light region ($m_V < m_h/2$), the model is also excluded by the invisible Higgs decay.

receives the contribution from the light DM, and the partial width is calculated as

$$\Gamma(h \to VV^*) = \frac{3av^2\lambda_{hV}^2}{16\pi m_h}\left(1 - \frac{m_h^2}{3m_V^2} + \frac{m_h^4}{12m_V^4}\right)\sqrt{1 - \frac{4m_V^2}{m_h^2}}. \tag{3.3.12}$$

The equation is basically similar to that of the scalar candidate except for the DM polarizations. If the vector DM is much lighter than the Higgs boson, there is an enhancement proportional to m_h^4/m_V^4 compared with the scalar DM. This factor comes from the longitudinal polarization of the massive vector boson. Thus, the lighter region will severely be constrained by the Higgs invisible decay. The cross section of the elastic scattering with nuclei is simply obtained by the replacement of $\lambda_{hS} \to \lambda_{hV}$ and $m_S \to m_V$.

We plot the constrains on the vector DM in Fig. 3.10. They are very close to the scalar DM. The DM mass is currently bounded for $m_V \lesssim 1160\,(1000)$ GeV for the complex (real) candidate from the direct detections. The XENON1T experiments will be able to search a coupling beyond the perturbativity.

3.3.2 Z portal dark matter

There is another simplified setup in which DM communicates with the visible matter through the Z boson. Such a DM candidate is called Z portal DM. There are some

possible ways to interact with the Z boson, but a simple way is that DM couples to the Z boson via current operators. Then, the interaction Lagrangian is written by, for fermionic DM,

$$\mathcal{L}_\chi \supset a\left[\bar{\chi}\gamma^\mu(g_{\chi v} - g_{\chi a}\gamma_5)\chi\right] Z_\mu, \tag{3.3.13}$$

with $a = 1(1/2)$ for a Dirac (Majorana) case again. There are two couplings in the model. Of these, the vector coupling, $g_{\chi v}$, suffers from direct detections, so that the model will be excluded unless $g_{\chi v} = 0$ or the DM particle is Majorana[4].

In the low mass region ($m_{DM} < m_Z/2$), the Z boson can decay into DM and anti-DM, and then the model is limited by the invisible width [37] as the Higgs portal models. The decay width is easily calculated and found to be

$$\Gamma(Z \to \chi\overline{\chi}) = \frac{a m_Z}{12\pi}\left(1 - \frac{4m_\chi^2}{m_Z^2}\right)^{1/2}\left[g_{\chi v}^2\left(1 + \frac{2m_\chi^2}{m_Z^2}\right) + g_{\chi a}^2\left(1 - \frac{4m_\chi^2}{m_Z^2}\right)\right]. \tag{3.3.14}$$

The elastic scattering of DM with nuclei also occurs through the Z exchanging. The low energy effective Lagrangian relevant for the scattering is

$$\mathcal{L} = \frac{a}{m_Z^2} g_Z\left[\overline{q}\gamma_\mu(C_V^q - C_A^q\gamma_5)q\right]\left[\overline{\chi}\gamma^\mu(g_{\chi v} - g_{\chi a}\gamma_5)\chi\right], \tag{3.3.15}$$

with $C_V^u = 1/2 - 4/3s_W^2$, $C_V^d = -1/2 + 2/3s_W^2$, $C_A^u = 1/2$ and $C_A^d = -1/2$. Since $\overline{\psi}\gamma^i\psi \to 0$ and $\overline{\psi}\gamma^0\gamma_5\psi \to 0$ for fermion ψ in the low velocity limit, we find only two pieces are left:

$$\mathcal{L} \approx \frac{a}{m_Z^2}\left[g_Z g_{\chi v} C_V^q(\overline{\chi}\gamma^\mu\chi)(\overline{q}\gamma_\mu q) + g_Z g_{\chi a} C_A^q(\overline{\chi}\gamma^\mu\gamma_5\chi)(\overline{q}\gamma_\mu\gamma_5 q)\right]. \tag{3.3.16}$$

The former contributes to the SI scattering and the latter to the SD scattering.

We show the constrains from the relic abundance, collider and direct detection experiments in Fig. 3.11 for the fermionic DM. In the left (right) panel, we assume that only the (axial-)vector coupling is non-vanishing. The lines showing the experimental bounds are similar to the Higgs portal models. In the case of the vector coupling dominance ($g_{\chi a} \ll g_{\chi v}$), the main bounds comes from the direct detections and the model is already excluded for $m_\chi \lesssim 6\,\text{TeV}$ by the LUX and PandaX experiments [12,13]. Besides, we will be able to search up to 10 TeV by the XENON1T [15] in near future. For the axial coupling dominance ($g_{\chi v} \ll g_{\chi a}$), the limits from the invisible decay are close to the vector coupling dominance. The relic abundance requires a larger axial coupling than the vector coupling for $m_\chi \lesssim 100$ GeV. In the heavy region ($m_\chi \gg 100\,\text{GeV}$), a similar coupling is sufficient, though. The direct detections are not so

[4]The vector current is vanishing for Majorana fermions due to the Majorana condition.

severe yet and the region of $m_\chi \gtrsim 230\,\mathrm{GeV}$ still survives. In the future, more sensitive search plans, e.g. LZ or DARWIN experiments [66, 67], will be able to probe the mass region over 1 TeV for this setup.

Finally, let us study a case of scalar DM. The interaction of DM and the Z boson is given by

$$\mathcal{L}_\varphi \supset i g_\varphi (\varphi^* \partial_\mu \varphi - \partial_\mu \varphi^* \varphi) Z^\mu + g_\varphi^2 \varphi^* \varphi Z_\mu Z^\mu. \tag{3.3.17}$$

The partial width of the $Z \to \varphi\varphi^*$ decay is

$$\Gamma(Z \to \varphi\varphi^*) = \frac{g_\varphi^2 m_Z}{48\pi} \left(1 - \frac{4m_\varphi^2}{m_Z^2}\right)^{3/2}. \tag{3.3.18}$$

For direct detections, since $\varphi^* \partial^i \varphi - \partial^i \varphi^* \varphi \to 0$ in the low velocity limit, the relevant effective Lagrangian is given in the form of

$$\mathcal{L} \approx \frac{1}{m_Z^2} g_Z g_\varphi C_V^q (i\varphi^* \partial_\mu \varphi - i\partial_\mu \varphi^* \varphi)(\overline{q}\gamma_\mu q). \tag{3.3.19}$$

We summarize the constraints in Fig. 3.12. The model is excluded up to over 10 TeV even at the current direct detections. At a glance, the scalar DM seems not a favorable choice under the Z portal assumption.

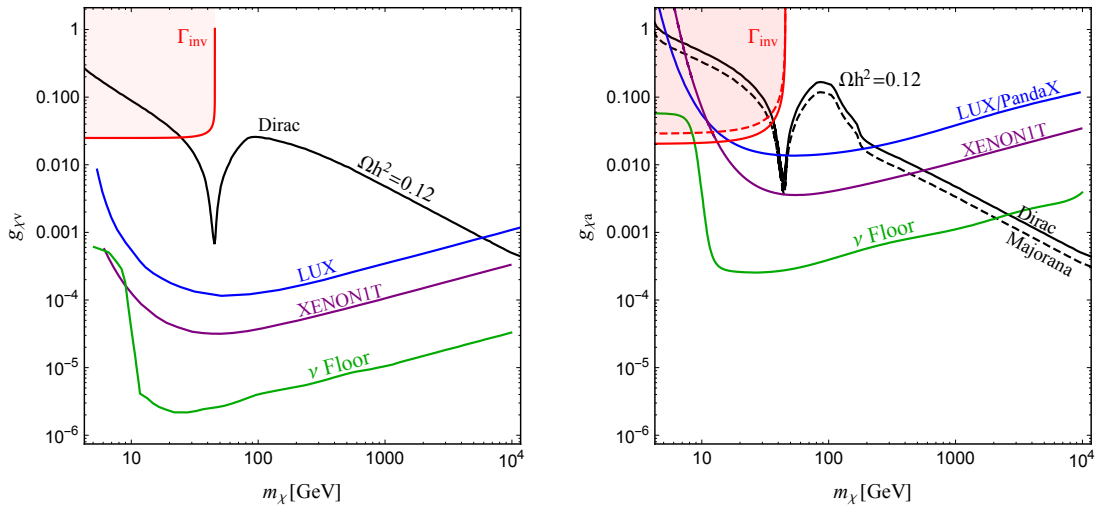

Figure 3.11. Constraints on fermionic DM in Z portal models with the vector coupling (*Left*) and the axial-vector coupling (*Right*). The DM abundance can be explained on the black lines, based on the thermal freeze-out scenario. The lower mass region is limited by the invisible Z decay that is depicted by the red region. For the vector coupling, the XENON1T can probe up to around 10 TeV. For the axial coupling, the bounds from the direct detections are not so strong yet, but more sensitive search plans, e.g. the LZ or DARWIN experiments [66, 67] will be able to probe the mass region over 1 TeV in the future.

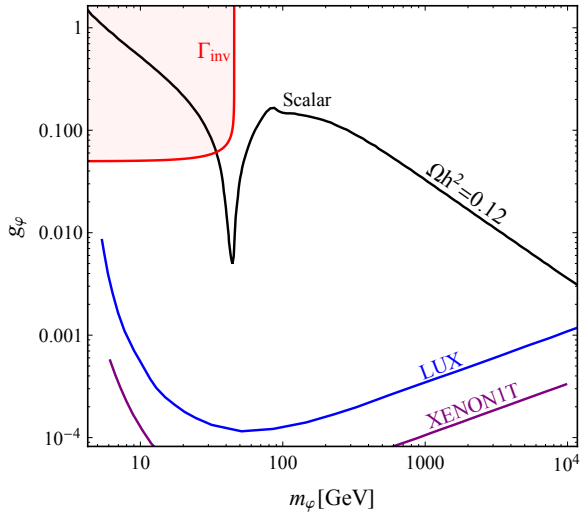

Figure 3.12. Bounds on Z portal scalar DM. The lines are similar to the fermionic DM, but the constraints are already very strong and the whole region looks contradicting with the experiments.

Chapter 4

Secluded DM scenarios

We have seen, in the previous chapter, that the WIMP DM paradigm gives us many chances to search the DM particles. Thus, considerable experimental efforts have been made to discover the direct evidences of DM, and some models are severely constrained from recently improved results in fact. Since the bounds are fully model dependent, we need not give up pursuing WIMP DM, but it is also important to look at other possibilities. One simple possibility is to consider that DM is highly secluded from us, while the observed abundance can be achieved by some production mechanisms. Based on this (or other individual) consideration, many novel and phenomenological DM scenarios have recently been proposed. In this chapter, we study secluded DM scenarios among these fresh possibilities. In particular, we restrict ourselves to cases of thermal relic DM in order to emphasize differences from the standard thermal WIMP DM scenario.

In Sec. 4.1, we study the original secluded DM scenario that was first proposed over ten years ago [21]. In the scenario, a DM particle has only tiny couplings to any SM particles and thus can elude the direct searches. To produce the correct abundance, an intermediate light particle (mediator particle) plays a crucial role as a thermal bath particle, instead of the SM ones. In Sec. 4.1, we show some concrete examples for the secluded scenario with a light mediator, and compare them with the WIMP models presented in Sec. 3.3. One will see that a correlation between the DM-nuclei elastic scattering and the total annihilation is drastically changed. In Sec. 4.2, we study a recent extension of the secluded DM scenario, that was first proposed by us [31], where a mediator particle has a non-negligible mass to DM. It is shown that the freeze-out behavior can considerably be altered while the observed relic is correctly explained even in the setup. Further, we also propose a renormalizable model that can realize the setup of the DM and mediator particles with the close mass by using a new strongly coupled gauge theory similar to QCD.

4.1 Secluded DM with a light mediator

WIMP DM commonly annihilates into the SM particles in order to transfer its entropy into the thermal plasma and reduce the number density to the correct abundance. The size of the annihilation cross section is therefore fixed via the observed abundance. This fact results in more or less a correlated cross section of DM elastic scattering off nuclei, and thus the DM particle easily shows up at the direct detection experiments. In this section, we show a way to considerably change this correlation by a seclusion mechanism [21].

4.1.1 General argument

When we carefully look over the thermal freeze-out process, we notice that the thermal relic abundance is determined by the total annihilation cross section alone. In the WIMP regime, the cross section is dominated by $2 \to 2$ annihilations into the SM particles. This leads to a sizable scattering with the SM and shows up the DM particle with ease. On the other hand, when we assume DM annihilation is dominated by processes into intermediate particles other than the SM ones, the thermal relic can correctly be produced without any conflict with the direct searches. In this case, the newly introduced particles may have to communicate with the SM sector, in order to transfer the DM entropy into others, so that they will provide some visible signatures. In most case, it requires much weaker condition than consistency with the direct searches, though.

Let us make the argument more concrete. We consider a hidden sector involving DM. It is also assumed that the DM particle has no couplings with the SM particles at the renormalizable level, but there is another particle, say mediator, communicating the both sectors (Fig. 4.1). For this setup, there are two parameter regions. One is the usual WIMP region where the mediator particle is heavier than DM. In the WIMP region, DM annihilation cannot create the on-shell mediators, so that the annihilation has to first produce the off-shell mediator that immediately decays into the SM particles. We can also say that the DM particle can annihilate into the SM only through a mixing between the mediator and a SM particle. Then, the evolution of the DM number density is governed by Eq.(3.1.2) and then the result will be similar to either of the WIMP models shown in Sec. 3.3.

Another is a secluded region that the mediator is adequately lighter than DM. In this region, DM can annihilate into the on-shell mediators, so that the Boltzmann

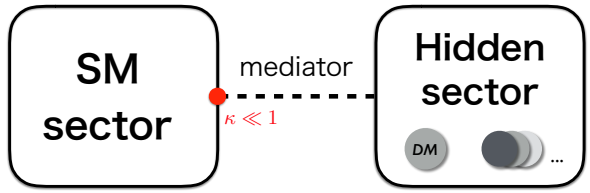

Figure 4.1. A rough sketch that describes a secluded setup. A DM particle is involved in a hidden sector that can communicate with the SM sector only via a (light) mediator particle. Even a small coupling between the SM and mediator ($\kappa \ll 1$) is sufficient to explain the DM abundance based on the thermal freeze-out scenario.

equation for DM becomes

$$\begin{aligned} \frac{1}{a^3}\frac{d(n_d a^3)}{dt} = &- \langle \sigma v \rangle_{d+d\to m+m} \left[n_d^2 - n_{d,\mathrm{eq}}^2 \left(\frac{n_m^2}{n_{m,\mathrm{eq}}^2} \right) \right] \\ &- \langle \sigma v \rangle_{d+d\to \mathrm{SMs}} \left[n_d^2 - n_{d,\mathrm{eq}}^2 \right], \end{aligned} \tag{4.1.1}$$

where the subscripts, d and m, stand for DM and mediator, respectively. Suppose that the second term is negligible to evade direct search bounds. It is further assumed that the mediator particle can maintain the thermal equilibrium with the SM plasma and hence can be regarded as a part of thermal bath, i.e., $n_m = n_{m,\mathrm{eq}}$[5]. In this case, we can see that Eq.(4.1.1) is reduced to the same as Eq.(3.1.2) and the DM abundance is completely controllable solely by the annihilation into the mediators, based on thermal freeze-out mechanism. Note that the DM abundance is no longer correlated to direct searches. That is a central difference from the WIMP regime. After the freeze-out, the mediator is left in a hot universe with a large entropy. The unexpected large entropy will spoil the great success of the standard cosmology in some ways, so that the mediator has to decay or annihilate into the SM particles before an important era, e.g. BBN. This puts a constraint on the mediator lifetime, but it is found to be weak. We would like to emphasize, from the above consideration, that the secluded regime can generically be accompanied with any WIMP DM models. In the successive subsections, we take some examples shown in the original secluded paper and study a powerful effect of the secluded mechanism.

[5]If the mediator is adequately lighter than the DM particle, this assumption is quit reasonable and can easily be fulfilled. I will discuss it later in the next subsection by taking a concrete example.

4.1.2 Vector mediator model

First, we consider an extension of the SM with a new $U(1)'$ gauge symmetry, whose Lagrangian is given by

$$\mathcal{L}_{DM+\text{med}} = -\frac{1}{4}V'_{\mu\nu}{}^2 - \frac{\kappa}{2}V'_{\mu\nu}B^{\mu\nu} - |D_\mu\varphi|^2 - V(|\varphi|) + \bar{\psi}(i\not{D} - m_\psi)\psi. \tag{4.1.2}$$

In this model, the DM particle is ψ that is singlet under the SM groups, but is charged under the $U(1)'$ group. The covariant derivative of ψ is defined as $D_\mu \equiv (\partial_\mu - ie'V'_\mu)\psi$ with e' being the gauge coupling of $U(1)'$. It is assumed that the scalar potential $V(|\varphi|)$ is arranged to break the $U(1)'$ symmetry. After the $U(1)'$ breaking, the Lagrangian takes the form,

$$\mathcal{L}_{DM+\text{med}} = -\frac{1}{4}V'_{\mu\nu}{}^2 + \frac{1}{2}m_{V'}^2 V'^2_\mu + \kappa V'_\nu \partial_\mu B^{\mu\nu} + \bar{\psi}(i\not{D} - m_\psi)\psi + \mathcal{L}_{h'}, \tag{4.1.3}$$

with $\mathcal{L}_{h'}$ being the Lagrangian for the physical $U(1)'$-Higgs boson. Since the $U(1)'$ gauge boson, V', is only particle to couple to ψ, it plays a role of a mediator. Note that we have four relevant model parameters, m_ψ, $m_{V'}$, κ and e'.

As mentioned above, there are a WIMP region and a secluded region in this kind of model. First, let us discuss the WIMP region ($m_{V'} > m_\psi$). In this region, there is no possible annihilation into the on-shell V', so that DM has to annihilate into the SM particles via kinetic mixing, κ. That will suffer from a strong bound of direct detection, however, because this is basically same as the Z portal model with the vector coupling. To simplify the presentation of the results, we consider a limiting case of $m_Z, m_h, m_t \ll m_\psi$. In this case, the annihilation cross section into the SM is approximated to

$$\sigma_{\text{ann}} v \simeq 1.3 \times 10^{-26}[\text{cm}^3/\text{s}] \times \beta \left(\frac{500\,\text{GeV}}{m_\psi}\right)^2 \times \left(\frac{4m_\psi^2}{4m_\psi^2 - m_{V'}^2}\right)^2, \tag{4.1.4}$$

at the freeze-out. We also define a typical coupling strength of the annihilation processes by

$$\beta \equiv \left(\frac{\kappa e'}{e\cos\theta_W}\right)^2. \tag{4.1.5}$$

Based on the thermal freeze-out mechanism, the size of this annihilation cross section determines the DM abundance. In addition, the DM particle can scatter off nuclei through photon exchanging induced by the charge radius operator, and the SI cross section is evaluated by

$$\sigma_{SI} = 16\pi\beta \left(\frac{Z\alpha\cos\theta_W}{m_{V'}^2}\right)^2 \times \left(\frac{m_\psi m_{\mathcal{A}}}{m_\psi + m_{\mathcal{A}}}\right)^2, \tag{4.1.6}$$

with Z being the atomic number of the target nucleus. Now, we can see that both the observables are dependent only on three free parameters, m_ψ, $m_{V'}$ and β. Thus, we can reduce β by equating Eqs.(4.1.4) and (4.1.6), and the SI cross section can be expressed independently of β. To compare with experimental results, we assume that the observed DM abundance can be explained by this DM candidate. Then, the predicted SI cross section with the nucleon is approximately given by

$$\sigma_{SI,N} \simeq 2 \times 10^{-43}\,\mathrm{cm}^2 \tag{4.1.7}$$

with $m_\psi = 500\,\mathrm{GeV}\,(\ll m_{V'})$. The latest direct detection experiments give limits on the cross section of $\mathcal{O}(10^{-46}\,\mathrm{cm}^2)$ for $m_{DM} = 500\,\mathrm{GeV}$. Then, we can see that the WIMP region will easily be excluded, as we anticipated above.

In the left panel of Fig. 4.2, we summarize constraints of the model for the WIMP region. All the observables are numerically calculated. The V' mass is fixed at $m_{V'} = 400\,\mathrm{GeV}$ in the analysis. The vertical axis is β defined by Eq.(4.1.5). The observed abundance can be explained on the black line. The upper-left corner filled with red is constrained by the invisible Z decay [37]. The gray regions above the horizontal lines are bounded from the measurement of the four-fermi interactions at LEP [54] for $\alpha' \equiv e'^2/4\pi = 1$ and $\alpha' = \alpha$. Limits from the XENON100 [47] and the LUX/PandaX [12, 13] at direct detection are also depicted in the figure. It can be seen that direct detection gives an especially strong bound on the model, and the whole parameter space consistent with the measured abundance has already been excluded.

In the secluded region ($m_\psi < m_{V'}$), on the other hand, the DM particle can annihilate into the on-shell V' bosons, so that we can achieve the observed DM abundance by appropriately tuning only the $U(1)'$ gauge coupling. Of importance is that what we need to tune is just e', not β that is a combination of e' and κ. Thus, we can take a tiny κ and the model is free from direct detection bounds, while keeping the relic abundance. The constraint on κ comes from other requirements. For instance, to validate the thermal relic scenario we have to require the kinetic equilibrium of the hidden sector and the SM sector. In most case, it will be much weaker than that of the WIMP region, however.

Let us derive the theoretical requirement to maintain the kinetic equilibrium. Since the DM and mediator are allowed to sizably couple with each other, it is sufficient to discuss only the equilibration between the mediator and the SM. Requiring the V' boson decay to occur frequently at the freeze-out, i.e., $\Gamma_{V'} \gtrsim H(T \simeq m_\psi/20)$, we obtain the inequality,

$$\kappa^2 \gtrsim 10^{-13} \left(\frac{10\,\mathrm{GeV}}{m_{V'}}\right) \left(\frac{m_\psi}{500\,\mathrm{GeV}}\right)^2, \tag{4.1.8}$$

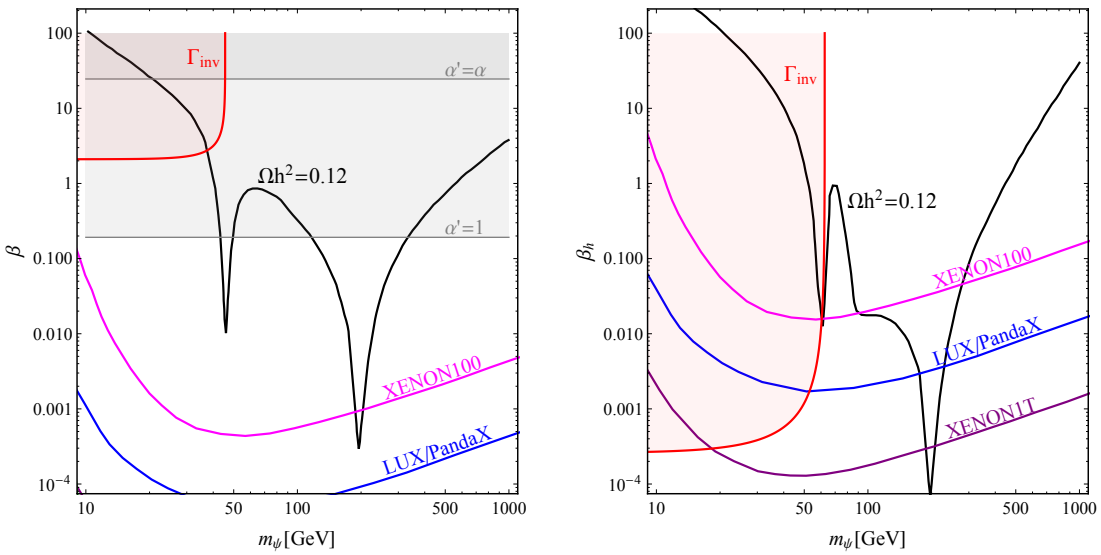

Figure 4.2. The observed DM abundance and experimental bounds in the WIMP region [21]. On the black line with two resonance poles, the observed abundance can be explained. The horizontal lines (gray) are bounds on the four-fermi operators from LEP measurements [54] for $\alpha' = 1$ and $\alpha' = \alpha$. The upper-left region filled with red is constrained by the invisible Z decay [37]. The direct detection bounds of the XENON100 [47] and the LUX/PandaX are also depicted.

that is a very weak condition and also consistent with the direct searches. Note that there is another requirement, which is that the V' boson has to decay before the BBN epoch ($t_{\rm BBN} \sim 1\,{\rm s}$). This gives another bound independent of the kinetic equilibration, that is

$$\kappa^2 \gtrsim 10^{-22} \left(\frac{10\,{\rm GeV}}{m_{V'}} \right). \tag{4.1.9}$$

We can see that the BBN bound is much weaker than the requirement of Eq.(4.1.8).

4.1.3 Scalar mediator model

Next, let us study another setup with a scalar mediator, whose Lagrangian is

$$\begin{aligned}\mathcal{L}_{DM+{\rm med}} = & \frac{1}{2}(\partial_\mu\varphi)^2 - \frac{1}{2}m_\varphi^2\varphi^2 + \bar{\psi}(i\partial\!\!\!/ - m_\psi - \lambda_\psi\varphi)\psi \\ & - \lambda_1 v\varphi\left(\phi^\dagger\phi - v^2/2\right) - \lambda_2\varphi^2\left(\phi^\dagger\phi - v^2/2\right) - V(\varphi).\end{aligned} \tag{4.1.10}$$

The DM candidate in this model is Dirac fermion, ψ, whose longevity is guaranteed by a global symmetry, while the mediator is an unstable real scalar, φ. Both the newly

introduced particles are SM singlet. If the mediator is much heavier than DM, i.e., in the WIMP regime, the mediator particle can be integrated out and this model returns to the Higgs portal model for a fermion, as shown in the Sec. 3.3.

We show the bounds on the WIMP region of this model in the right panel of Fig. 4.2. In the figure, λ_2 is assumed to be vanishing for simplicity. Again, the mediator mass is fixed at $m_\varphi = 400\,\mathrm{GeV}$ and a typical coupling strength is defined by

$$\beta_h \equiv \left(\frac{\lambda_\psi \lambda_1 v^2}{m_\varphi^2}\right)^2 . \tag{4.1.11}$$

The lines in the plot are similar to before. The lower mass region is strongly constrained by the invisible decay of the Higgs boson. In the higher mass region, the direct detections are main limits and found to be very severe. Thus, we can expect that in the secluded region ($m_\varphi < m_\psi$), the model will be able to evade these strong limits, because the DM annihilations can be dominated by the one into the mediator particles and a value of the λ_1 coupling can be chosen free from the observed abundance. In the region, there exists a bound from the kinetic equilibration of the hidden sector again. The kinetic equilibrium of the hidden and SM sector requires

$$\lambda_1^2 \gtrsim 10^{-12} \left(\frac{10\,\mathrm{GeV}}{m_\varphi}\right) \left(\frac{m_\psi}{500\,\mathrm{GeV}}\right)^2 , \tag{4.1.12}$$

but this is very weak condition. Besides, the mediator decay before the BBN imposes a very loose requirement on the coupling: $\lambda_1^2 \gtrsim 10^{-21} \times (10\,\mathrm{GeV}/m_\varphi)$.

4.1.4 Fermionic mediator model

Fermion can be a mediator particle, of course. Let us introduce the following setup,

$$\begin{aligned}\mathcal{L}_{DM+\mathrm{med}} = & \frac{1}{2}(\partial_\mu S)^2 - \frac{1}{2}m_S^2 S^2 + \overline{N'} i\partial\!\!\!/ N' - \frac{1}{2}m_{N'}\overline{N'^c}N' \\ & + \overline{N_R} i\partial\!\!\!/ N_R - \frac{1}{2}m_{N_R}\overline{N_R^c}N_R - \frac{\lambda}{2}S^2\phi^\dagger\phi \\ & - \left[Y_\nu \overline{L_L}\phi N_R - Y_{N'} S\overline{N_R^c}N' + (h.c.)\right] ,\end{aligned} \tag{4.1.13}$$

where a Z_2 symmetry is introduced into N' and S in order to guarantee the DM stability. They are also in the trivial representation of the SM gauges. The lighter one among them can be a DM candidate. We also introduce a right-handed neutrino, N_R, in the model to connect the mediator with the SM sector. This setup looks like neutrino portal models [68].

To operate a seclusion mechanism well, a relation, $m_{N'}, m_S > m_{N_R}$, is required. For $m_{N'} < m_S$, N' becomes a DM candidate. In this case, an annihilation process via

S exchanging in t-channel should be dominant in N'-annihilations, so that the DM abundance is fixed by $Y_{N'}$. The kinetic equilibrium is achieved by Y_ν or λ couplings, on the other hand. Thus, one can see that some correlations among the DM observables are resolved in the model. For $m_{N'} > m_S$, the role of S and N' is reversed, but the other discussion is totally same. In both cases, the model will be far from the direct detection bounds.

4.2 Secluded DM with a massive mediator

In the previous section, we introduced the secluded DM scenario and pointed out that it is a generic option of the WIMP DM paradigm. It was assumed that there is a large mass splitting between the DM and mediator particles, $m_{DM} \gg m_{\rm med}$, to operate the seclusion mechanism well. Then, if we construct a secluded DM model, we have to introduce a hierarchical mass scale in the model. In this section, we explore another setup of the secluded DM with a tiny mass splitting. If the setup is feasible, it will open a novel possibility to construct a hidden sector in which DM and mediator particles are unified in a (an approximate) symmetry multiplet. At the end of this section, we propose a renormalizable model involving nearly degenerate DM and mediator. In the model, they appear as dark pions in a new strong sector.

Before getting to the point, we try to guess whether there is something new in the setup. If DM and mediator particles have close mass, the mediator can no longer be treated as a thermal bath particle, so that the evolution of the mediator number will be crucial to determine the DM abundance. Now, let us assume that the main process in the hidden sector is a pair annihilation ($d + d \leftrightarrow m + m$) and we can neglect annihilations into the SM. Then, a set of the Boltzmann equations including the mediator is collected into the following two:

$$\frac{1}{a^3}\frac{d(n_d a^3)}{dt} = -\langle\sigma v\rangle_{d+d\to m+m}\left[n_d^2 - n_m^2\left(\frac{n_{d,\rm eq}^2}{n_{m,\rm eq}^2}\right)\right], \tag{4.2.1}$$

$$\frac{1}{a^3}\frac{d(n_m a^3)}{dt} = -\langle\sigma v\rangle_{m+m\to d+d}\left[n_m^2 - n_d^2\left(\frac{n_{m,\rm eq}^2}{n_{d,\rm eq}^2}\right)\right] - \langle\Gamma\rangle_m\left[n_m - n_{m,\rm eq}\right], \tag{4.2.2}$$

up to negligible contributions from the annihilations into the SM. Note that we take the mediator decay into account. Summing up both the equations, we obtain

$$\frac{1}{a^3}\frac{d(n_d a^3 + n_m a^3)}{dt} = -\langle\Gamma\rangle_m\left[n_m - n_{m,\rm eq}\right]. \tag{4.2.3}$$

From the equation, we find that the total number of the hidden sector particles will be unchanged in the limit of the stable mediator, as far as the annihilations into the SM is inefficient. Then, we can expect the freeze-out epoch can be much delayed by tuning the mediator lifetime. Below, we employ a toy model to verify this phenomenon and study effects of other ingredients.

4.2.1 Setup

We introduce a toy model with a simple hidden sector in which there are two real scalars. One is a DM particle ϕ_d and another a mediator particle ϕ_m, both of which are singlet under the SM gauges. The model Lagrangian is given by

$$\begin{aligned}\mathcal{L}_{DM+\text{med}} = & \frac{1}{2}(\partial_\mu\phi_d)^2 + \frac{1}{2}(\partial_\mu\phi_m)^2 - \frac{1}{2}m_d^2\phi_d^2 - \frac{1}{2}m_m^2\phi_m^2 \\ & - \lambda_1\phi_d^2|\phi|^2 - \lambda_2\phi_m^2|\phi|^2 - \lambda_3\phi_m^2\phi_d^2 \\ & - gm_m\phi_m|\phi|^2,\end{aligned} \tag{4.2.4}$$

in addition to the SM Lagrangian. Here, the SM doublet Higgs field is denoted by ϕ. The DM particle is stable thanks to a Z_2 symmetry, $\phi_d \to -\phi_d$, while the longevity of the mediator particle is not protected by the symmetry, due to the last term in Eq.(4.2.4). Note that in the above Lagrangian we omit terms that are consistent with the Z_2 symmetry and renomalizability, such as $\phi_d^2\phi_m$. As we will see later, however, it is not crucial to our discussion whether we involve these terms in the model Lagrangian. Thus, we consider it as just a toy model and survey its parameter space.

This model involves several well-known thermal relic scenarios of DM. If we take $m_m \gg m_d$, for example, the mediator particle can be integrated out from the theory below the DM mass scale. Then, to study the freeze-out phenomenon of the DM density, we can use a low energy effective model in which the mediator is absent. The obtained effective model is the same as the Higgs portal scalar DM model shown in Sec. 3.3. For another example, if we consider a case of $m_d \gg m_m$, the mediator particle may behave as a part of thermal plasma until the DM density freezes out. This parameter choice corresponds to the original secluded proposal [21], so that the observed DM abundance can be achieved by appropriately choosing the annihilation cross section of DM into the mediator, even if $\lambda_1 \ll 1$. This possibility has already been studied above. Here, we are interested in another parameter region, $m_d \simeq m_m$ and $\lambda_1 \ll 1$, which has not been investigated in the literature.

4.2.2 Evolution examples

In this subsection, we show some examples of number density evolution for the DM and mediator particles introduced in Eq.(4.2.4). Motivated by an unified description of the DM and mediator particles, we assume

$$m_d = m_m \equiv m, \quad \lambda_1 = \lambda_2 \equiv \lambda \, (\ll 1), \tag{4.2.5}$$

everywhere. It is also assumed that both the DM and mediator maintain the kinetic equilibrium with the SM, so that their distributions can be characterized in terms of the SM temperature in common. The validity of this assumption will be discussed in Sec. 4.2.4.

The Boltzmann equations are, for DM,

$$\begin{aligned} \frac{1}{a^3}\frac{d(n_d a^3)}{dt} = &- \langle \sigma v \rangle_{dd\to mm} \left[n_d^2 - n_m^2 \left(\frac{n_{d,\mathrm{eq}}^2}{n_{m,\mathrm{eq}}^2} \right) \right] \\ &- \langle \sigma v \rangle_{dd\to \phi\phi^\dagger} \left[n_d^2 - n_{d,\mathrm{eq}}^2 \right], \end{aligned} \tag{4.2.6}$$

and, for the mediator,

$$\begin{aligned} \frac{1}{a^3}\frac{d(n_m a^3)}{dt} = &- \langle \sigma v \rangle_{mm\to dd} \left[n_m^2 - n_d^2 \left(\frac{n_{m,\mathrm{eq}}^2}{n_{d,\mathrm{eq}}^2} \right) \right] \\ &- \langle \Gamma \rangle_m \left[n_m - n_{m,\mathrm{eq}} \right] \\ &- \langle \sigma v \rangle_{mm\to \phi\phi^\dagger} \left[n_m^2 - n_{m,\mathrm{eq}}^2 \right], \end{aligned} \tag{4.2.7}$$

where the Higgs field is assumed to keep the chemical equilibrium with the thermal plasma, i.e., $n_\phi = n_{\phi,\mathrm{eq}}$. These equations will numerically be solved, assuming the radiation dominated universe: $H^2 = 8\pi G \rho_{SM}/3$.

Example I We first show an extreme example. The parameters are fixed at

$$m = 1 \text{ TeV}, \quad \lambda = 1 \times 10^{-3}, \quad \lambda_3 = 4.0, \quad g = 2 \times 10^{-9}. \tag{4.2.8}$$

Note that the value of λ leads to $(\sigma v)_{dd\to\phi\phi^\dagger} \sim 10^{-30}\,[\mathrm{cm}^3/\mathrm{s}]$ that is rather smaller than the canonical cross section, $(\sigma v)_{\mathrm{can}} = 3 \times 10^{-26}\,[\mathrm{cm}^3/\mathrm{s}]$. In Fig. 4.3, we show the time evolution of the number densities divided by the entropy density: $Y \equiv n/s$. The red (blue) line represents the DM (mediator) density and the black dashed line does the equilibrium one. The horizontal band stands for the observed value of the DM abundance within 1σ by the Planck Collaboration, $\Omega_{\mathrm{CDM}} h^2 = 0.1188 \pm 0.0010$ [37], that corresponds to the yield, $Y_d = (4.330 \pm 0.036) \times 10^{-13}$.

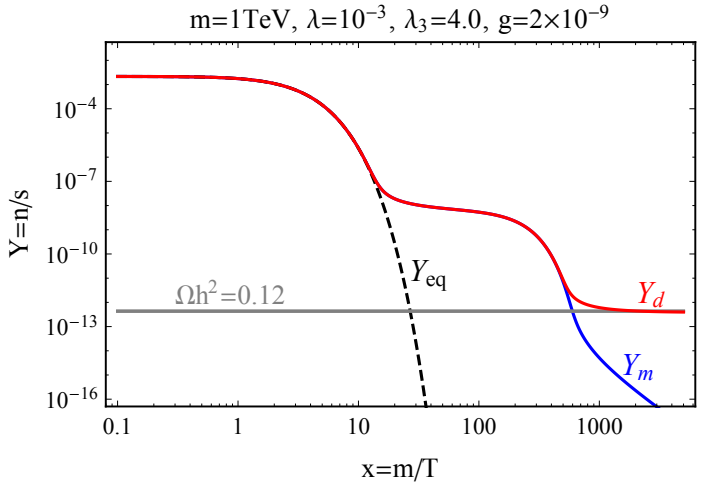

Figure 4.3. The evolution of the yields, $Y \equiv n/s$, for the DM and mediator particles. The parameters are fixed at $m = 1$ TeV, $\lambda = 10^{-3}$, $\lambda_3 = 4.0$, $g = 2 \times 10^{-9}$. The horizontal axis is the inverse temperature, $x \equiv m/T$.

In the figure, one can see that the thermal history is obviously unlike the standard thermal relic scenario, while the observed abundance can be achieved properly. At high temperature ($x \ll 1$), both the DM and mediator particles keep in chemical equilibrium with the SM sector through $dd, mm \leftrightarrow \phi\phi^\dagger$, so that their number densities trace the equilibrium ones. As temperature decreases down to $x \sim 20$, however, they chemically decouple from the SM sector; on the other hand, the chemical equilibrium between the DM and mediator particles is fulfilled even at this time due to the largeness of the coupling λ_3. Note that the mediator (inverse) decay process is not efficient for the thermalization with the SM sector, because the mediator lifetime is much longer than the Hubble time, i.e. $\tau_m \gg 1/H(x \simeq 20)$.

For a while after the decoupling, the DM number in a comoving volume can hardly change, and behaves as if it freezes out. However, this behavior is temporary and it starts to considerably decrease around $x \sim 800$. The trigger of the decrease is mediator decay. Once the mediator decay becomes active, the DM number also decreases along with that of the mediator. In this regime, because of the chemical equilibrium of the DM and mediator, the DM particle can rapidly convert to the mediator particle via the $dd \to mm$ process, to keep the balance between their number densities. As a result, the DM density reduces down to the observed one, though the thermal history is quite unusual. Now, we have confirmed our guess at the beginning of this section. We would like to emphasize that a large coupling λ_3 is required to keep the chemical equilibrium at high x.

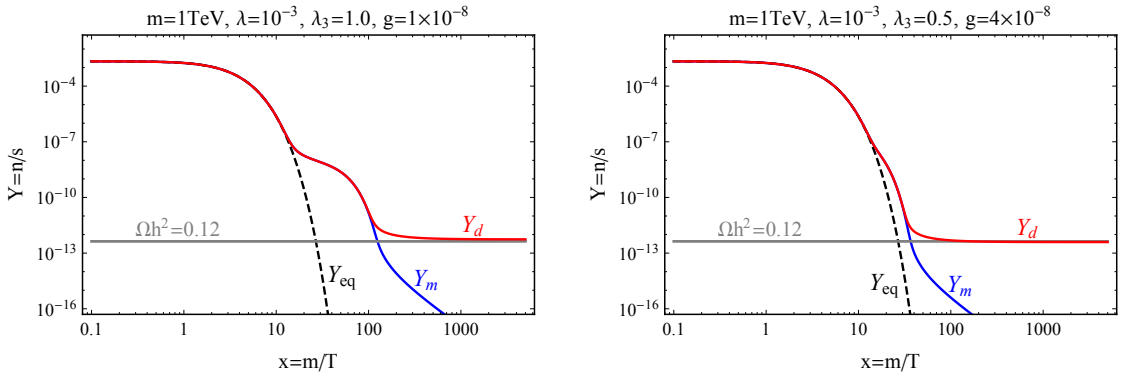

Figure 4.4. Other examples for time evolution of the particle yields, $Y \equiv n/s$, for the DM and mediator. The parameters are fixed as follows; (*Left*) $\lambda_3 = 0.95,\ g = 1 \times 10^{-8}$. (*Right*) $\lambda_3 = 0.5,\ g = 4 \times 10^{-8}$. The DM and mediator mass and the Higgs portal couplings are common in both examples: $m = 1$ TeV and $\lambda = 10^{-3}$.

Example II & III We show other examples for the time evolution in Fig. 4.4. The DM and mediator mass and the Higgs portal coupling are taken the same values as before: $m = 1\,\text{TeV}$ and $\lambda = 10^{-3}$. The other parameters are fixed at, for the left panel,

$$\lambda_3 = 1.0, \quad g = 1 \times 10^{-8}, \tag{4.2.9}$$

and, for the right panel,

$$\lambda_3 = 0.5, \quad g = 4 \times 10^{-8}. \tag{4.2.10}$$

In the left panel, the mediator lifetime is shorter than the example I. Then, the *thaw* phenomenon of the temporary freezee-out occurs earlier, but the two step decreasing of the DM number is still clear. The required quartic coupling is smaller than before: $\lambda_3 = 1.0$. Further, in the right panel, the mediator is more unstable than the left panel. We cannot see a big difference from the ordinary thermal history and can only notice a slight slope change before and after the decoupling of $dd, mm \leftrightarrow \phi\phi^\dagger$. Now, we can know that the quartic coupling, λ_3, can be tuned to realize the correct abundance for a fixed lifetime.

We can imagine that one of our assumptions, $\lambda_1 = \lambda_2$, is not essential to the thermal history, as far as the quartic coupling between the DM and mediator is large enough to maintain the chemical equilibrium between them. Even if the DM is completely Higgs-phobic ($\lambda_1 = 0$), their chemical contact enables the DM particle to be indirectly in the equilibrium with the Higgs through the DM-mediator coupling.

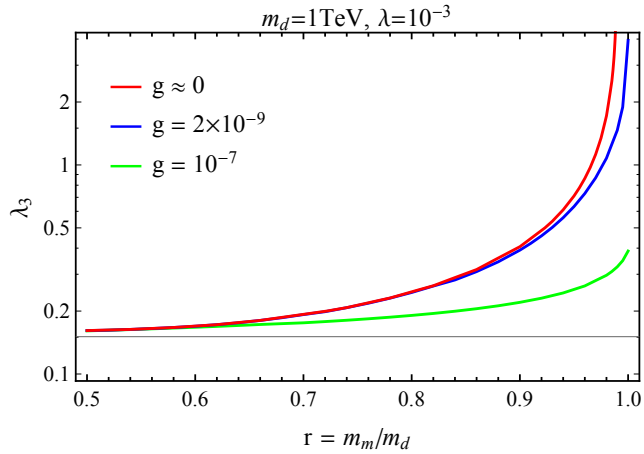

Figure 4.5. Effects of mass difference between the DM and mediator particles. The correct DM abundance is realized on lines for each value of g.

4.2.3 Effects of mass difference

It seems that in the degenerate setup we can produce the DM abundance with correct amount by tuning some parameters, mainly two parameters: the mediator lifetime and λ_3. However, if we introduce a mass splitting, the prediction can be changed. Here, we study the impacts on the relic abundance of DM.

We show the results in Fig. 4.5, when we fix some parameters at $m_d = 1\,\text{TeV}$ and $\lambda = 10^{-3}$. In the plot, we change the values of the coupling that induce the mediator decay, as $g = 10^{-7}$ (green), $g = 2 \times 10^{-9}$ (blue) and $g \approx 0$ (red). The DM abundance can be explained on the lines. The region below the lines is excluded by the overclosure of the universe. In the figure, we can see that when we fix the mediator lifetime, smaller mass splitting requires lager λ_3. On the other hand, when we fix the mass splitting, longer lifetime requires larger λ_3. Therefore, the longevity of the mediator puts a severe constraint on λ_3, especially in the region of the tiny mass splitting ($m_d \approx m_m$). We also find that the mass difference can significantly help reducing the DM abundance. A moderate mass splitting of $\mathcal{O}(10\,\%)$ allows the λ_3-coupling to be smaller than unity, even in the longevity limit ($g \approx 0$). Further, we can see that in a case of a mass difference more than $50\,\%$, the model prediction is nearly same as the original secluded DM ($\lambda_3 \to 0.16$), independently of the mediator lifetime.

4.2.4 Validity of kinetic equilibrium

It has been assumed so far that the particles in the hidden sector have the distribution characterized in terms of the SM temperature. In other words, we assumed that the hidden sector particles were in kinetic equilibrium with the SM thermal bath until

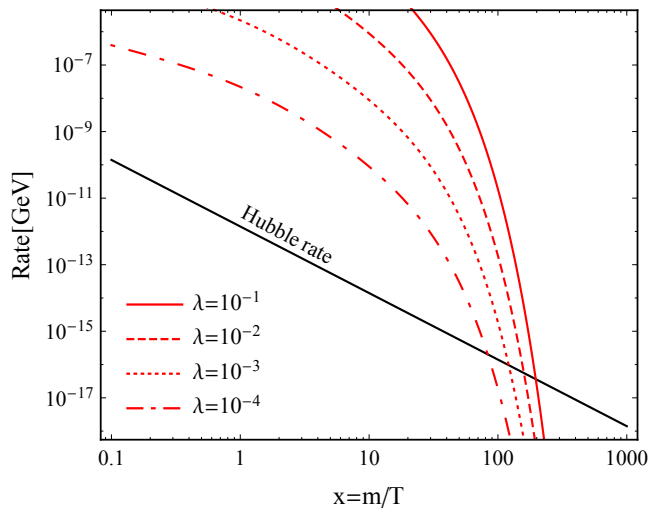

Figure 4.6. Comparison of reaction rates with the Hubble expansion rate. The black line shows the Hubble expansion rate and the red lines are the reaction rates of the elastic scattering process, $\phi_d\phi \to \phi_d\phi$. The values of λ are different for the lines; $\lambda = 10^{-1}$ (solid), 10^{-2} (dashed), 10^{-3} (dotted) and 10^{-4} (dot-dashed), respectively.

the freeze-out. Here, we observe the validity of our assumption on the kinematic equilibrium between the hidden and the SM sectors.

Let us concentrate on an elastic scattering process, $\phi_d\phi \to \phi_d\phi$. It is enough to study this process as far as $\lambda_1 = \lambda_2$ is assumed. We plot the Hubble rate and the reaction rate of the process in Fig. 4.6 for each value of the Higgs portal coupling, λ. It can be seen that the expansion rate gets superior to the reaction rate of the $\phi_d\phi \to \phi_d\phi$ process at $x \sim$100-200, because the Higgs boson and the weak bosons are already non-relativistic and their number densities become rather dilute at that time. Then, we can consider that the hidden sector is kinematically decoupled from the SM around the time. When we back to the thermal history in the degenerate setup, it is found that the DM freeze-out can occur later than the kinetic decoupling in some cases, because of the longevity of the mediator. Therefore, the assumption we made on the distribution of DM and mediator may not be reasonable, at least, for the example I. However, we believe that some generic features, such as delayed freeze-out and two step decreasing, will be carried on even if we improve the treatment of the phase-space distributions for the DM and mediator. The effects of the temperature deviation will be pursued in the future.

4.2.5 A renormalizable model

We have carefully surveyed the parameter space of the secluded DM scenario, and found a novel parameter region and interesting phenomena, e.g. delay of freeze-out, that have not been studied yet. It was also pointed out, however, that we need a strong coupling between DM and mediator to see the phenomena. Then, if DM and mediator are assumed to be elementary, it seems much difficult to obtain such a strong coupling without appearance of Landau pole much below the Planck scale. Further, one may think that the parameter region responsible for the delayed freeze-out is quite unusual and requires some unnatural tunings, because we have to arrange couplings that are many orders of magnitude different from each other.

Here, we introduce a renomalizable model that implements the coupling hierarchy and the non-traditional thermal history of DM as presented above. The model is build on a newly introduced strong sector in which DM and mediator particles appear as dark pions resulting from the strong dynamics, so that a strong coupling of the DM and mediator can be understood without any conflict with the Landau pole problem. Of great interest is that the degenerate setup of the DM and mediator, the coupling hierarchy and the long lifetime of the mediator in our secluded scenario are all explained by symmetries in the model.

Our model Lagrangian is divided into five parts,

$$\mathcal{L} = \mathcal{L}_{SM} + \mathcal{L}_{DQCD} + \mathcal{L}_{\text{yukawa}} + \mathcal{L}_{LSM} + \mathcal{L}_{M}, \tag{4.2.11}$$

where $\mathcal{L}_{SM}$ is the SM Lagrangian involving the Higgs potential. We introduce a new confining gauge theory, dubbed dark quantum chromodynamics (DQCD),

$$\mathcal{L}_{\text{DQCD}} = -\frac{1}{4g_{Ds}^2} G^a_{\mu\nu} G^{a\mu\nu} + \bar{\psi} i \not{D} \psi. \tag{4.2.12}$$

Here, $\psi_{L,R} = (U_{L,R}, D_{L,R})^T$ denote left- and right-handed dark quark fields in the fundamental representation of DQCD and form doublet of a dark chiral flavor $SU(2)$. We assume that the DQCD dynamics is analogous to the SM QCD. As will see below, candidates of DM and mediator particles show up as dark pions that are pseudo-Nambu-Goldstone bosons resulting from the dynamical dark chiral symmetry breaking due to a dark quark pair condensate, $\langle \bar{\psi}\psi \rangle \neq 0$. We refer to the strong scale as Λ_{DQCD}.

A linear sigma model is also introduced,

$$\mathcal{L}_{LSM} = \frac{1}{2}(\partial_\mu S)^2 + \frac{1}{2}(\partial_\mu P)^2 - V(S, P), \tag{4.2.13}$$

with the potential,

$$V = \frac{\lambda}{4}\left(S^2 + P^2 - F^2\right)^2 + \frac{1}{4}\epsilon_\Delta F^2 (S^2 - P^2) - \epsilon_S F^3 S - \epsilon_P F^3 P. \tag{4.2.14}$$

The first term in Eq.(4.2.14) preserves a $U(1)$ symmetry ($\Phi \equiv S + iP \to e^{i\theta}\Phi$), while the second term breaks it down to a Z_2 symmetry. The discrete symmetry is also broken by the third term completely. The interactions between the SM and DQCD sectors are mediated by these fields, S and P, and the Lagrangian is given by

$$\mathcal{L}_M = -\left[y\bar{\psi}_L(S + i\tau^3 P)\psi_R + h.c.\right] - \frac{\lambda_M}{2}(S^2 + P^2)(\phi^\dagger\phi - v^2/2), \tag{4.2.15}$$

where ϕ and v denote the SM doublet Higgs field and the VEV, respectively. Note that the first term in Eq.(4.2.15) also plays a role of an explicit dark chiral symmetry breaking, which makes the dark pions massive. In addition, it is also interesting that the $U(1)$ symmetry acting on $\Phi = S + iP$ is respected in this Lagrangian when we identify it as the third component of the dark chiral symmetry ($\psi \to e^{i\tau^3\gamma_5\theta}\psi$).

From the potential structure, the field configuration, $S = P = 0$, is unstable and the scalar fields have the VEVs of order of F. Now, we parametrize them as

$$\langle S\rangle = F\cos\bar{\theta}, \quad \langle P\rangle = F\sin\bar{\theta}, \tag{4.2.16}$$

with $F > 0$ in our convention. In addition, the Z_2 breaking couplings are rewritten by

$$\epsilon_S = |\epsilon|\cos\theta_\epsilon, \quad \epsilon_P = |\epsilon|\cos\theta_\epsilon. \tag{4.2.17}$$

Let $\tilde{s}$ and $\tilde{p}$ denote the fluctuation fields of the scalars from the VEVs. Due to the complicated structure of the potential, the mass eigenstates do not necessarily align the VEV direction. After a little tedious calculation, we find the mass eigenstates, s and p, are given by an orthogonal transformation of $\tilde{s}$ and $\tilde{p}$,

$$\begin{pmatrix} s \\ p \end{pmatrix} = \begin{pmatrix} \cos\theta & \sin\theta \\ -\sin\theta & \cos\theta \end{pmatrix} \begin{pmatrix} \tilde{s} \\ \tilde{p} \end{pmatrix}, \tag{4.2.18}$$

with the eigenvalues, M_s and M_p, respectively.

Now, we have three mass scales, v, Λ_{HQCD} and F. Assuming $v \ll \Lambda_{DQCD} \ll F$[6] and integrating out the heavy degrees of freedom, we obtain the low energy effective Lagrangian described by the SM particles and the dark pions, $\mathcal{L}_{\rm eff} = \mathcal{L}_{SM} + \mathcal{L}_{\chi,\rm eff}$. The chiral part, $\mathcal{L}_{\chi,\rm eff}$, is expressed in terms of a dark chiral field, U, into which the dark pions are collected:

$$\mathcal{L}_{\chi,\rm eff} = \frac{f^2}{4}\mathrm{tr}\left[\partial_\mu U^\dagger \partial^\mu U\right] + \frac{f^2}{4}\mathrm{tr}\left[\chi^\dagger U + U^\dagger \chi\right], \tag{4.2.19}$$

[6]The model will have baryon-like state DM candidates. If they are produced as symmetric relic in the thermal relic scenario, $m_{\rm baryons} \gtrsim 200\,\mathrm{TeV}$ will result in the overclosure by the naïve scaling of the SM QCD. Since the baryons have their masses comparable to the intrinsic strong scale, Λ_{DQCD} should be less than $\mathcal{O}(100\,\mathrm{TeV})$ unless the thermal history is changed.

with

$$U = \exp\left(i\frac{\pi^a\tau^a}{f}\right), \quad \chi = 2Bm_\psi\left(1 - \frac{1}{\Lambda_s^2}\phi^\dagger\phi + \frac{1}{\Lambda_p^2}i\tau^3\phi^\dagger\phi\right), \tag{4.2.20}$$

where f denotes a decay constant of the dark pions, B a low energy constant associated with the dark quark pair condensation, and τ^a the Pauli matrices. The scalar and pseudo-scalar terms can be given in terms of the parameters in the UV Lagrangian,

$$\frac{1}{\Lambda_s^2} = \lambda_M\left(\frac{\cos^2\theta}{M_s^2} + \frac{\sin^2\theta}{M_p^2}\right), \tag{4.2.21}$$

$$\frac{1}{\Lambda_p^2} = \lambda_M \sin\theta\cos\theta\left(\frac{1}{M_s^2} - \frac{1}{M_p^2}\right). \tag{4.2.22}$$

Expanding the chiral field, U, in terms of the dark pion fields, we find

$$\begin{aligned}\mathcal{L}_{\chi,\text{eff}} = &\frac{1}{2}\partial_\mu\pi^a\partial^\mu\pi^a - \frac{1}{2}m_\pi^2\pi^a\pi^a + \lambda_{\pi\phi}\pi^a\pi^a\phi^\dagger\phi + g_\pi m_\pi\pi^3\phi^\dagger\phi \\ &- \frac{1}{6f^2}\left[(\pi^a\partial_\mu\pi^b)^2 - (\pi^a\partial_\mu\pi^b)(\pi^b\partial^\mu\pi^a)\right] + \frac{m_\pi^2}{24f^2}(\pi^a\pi^a)^2 + \cdots,\end{aligned} \tag{4.2.23}$$

up to $\mathcal{O}(\pi^6)$ and irrelevant terms. The dark pions mass and the Higgs portal couplings are given by

$$m_\pi^2 = 2Bm_\psi, \quad \lambda_{\pi\phi} = \frac{1}{2}\frac{m_\pi^2}{\Lambda_s^2}, \quad g_\pi = \frac{fm_\pi}{\Lambda_p^2}. \tag{4.2.24}$$

It can be seen that $\pi^{1,2}$ and π^3 play roles of DM and mediator particles, respectively, and they are actually degenerate in mass at a leading order[7]. The couplings, $\lambda_{\pi\phi}$ and g_π, correspond to λ and g in Sec.4.2.2, respectively. Note that the conversion process, $\phi_d\phi_d \to \phi_m\phi_m$, proceeds through the interaction terms in the second line. The amplitude of the π-π scattering through the interactions is evaluated as

$$\mathcal{M}(\pi^1\pi^1 \to \pi^3\pi^3) = \mathcal{M}(\pi^2\pi^2 \to \pi^3\pi^3) = \frac{s - m_\pi^2}{f^2}, \tag{4.2.25}$$

so that the correspondence is

$$\lambda_3 = \frac{3m_\pi^2}{4f^2}, \tag{4.2.26}$$

at the low energy threshold ($s = 4m_\pi^2$). Now we can find that all the significant terms are derived from the Lagrangian Eq.(4.2.11).

[7]The masses of $\pi^{1,2}$ and π^3 slightly split at a higher order.

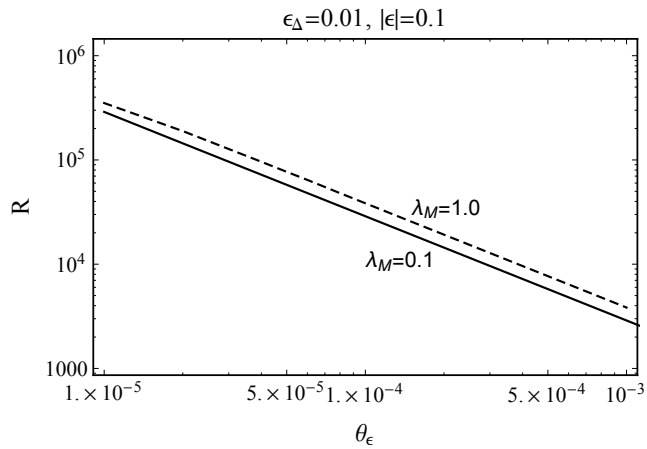

Figure 4.7. Ratio of the couplings, $g_{\pi\phi}$ and g_π, defined by Eq.(4.2.28). In our scenario, a large ratio is favorable to make the mediator particle long-lived enough.

Finally, we would like to demonstrate that the model encompasses the hierarchy between the couplings, $\lambda_{\pi\phi}$, g_π and λ_3. Since the largeness of λ_3 can be free from the details of the linear sigma model, we focus on $\lambda_{\pi\phi}$ and g_π. Taking the following parameter set as a reference,

$$\epsilon_\Delta = 0.01, \quad |\epsilon| = 0.1, \quad 0 < \theta_\epsilon < \frac{\pi}{4}, \tag{4.2.27}$$

we plot in Fig. 4.7 the ratio of the couplings,

$$R = \frac{f}{m_\pi}\frac{g_{\pi\phi}}{g_\pi}. \tag{4.2.28}$$

The solid and dashed lines correspond to $\lambda_M = 0.1$ and $\lambda_M = 1.0$. A large ratio is favorable to make the mediator particle long-lived enough. It can be seen that the large ratio is obtained in fact, if we take θ_ϵ small enough. Note that if $\theta_\epsilon = 0$, a discrete symmetry ($P \to -P$) is restored, so that the smallness of θ_ϵ can be explained in a technically natural manner.

Chapter 5

Summary and Conclusion

There are a lot of cosmological and astrophysical observations that support existence of DM that occupies about 80% of the pressureless component in our universe. However, only a few properties of DM have been known and the fundamental nature remains mysterious. The lack of our knowledge of DM has therefore driven particle theorists to propose various DM candidates.

Weakly Interacting Massive Particles (WIMPs) that are often predicted in BSM physics can provide a good explanation of DM, based on the thermal freeze-out scenario. In the standard WIMP DM scenario, the DM relic abundance is determined by the pair annihilations into the SM particles, so that we can expect the DM direct production and the elastic scattering off nuclei are correlated through the measured abundance to some extent. Based on this observation, a lot of efforts have been made to directly or indirectly discover DM particles at colliders, at underground detectors and in cosmic rays. Unfortunately, however, there are no positive results in these DM searches up to now.

Motivated by the current experimental status, many novel mechanisms for thermal DM production have recently been proposed. A representative example is a Strongly Interacting Massive Particle (SIMP) scenario [22], in which number changing processes within DM particles, e.g., $3 \to 2$ process, are relevant to produce the DM abundance. Besides, there is another proposal, dubbed a secluded DM scenario [21], in which a DM particle annihilates predominantly into intermediate particles (mediator) other than the SM ones. Then, the DM abundance is fixed by the annihilation into the mediator, unlike the WIMP DM scenario. This makes it possible to untie correlations between the DM abundance and the DM scatterings with the SM, and to evade strong direct detection bounds. In Ref. [21], the authors assumed that the mediator particle is sufficiently lighter than the DM particle, so that the mediator can be treated as a part of background thermal plasma. In this case, the thermal history is hardly changed,

while the DM abundance can correctly be produced by appropriately choosing the cross section.

In this thesis, we study a novel possibility of the secluded DM scenario that DM and mediator particles have close mass with each other. We first introduce a toy model with one DM and one mediator slightly coupled to the SM Higgs field. The mediator is also assumed to decay into the SM particles later. In the model, we carefully survey the parameter space and examine the time evolution of the DM and mediator number densities. As a result, it has been found that in a case of degenerate DM-mediator, the freeze-out phenomenon can be delayed if the mediator is long-lived. Then, the evolution of the DM number can exhibit an unusual behavior like a "terrace" in the thermal history. Further, we study the effects of the mass splitting and point out that the required splitting for the delayed freeze-out is less than 50 %.

This observation enables us to find a new potential of DM model constructions that DM and mediator particles are unified in a symmetry multiplet. Then, we propose a renormalizable model that realizes the nearly degenerate setup in a natural way. The model is built on a new strongly coupled gauge theory, dubbed dark QCD (DCD), that is analogous to the SM QCD with two flavor light quarks. The DQCD is introduced in a hidden sector and communicates with the SM sector only through a linear sigma model. Emphasize that all parts of the model are constructed at a renormalizable level. In this model, we investigate the low energy effective Lagrangian around TeV scale, and find that the DM and mediator particles are unified in a multiplet of an approximate flavor symmetry as dark pions that are pseudo-Nambu-Goldstone bosons associated with the dark chiral symmetry breaking of DQCD. It is intriguing that all the required features for the delayed freeze-out, such as degenerate mass and longevity of mediator, can be realized in our model in a (technically) natural manner.

Acknowledgements

I would like to express my sincere gratitude to my supervisor Masaharu Tanabashi for various instructive discussions and collaborations. His suggestions always improved and enriched my study and research in great amount. I also would like to thank Masato Yamanaka, who is a collaborator for a central part of this thesis, for discussions and helpful advice. I am very grateful to Shinya Matsuzaki, Yuji Omura, Tomohiro Abe and Kei Yamamoto for fruitful discussions, invaluable comments and encouragements. Finally, I would like to express my gratitude to all the members of theoretical particle physics group at Nagoya University and to my family for their hospitality and nontrivial supports.

Appendix A

Thermodynamics and Boltzmann equations

In this appendix, we summarize thermodynamical description of the early universe with the FRW metric. We also derive Boltzmann equations governing time evolution of some quantities in the expanding universe.

A.1 Thermodynamical quantities

The number density, energy density and pressure of a particle species with g internal degrees of freedom are given in terms of the phase space integral of a distribution function $f(\vec{p})$,

$$n = g \int \frac{d^3\vec{p}}{(2\pi)^3} f(\vec{p}), \tag{A.1.1}$$

$$\rho = g \int \frac{d^3\vec{p}}{(2\pi)^3} E(\vec{p}) f(\vec{p}), \tag{A.1.2}$$

$$p = g \int \frac{d^3\vec{p}}{(2\pi)^3} \frac{|\vec{p}|^2}{3E(\vec{p})} f(\vec{p}), \tag{A.1.3}$$

where $E(\vec{p}) = \sqrt{m^2 + |\vec{p}|^2}$ denotes the energy of the particle with the mass, m.

If the particle species is in thermal equilibrium with a thermal bath with temperature T, the particle distribution obeys the thermal one,

$$f(\vec{p}, T) = \frac{1}{e^{(E-\mu)/T} \mp 1}, \tag{A.1.4}$$

where in the denominator, minus $(-)$ is taken into account for bosons and plus $(+)$ for fermions. These are nothing but the Bose-Einstein and Fermi-Dirac distributions.

For the equilibrium distribution, the number density, energy density and pressure of the particle species are written by

$$n(T) = \frac{g}{2\pi^2}\int_m^\infty \frac{(E^2-m^2)^{1/2}}{e^{(E-\mu)/T}\mp 1}EdE, \tag{A.1.5}$$

$$\rho(T) = \frac{g}{2\pi^2}\int_m^\infty \frac{(E^2-m^2)^{1/2}}{e^{(E-\mu)/T}\mp 1}E^2dE, \tag{A.1.6}$$

$$p(T) = \frac{g}{6\pi^2}\int_m^\infty \frac{(E^2-m^2)^{3/2}}{e^{(E-\mu)/T}\mp 1}dE. \tag{A.1.7}$$

The entropy density is also defined by

$$s(T) = \frac{\rho(T)+p(T)-\mu(T)n(T)}{T}. \tag{A.1.8}$$

In the relativistic limit ($m \ll T$), they are approximated to, for $\mu \ll T$,

$$n \simeq \begin{cases} (\zeta(3)/\pi^2)gT^3 & \text{(Boson)} \\ (\zeta(3)/\pi^2)(3/4)gT^3 & \text{(Fermion)} \end{cases}, \tag{A.1.9}$$

$$\rho \simeq \begin{cases} (\pi^2/30)gT^4 & \text{(Boson)} \\ (\pi^2/30)(7/8)gT^4 & \text{(Fermion)} \end{cases}, \tag{A.1.10}$$

$$p \simeq \frac{1}{3}\rho, \tag{A.1.11}$$

and for $\mu \gg T$,

$$n \simeq \frac{g}{6\pi^2}\mu^3 \tag{A.1.12}$$

$$\rho \simeq \frac{g}{8\pi^2}\mu^4, \tag{A.1.13}$$

$$p \simeq \frac{1}{3}\rho. \tag{A.1.14}$$

In the non-relativistic limit, we find

$$n \simeq \left(\frac{mT}{2\pi}\right)^{3/2} e^{-(m-\mu)/T}, \tag{A.1.15}$$

$$\rho \simeq (m+\frac{3}{2}T)n, \tag{A.1.16}$$

$$p \simeq Tn. \tag{A.1.17}$$

Moreover, it may be instructive to give explicit expressions for n, ρ and p for the Maxwell-Boltzmann distribution with a zero chemical potential, $f(\vec{p},T) = \exp(-E/T)$.

After some calculation, we obtain

$$n = \frac{m^2 T}{2\pi^2} K_2(m/T), \tag{A.1.18}$$

$$\rho = \frac{m^2 T}{2\pi^2} \left[m K_1(m/T) + 3T K_2(m/T) \right], \tag{A.1.19}$$

$$p = \frac{m^2 T^2}{2\pi^2} K_2(m/T). \tag{A.1.20}$$

where $K_\alpha(x)$ denotes the modified Bessel function of second kind of order α. Later, we will use them in thermal averaged cross section and decay rate in the Boltzmann equations.

A.2 Boltzmann equations

A.2.1 Derivation

Let us consider a distribution function, $f(x, p)$, and its time evolution of a particle species that obeys a relativistic equation. According to Liouville's theorem, if non-gravitational interaction does not work between the particles, one can derive the collisionless Boltzmann equation,

$$\hat{L}[f] = 0, \tag{A.2.1}$$

with the Liouville operator defined by

$$\hat{L}[f] \equiv \left[p^\mu \frac{\partial}{\partial x^\mu} - \Gamma^\mu_{\alpha\beta} p^\alpha p^\beta \frac{\partial}{\partial p^\mu} \right] f(x, p). \tag{A.2.2}$$

Now we consider the FRW metric in flat space, Eq.(2.2.1), and find

$$\hat{L}[f] = \left[E \frac{\partial}{\partial t} - H |\vec{p}|^2 \frac{\partial}{\partial E} \right] f(t, E) \tag{A.2.3}$$

where we take time coordinate as $x^0 = t$. We can find

$$\frac{d(na^3)}{dt} = 0, \tag{A.2.4}$$

which means the number density follows an adiabatic expansion law.

In actual cases, we are interested in interacting particles, so that the collisionless Boltzmann equation should be modified, taking into account particle interactions. The appropriately modified Boltzmann equation is expressed in the form of

$$\hat{L}[f] = C[f], \tag{A.2.5}$$

where $C[f]$ is called a collision term that describes contributions from particle interactions. Now, substituting Eq.(A.2.3) into Eq.(A.2.5), we obtain

$$E\left(\frac{\partial}{\partial t} - H|\vec{p}|\frac{\partial}{\partial|\vec{p}|}\right) f(\vec{p},t) = C[f]. \tag{A.2.6}$$

Integrating both sides with respect to the Lorentz invariant phase space, $d\Pi \equiv \frac{d^3\vec{p}}{2E(2\pi)^3}$, we obtain

$$\frac{dn}{dt} + 3Hn = 2\int d\Pi C[f]. \tag{A.2.7}$$

Note that we performed the integration-by-parts against the second term in the left-hand-side. Further, after multiplying the energy by the both sides of Eq.(A.2.6), we take the same step as before, then we obtain the Boltzmann equation for the energy density,

$$\frac{d\rho}{dt} + 3H(\rho + p) = 2\int d\Pi E C[f]. \tag{A.2.8}$$

Now, we focus on a particle X. Suppose thta the particle collision procees through a scattering process $(X + i + j + \cdots \leftrightarrow k + l + \cdots)$, the collision term is given by

$$\begin{aligned} C[f_X] = -\frac{1}{2}\int & d\Pi_i d\Pi_j \cdots d\Pi_k d\Pi_l \cdots (2\pi)^4\delta^{(4)}(p_X + p_i + p_j + \cdots - p_k - p_l - \cdots) \\ & \times \Big[f_X f_i f_j \cdots (1 \mp f_k)(1 \mp f_l) \cdots |\mathcal{M}_{Xij\cdots\to kl\cdots}|^2 \\ & \quad - f_k f_l \cdots (1 \mp f_X)(1 \mp f_i)(1 \mp f_j) \cdots |\mathcal{M}_{kl\cdots\to Xij\cdots}|^2 \Big], \end{aligned} \tag{A.2.9}$$

where $\mathcal{M}$ denotes the Lorentz invariant scattering amplitude for the process. Further, for simplicity, we assume that the particle density is dilute and the scattering process respects the time reversal symmetry. In this case, the effects of quantum statistics can be neglected, $1 \mp f \simeq 1$, and the Boltzmann equations, (A.2.7) and (A.2.8), are reduced to

$$\begin{aligned} \frac{dn_X}{dt} + 3Hn_X = -\int & d\Pi_X d\Pi_i d\Pi_j \cdots d\Pi_k d\Pi_l \cdots \\ & \times (2\pi)^4\delta^{(4)}(p_X + p_i + p_j + \cdots - p_k - p_l - \cdots) \\ & \times [f_X f_i f_j \cdots - f_k f_l \cdots] \, |\mathcal{M}_{Xij\cdots\to kl\cdots}|^2, \end{aligned} \tag{A.2.10}$$

$$\begin{aligned} \frac{d\rho_X}{dt} + 3H(\rho_X + p_X) = -\int & d\Pi_X d\Pi_i d\Pi_j \cdots d\Pi_k d\Pi_l \cdots \\ & \times (2\pi)^4\delta^{(4)}(p_X + p_i + p_j + \cdots - p_k - p_l - \cdots) \\ & \times E_X \, [f_X f_i f_j \cdots - f_k f_l \cdots] \, |\mathcal{M}_{Xij\cdots\to kl\cdots}|^2. \end{aligned} \tag{A.2.11}$$

A.2.2 Thermally averaged cross section and decay rate

In this subsection, we introduce the thermally averaged decay rate and cross section, in order to apply the Boltzmann equations for a thermodynamical system later. First of all, the equilibrium number density $n^{\rm eq}(T)$ at a temperature T is defined by

$$n^{\rm eq}(T) \equiv \frac{g}{(2\pi)^3}\int d^3\vec{p}\, e^{-E/T}. \tag{A.2.12}$$

Then, for a particle decay into a two-body final state, $i \to kl$, the thermally averaged decay rate is defined by

$$\langle \Gamma_{i\to kl}\rangle_T \equiv \frac{1}{n_i^{\rm eq}(T)}\int d\Pi_i d\Pi_k d\Pi_l \delta^{(4)}(p_i - p_k - p_l)\; e^{-E_i/T}|\mathcal{M}_{i\to kl}|^2, \tag{A.2.13}$$

with the Lorentz invariant phase space (LIPS),

$$d\Pi \equiv \frac{g}{(2\pi)^3}\frac{d^3\vec{p}}{2E}. \tag{A.2.14}$$

Recalling the decay rate at zero temperature is given by

$$\Gamma_{i\to kl} = \frac{1}{2m_i}\int d\Pi_k d\Pi_l \delta^{(4)}(p_i - p_k - p_l)|\mathcal{M}_{i\to kl}|^2, \tag{A.2.15}$$

the averaged one is written with

$$\langle \Gamma_{i\to kl}\rangle_T = \frac{\Gamma_{i\to kl}}{n_i^{\rm eq}(T)}\int \frac{g_i d^3\vec{p}_i}{(2\pi)^3}\frac{m_i}{E_i}e^{-E_i/T}. \tag{A.2.16}$$

Using the integration formulae,

$$\int \frac{d^3\vec{p}_i}{(2\pi)^3}\; e^{-E_i/T} = \frac{m_i^2 T}{2\pi^2}K_2(m_i/T), \tag{A.2.17}$$

$$\int \frac{d^3\vec{p}_i}{(2\pi)^3}\frac{m_i}{E_i}e^{-E_i/T} = \frac{m_i^2 T}{2\pi^2}K_1(m_i/T), \tag{A.2.18}$$

we obtain

$$\langle \Gamma_{i\to kl}\rangle_T = \Gamma_{i\to kl}\frac{K_1(m_i/T)}{K_2(m_i/T)}, \tag{A.2.19}$$

where $K_\alpha(x)$ denotes the modified Bessel function of second kind of order α. The extension to the multi-particle final state is straightforward.

Next, we express the thermally averaged cross section for a scattering process, $ij \to kl$, in terms of zero temperature cross section and the equilibrium number density.

Similarly to the decay rate, it is defined by

$$\langle\sigma v\rangle_{ij\to kl}(T) \equiv \frac{1}{n_i^{\rm eq}(T)n_j^{\rm eq}(T)}\int d\Pi_i d\Pi_j d\Pi_k d\Pi_l \times \delta^{(4)}(p_i+p_j-p_k-p_l)|\mathcal{M}_{ij\to kl}|^2 e^{-E_i/T}e^{-E_j/T}$$

$$= \frac{g_i g_j}{n_i^{\rm eq}(T)n_j^{\rm eq}(T)}\int \frac{d^3\vec{p}_i}{(2\pi)^3}\frac{d^3\vec{p}_j}{(2\pi)^3}(\sigma v)_{ij\to kl}e^{-E_i/T}e^{-E_j/T}, \tag{A.2.20}$$

where $(\sigma v)_{ij\to kl}$ denotes the zero temperature cross section for the process. This equation can be reduced to

$$\langle\sigma v\rangle_{ij\to kl} = \frac{\frac{T}{32\pi^4}\int ds K_1(\sqrt{s}/T)\frac{|\vec{p}_i||\vec{p}_k|}{4\pi\sqrt{s}}\int\frac{d\Omega_{kl}}{4\pi}|\mathcal{M}|^2_{ij\to kl}}{n_i^{\rm eq}(T)n_j^{\rm eq}(T)/(g_i g_j)}, \tag{A.2.21}$$

where $|\vec{p}_{i(k)}|$ denotes the momentum of the particle $i(k)$ in the center-of-mass frame of the reaction, and is explicitly written by

$$|\vec{p}_i| = \frac{\sqrt{s-(m_i+m_j)^2}\sqrt{s-(m_i-m_j)^2}}{2\sqrt{s}}, \tag{A.2.22}$$

$$|\vec{p}_k| = \frac{\sqrt{s-(m_k+m_l)^2}\sqrt{s-(m_k-m_l)^2}}{2\sqrt{s}}. \tag{A.2.23}$$

The integration range of s is

$$\max\left[(m_i+m_j)^2,(m_k+m_l)^2\right] \le s \le \infty. \tag{A.2.24}$$

The above thermally averaged quantities, Eqs.(A.2.19) and (A.2.21), will appear in the Boltzmann equations. In particular, for a pair annihilation $i\bar{i}\to k\bar{k}$, Eq.(A.2.21) becomes

$$\langle\sigma v\rangle_{ij\to kl} = \frac{\frac{T}{64\pi^4}\int ds(\sigma v)_{i\bar{i}\to k\bar{k}}(s)s(s-4m_i^2)^{1/2}K_1(\sqrt{s}/T)}{n_i^{\rm eq}(T)n_j^{\rm eq}(T)/(g_i g_j)}, \tag{A.2.25}$$

which is rather practical in numerical calculation in a case.

A.2.3 Application for a thermodynamical system

Now that we have the general expression of the Boltzmann equations including the collision processes, let us apply them for a thermodynamical system in which the

particle collision mainly occurs via a decay ($i \to kl\cdots$) and $2 \to 2$ annihilations ($ij \to kl$). We assume the distribution function to be the Maxwell-Boltzmann form;

$$n(t) = \frac{g}{(2\pi)^3}\int d^3\vec{p}\, e^{-(E-\mu)/T} = e^{\mu/T}\frac{g}{(2\pi)^3}\int d^3\vec{p}\, e^{-E/T} = e^{\mu/T} n^{\rm eq}(T). \tag{A.2.26}$$

Further, it is also assumed that the initial and final state particles are in kinematic equilibrium with a thermal bath at a temperature T.

For the number density of a particle species, i, the Boltzmann equation turns to

$$\begin{aligned}\frac{dn_i}{dt} + 3Hn_i = &-\int d\Pi_i d\Pi_k d\Pi_l \cdots (2\pi)^4\delta^{(4)}(p_i - p_k - p_l - \cdots) \\ &\times \left[e^{-(E_i-\mu_i)/T} - e^{-(E_k-\mu_k)/T}e^{-(E_l-\mu_l)/T}\cdots\right]|\mathcal{M}_{i\to kl\cdots}|^2 \\ &-\int d\Pi_i d\Pi_j d\Pi_k d\Pi_l (2\pi)^4\delta^{(4)}(p_i + p_j - p_k - p_l) \\ &\times \left[e^{-(E_i-\mu_i)/T}e^{-(E_j-\mu_j)/T} - e^{-(E_k-\mu_k)/T}e^{-(E_l-\mu_l)/T}\right]|\mathcal{M}_{ij\to kl}|^2,\end{aligned} \tag{A.2.27}$$

where the first (second) term in the right-hand-side is the contribution from the decay (annihilation) process. They are evaluated as follows:

$$\begin{aligned}(\text{1st-term}) &= -\int d\Pi_i d\Pi_k d\Pi_l \cdots (2\pi)^4\delta^{(4)}(p_i - p_k - p_l - \cdots) \\ &\quad\times \left[e^{-(E_i-\mu_i)/T} - e^{-(E_k-\mu_k)/T}e^{-(E_l-\mu_l)/T}\cdots\right]|\mathcal{M}_{i\to kl\cdots}|^2 \\ &= -\Gamma_i\int\frac{g_i d^3\vec{p}_i}{(2\pi)^3}\frac{m_i}{E_i}\left[\frac{n_i}{n_i^{\rm eq}}e^{-E_i/T} - \left(\frac{n_k}{n_k^{\rm eq}}\frac{n_l}{n_l^{\rm eq}}\cdots\right)e^{-E_i/T}\right] \\ &= -\langle\Gamma_i\rangle\left[n_i - n_i^{\rm eq}\left(\frac{n_k}{n_k^{\rm eq}}\frac{n_l}{n_l^{\rm eq}}\cdots\right)\right].\end{aligned} \tag{A.2.28}$$

$$\begin{aligned}(\text{2nd-term}) &= -\int d\Pi_i d\Pi_j d\Pi_k d\Pi_l (2\pi)^4\delta^{(4)}(p_i + p_j - p_k - p_l) \\ &\quad\times \left[e^{-(E_i-\mu_i)/T}e^{-(E_j-\mu_j)/T} - e^{-(E_k-\mu_k)/T}e^{-(E_l-\mu_l)/T}\right]|\mathcal{M}_{ij\to kl}|^2 \\ &= -\int\frac{g_i d^3\vec{p}_i}{(2\pi)^3}\frac{g_j d^3\vec{p}_j}{(2\pi)^3}(\sigma v)_{ij\to kl} \\ &\quad\times\left[\frac{n_i}{n_i^{\rm eq}}\frac{n_j}{n_j^{\rm eq}}e^{-(E_i+E_j)/T} - \frac{n_k}{n_k^{\rm eq}}\frac{n_l}{n_l^{\rm eq}}e^{-(E_i+E_j)/T}\right] \\ &= -\langle\sigma v\rangle_{ij\to kl}\left[n_i n_j - n_i^{\rm eq}n_j^{\rm eq}\frac{n_k}{n_k^{\rm eq}}\frac{n_l}{n_l^{\rm eq}}\right].\end{aligned} \tag{A.2.29}$$

Note that all of the thermal quantities are evaluated at the temperature T. Combining the equations, we find

$$\begin{aligned}\frac{dn_i}{dt} + 3Hn_i = &- \langle \Gamma_i \rangle \left[n_i - n_i^{\rm eq} \left(\frac{n_k}{n_k^{\rm eq}} \frac{n_l}{n_l^{\rm eq}} \cdots \right) \right] \\ &- \langle \sigma v \rangle_{ij \to kl} \left[n_i n_j - n_i^{\rm eq} n_j^{\rm eq} \frac{n_k}{n_k^{\rm eq}} \frac{n_l}{n_l^{\rm eq}} \right] .\end{aligned} \tag{A.2.30}$$

We can also formulate the Boltzmann equation for the energy density. It is not used in this thesis, but we give it here. The equation is written in the form of

$$\begin{aligned}&\frac{d\rho_i}{dt} + 3H(\rho_i + p_i) \\ &\quad = - \int d\Pi_i d\Pi_k d\Pi_l \cdots (2\pi)^4 \delta^{(4)}(p_i - p_k - p_l - \cdots) \\ &\qquad \times E_i \left[e^{-(E_i - \mu_i)/T} - e^{-(E_k - \mu_k)/T} e^{-(E_l - \mu_l)/T} \cdots \right] |\mathcal{M}_{i \to kl \cdots}|^2 \\ &\qquad - \int d\Pi_i d\Pi_j d\Pi_k d\Pi_l (2\pi)^4 \delta^{(4)}(p_i + p_j - p_k - p_l) \\ &\qquad \times E_i \left[e^{-(E_i - \mu_i)/T} e^{-(E_j - \mu_j)/T} - e^{-(E_k - \mu_k)/T} e^{-(E_l - \mu_l)/T} \right] |\mathcal{M}_{ij \to kl}|^2 ,\end{aligned} \tag{A.2.31}$$

where the first (second) term in the right-hand-side is the contribution from the decay (annihilation) process. Again, they can be evaluated as

$$\begin{aligned}(\text{1st-term}) &= - \int d\Pi_i d\Pi_k d\Pi_l \cdots (2\pi)^4 \delta^{(4)}(p_i - p_k - p_l - \cdots) \\ &\qquad \times E_i \left[e^{-(E_i - \mu_i)/T} e^{-(E_k - \mu_k)/T'} e^{-(E_l - \mu_l)/T'} \right] |\mathcal{M}_{i \to kl \cdots}|^2 \\ &= -m_i \Gamma_i \int \frac{g_i d^3 \vec{p}_i}{(2\pi)^3} \left[\frac{n_i}{n_i^{\rm eq}(T)} e^{-E_i/T} - \left(\frac{n_k}{n_k^{\rm eq}} \frac{n_l}{n_l^{\rm eq}} \cdots \right) e^{-E_i/T} \right] \\ &= -m_i \Gamma_i \left[n_i - \left(\frac{n_k}{n_k^{\rm eq}} \frac{n_l}{n_l^{\rm eq}} \cdots \right) n^{\rm eq} \right] ,\end{aligned} \tag{A.2.32}$$

and

$$\begin{aligned}(\text{2nd-term}) &= - \int d\Pi_i d\Pi_j d\Pi_k d\Pi_l (2\pi)^4 \delta^{(4)}(p_i + p_j - p_k - p_l) \\ &\qquad \times E_i \left[e^{-(E_i - \mu_i)/T} e^{-(E_j - \mu_j)/T} - e^{-(E_k - \mu_k)/T} e^{-(E_l - \mu_l)/T} \right] |\mathcal{M}_{ij \to kl}|^2 \\ &= - \int \frac{g_i d^3 \vec{p}_i}{(2\pi)^3} \frac{g_j d^3 \vec{p}_j}{(2\pi)^3} E_i (\sigma v)_{ij \to kl} \\ &\qquad \times \left[\frac{n_i}{n_i^{\rm eq}} \frac{n_j}{n_j^{\rm eq}(T)} e^{-(E_i + E_j)/T} - \frac{n_k}{n_k^{\rm eq}} \frac{n_l}{n_l^{\rm eq}} e^{-(E_i + E_j)/T} \right] \\ &= - \langle E_i \cdot \sigma v \rangle_{ij \to kl} \left[n_i n_j - n_i^{\rm eq} n_j^{\rm eq} \frac{n_k}{n_k^{\rm eq}} \frac{n_l}{n_l^{\rm eq}} \right] ,\end{aligned} \tag{A.2.33}$$

where we define in the last line

$$\langle E_i \cdot \sigma v \rangle_{ij\to kl}(T) \equiv \frac{g_i g_j}{n_i^{\rm eq}(T) n_j^{\rm eq}(T)} \int \frac{d^3\vec{p}_i}{(2\pi)^3} \frac{d^3\vec{p}_j}{(2\pi)^3} E_i (\sigma v)_{ij\to kl}\, e^{-(E_i+E_j)/T}. \tag{A.2.34}$$

Combining the equations, Eq.(A.2.31) becomes

$$\begin{aligned} \frac{d\rho_i}{dt} + 3H(\rho_i + p_i) = & -m_i \Gamma_i \left[n_i - n^{\rm eq} \left(\frac{n_k}{n_k^{\rm eq}} \frac{n_l}{n_l^{\rm eq}} \cdots \right) \right] \\ & - \langle E_i \cdot \sigma v \rangle_{ij\to kl} \left[n_i n_j - n_i^{\rm eq} n_j^{\rm eq} \frac{n_k}{n_k^{\rm eq}} \frac{n_l}{n_l^{\rm eq}} \right]. \end{aligned} \tag{A.2.35}$$

Appendix B

Direct detection of DM

In Sec. 3.2, we study the DM-nucleon effective interactions relevant for the elastic scattering of DM with nuclei, and derive the expressions of the cross section for scalar, fermion and vector DM candidates. Since in most cases we only know interactions between DM and partons (quarks and gluon) in DM models, we have to evaluate the contributions from DM-parton effective interactions to the DM-nucleon interactions. In general, there are many effective operators that contributes to the DM-nucleon interactions, Eqs.(3.2.1), (3.2.4), (3.2.6) and (3.2.7). In this appendix, we explain a way of moving from a quark-gluon level to the nucleon level in short.

B.1 Scalar operators

Operators that contribute to $f_{N,e}$ are

$$\mathcal{L}_{\text{eff}} \supset \left[\sum_{q=u,d,s} c_S^{(q)} \mathcal{O}_S \overline{q} q - c_S^{(g)} \mathcal{O}_S \frac{\alpha_s}{12\pi} G^{\alpha}_{\mu\nu} G^{\alpha\mu\nu} \right], \tag{B.1.1}$$

where $\mathcal{O}_S$ is defined by

$$\mathcal{O}_S = \begin{cases} 2m_X X^* X & \text{(Scalar)} \\ \overline{\chi}\chi & \text{(Fermion)} \\ 2m_V V^*_\mu V^\mu & \text{(Vector)} \end{cases}, \tag{B.1.2}$$

for each candidate. Note that the contributions from the heavy quarks are taken into account by the gluon operator. When we would like to evaluate the amplitude of the

elastic scattering of DM with a nucleon, N, we have to know nuclear matrix elements,

$$m_N f_{N,q} \equiv \langle N|m_q \bar{q}q|N\rangle, \tag{B.1.3}$$

$$\frac{2}{27} m_N f_{N,g} \equiv \frac{1}{12\pi}\langle N|\alpha_s G^{\alpha}_{\mu\nu} G^{\alpha\mu\nu}|N\rangle. \tag{B.1.4}$$

The form factor for the gluon is related to that of light quarks through the trace anomaly of QCD and we find the relation to be

$$f_{N,g} = 1 - \sum_{q=u,d,s} f_{N,q}. \tag{B.1.5}$$

As a result, by summing up all the contributions, we obtain

$$f_{N,e} = \sum_{q=u,d,s} c_S^{(q)} f_{N,q} + c_S^{(g)} f_{N,g}. \tag{B.1.6}$$

That is what we have in Eq.(3.2.4), for example. Note that $c_S^{(q)}$ and $c_S^{(g)}$ depend on DM models.

B.2 Vector operators

The contributions to $f_{N,o}$ come from the operators,

$$\mathcal{L}_{\text{eff}} \supset \sum_{q=u,d,s} c_V^{(q)} \mathcal{O}_V^{\mu} \bar{q}\gamma_\mu q, \tag{B.2.1}$$

where $\mathcal{O}_V^{\mu}$ is defined by

$$\mathcal{O}_V^{\mu} = \begin{cases} X^* i\overleftrightarrow{\partial^\mu} X & \text{(Scalar)} \\ \overline{\chi}\gamma^\mu \chi & \text{(Fermion)} \\ V_\nu^* i\overleftrightarrow{\partial^\mu} V^\nu & \text{(Vector)} \end{cases}, \tag{B.2.2}$$

These are couplings to the baryon number current, so that there is no suppression by the form factor and we are free from theoretical uncertainty in moving to the nucleon level. Thus, it is easy to obtain

$$f_{N,o} = \sum_{q=u,d} c_V^{(q)} g_{N,q}\,, \tag{B.2.3}$$

with $g_{p,u} = 2$, $g_{p,d} = 1$, $g_{n,u} = 1$ and $g_{n,d} = 2$.

B.3 Axial vector operators

Next, we study the SD terms. They are similarly defined and evaluated. The relevant operators are given by

$$\mathcal{L}_{\text{eff}} \supset \sum_q c_A^{(q)} \mathcal{O}_A^\mu \overline{q}\gamma_\mu\gamma_5 q \tag{B.3.1}$$

with

$$\mathcal{O}_A^\mu = \begin{cases} \overline{\chi}\gamma_\mu\gamma_5\chi & \text{(Fermion)} \\ -\sqrt{6}(V_\sigma^* i \overleftrightarrow{\partial_\nu} V_\rho)\varepsilon^{\mu\nu\sigma\rho} & \text{(Vector)} \end{cases}, \tag{B.3.2}$$

The coefficients, $a_{N,e}$, are

$$a_{N,e} = \sum_q c_A^{(q)} \Delta_q^N, \tag{B.3.3}$$

where Δ_q^N are defined by

$$2s_\mu \Delta_q^N \equiv \langle N|\overline{q}\gamma_\mu\gamma_5 q|N\rangle, \tag{B.3.4}$$

with s_μ being the nucleon spin. In this thesis, we use the micrOMEGAs default values,

$$\Delta_u^p = 0.842 \pm 0.012, \quad \Delta_d^p = -0.427 \pm 0.013, \quad \Delta_s^p = -0.085 \pm 0.018, \tag{B.3.5}$$

that is determined in Ref. [69]. The heavy quark contributions are shown to be small [70], and then we neglect them. The quantities for the neutron are obtained by a simple isospin rotation,

$$\Delta_u^n = \Delta_d^p, \quad \Delta_d^n = \Delta_u^p, \quad \Delta_s^n = \Delta_s^n. \tag{B.3.6}$$

We will end this appendix here. For further detail, please see Refs. [71,72], for example.

References

[1] F. Zwicky, Helv. Phys. Acta **6**, 110 (1933) [Gen. Rel. Grav. **41**, 207 (2009)]; Astrophys. J. **86**, 217 (1937).

[2] V. C. Rubin and W. K. Ford, Jr., Astrophys. J. **159**, 379 (1970); V. C. Rubin, W. K. Ford, Jr. and N. Thonnard, Astrophys. J. **225**, L107 (1978); V. C. Rubin, N. Thonnard and W. K. Ford, Jr., Astrophys. J. **238**, 471 (1980); V. C. Rubin, D. Burstein, W. K. Ford, Jr. and N. Thonnard, Astrophys. J. **289**, 81 (1985); K. G. Begeman, A. H. Broeils and R. H. Sanders, Mon. Not. Roy. Astron. Soc. **249**, 523 (1991).

[3] D. Clowe, M. Bradac, A. H. Gonzalez, M. Markevitch, S. W. Randall, C. Jones and D. Zaritsky, Astrophys. J. **648**, L109 (2006) [astro-ph/0608407].

[4] D. N. Spergel *et al.* [WMAP Collaboration], Astrophys. J. Suppl. **148**, 175 (2003) [astro-ph/0302209].

[5] P. A. R. Ade *et al.* [Planck Collaboration], Astron. Astrophys. **571**, A16 (2014) [arXiv:1303.5076 [astro-ph.CO]]; Astron. Astrophys. **594**, A13 (2016) [arXiv:1502.01589 [astro-ph.CO]].

[6] J. L. Feng, Ann. Rev. Astron. Astrophys. **48**, 495 (2010) [arXiv:1003.0904 [astro-ph.CO]].

[7] G. Bertone, D. Hooper and J. Silk, Phys. Rept. **405**, 279 (2005) [hep-ph/0404175].

[8] G. Arcadi, M. Dutra, P. Ghosh, M. Lindner, Y. Mambrini, M. Pierre, S. Profumo and F. S. Queiroz, arXiv:1703.07364 [hep-ph].

[9] G. Jungman, M. Kamionkowski and K. Griest, Phys. Rept. **267**, 195 (1996) [hep-ph/9506380].

[10] B. W. Lee and S. Weinberg, Phys. Rev. Lett. **39**, 165 (1977).

[11] D. Abercrombie *et al.*, arXiv:1507.00966 [hep-ex].

[12] D. S. Akerib *et al.* [LUX Collaboration], Phys. Rev. Lett. **118**, no. 2, 021303 (2017) [arXiv:1608.07648 [astro-ph.CO]].

[13] A. Tan *et al.* [PandaX-II Collaboration], Phys. Rev. Lett. **117**, no. 12, 121303 (2016) [arXiv:1607.07400 [hep-ex]]; X. Cui *et al.* [PandaX-II Collaboration], Phys. Rev. Lett. **119**, no. 18, 181302 (2017) [arXiv:1708.06917 [astro-ph.CO]].

[14] E. Aprile *et al.* [XENON Collaboration], Phys. Rev. Lett. **119**, no. 18, 181301 (2017) [arXiv:1705.06655 [astro-ph.CO]].

[15] E. Aprile *et al.* [XENON Collaboration], JCAP **1604**, no. 04, 027 (2016) [arXiv:1512.07501 [physics.ins-det]].

[16] M. Ackermann *et al.* [Fermi-LAT Collaboration], Phys. Rev. Lett. **115**, no. 23, 231301 (2015) [arXiv:1503.02641 [astro-ph.HE]]; M. Ackermann *et al.* [Fermi-LAT Collaboration], Astrophys. J. **812**, no. 2, 159 (2015) [arXiv:1510.00004 [astro-ph.HE]].

[17] M. L. Ahnen *et al.* [MAGIC and Fermi-LAT Collaborations], JCAP **1602**, no. 02, 039 (2016) [arXiv:1601.06590 [astro-ph.HE]].

[18] H. Abdallah *et al.* [H.E.S.S. Collaboration], Phys. Rev. Lett. **117**, no. 11, 111301 (2016) [arXiv:1607.08142 [astro-ph.HE]].

[19] M. Aguilar *et al.* [AMS Collaboration], Phys. Rev. Lett. **113**, 121102 (2014); M. Aguilar *et al.* [AMS Collaboration], Phys. Rev. Lett. **117**, no. 9, 091103 (2016).

[20] G. Ambrosi *et al.* [DAMPE Collaboration], arXiv:1711.10981 [astro-ph.HE].

[21] M. Pospelov, A. Ritz and M. B. Voloshin, Phys. Lett. B **662**, 53 (2008) [arXiv:0711.4866 [hep-ph]]; M. Pospelov and A. Ritz, Phys. Lett. B **671**, 391 (2009) [arXiv:0810.1502 [hep-ph]]; N. Arkani-Hamed, D. P. Finkbeiner, T. R. Slatyer and N. Weiner, Phys. Rev. D **79**, 015014 (2009) [arXiv:0810.0713 [hep-ph]].

[22] Y. Hochberg, E. Kuflik, T. Volansky and J. G. Wacker, Phys. Rev. Lett. **113**, 171301 (2014) [arXiv:1402.5143 [hep-ph]]; Y. Hochberg, E. Kuflik, H. Murayama, T. Volansky and J. G. Wacker, Phys. Rev. Lett. **115**, no. 2, 021301 (2015) [arXiv:1411.3727 [hep-ph]];

[23] T. Goerdt, B. Moore, J. I. Read, J. Stadel and M. Zemp, Mon. Not. Roy. Astron. Soc. **368**, 1073 (2006) [astro-ph/0601404]; A. A. Klypin, A. V. Kravtsov, O. Valenzuela and F. Prada, Astrophys. J. **522**, 82 (1999) [astro-ph/9901240]; B. Moore, S. Ghigna, F. Governato, G. Lake, T. R. Quinn, J. Stadel and P. Tozzi, Astrophys. J. **524**, L19 (1999) [astro-ph/9907411]; M. Boylan-Kolchin, J. S. Bullock and M. Kaplinghat, Mon. Not. Roy. Astron. Soc. **415**, L40 (2011) [arXiv:1103.0007 [astro-ph.CO]]; M. Boylan-Kolchin, J. S. Bullock and M. Kaplinghat, Mon. Not. Roy. Astron. Soc. **422**, 1203 (2012) [arXiv:1111.2048 [astro-ph.CO]].

[24] E. D. Carlson, M. E. Machacek and L. J. Hall, Astrophys. J. **398**, 43 (1992).

[25] A. A. de Laix, R. J. Scherrer and R. K. Schaefer, Astrophys. J. **452**, 495 (1995) [astro-ph/9502087]. D. N. Spergel and P. J. Steinhardt, Phys. Rev. Lett. **84**, 3760 (2000) [astro-ph/9909386]; R. Dave, D. N. Spergel, P. J. Steinhardt and B. D. Wandelt, Astrophys. J. **547**, 574 (2001) [astro-ph/0006218]; B. D. Wandelt, R. Dave, G. R. Farrar, P. C. McGuire, D. N. Spergel and P. J. Steinhardt, [astro-ph/0006344]; M. C. Bento, O. Bertolami, R. Rosenfeld and L. Teodoro, Phys. Rev. D **62**, 041302 (2000) [astro-ph/0003350]; S. Tulin, H. B. Yu and K. M. Zurek, Phys. Rev. Lett. **110**, no. 11, 111301 (2013) [arXiv:1210.0900 [hep-ph]]; J. M. Cline, Z. Liu, G. Moore and W. Xue, Phys. Rev. D **90**, no. 1, 015023 (2014) [arXiv:1312.3325 [hep-ph]]; M. Kaplinghat, S. Tulin and H. B. Yu, Phys. Rev. D **89**, no. 3, 035009 (2014) [arXiv:1310.7945 [hep-ph]]; C. Kouvaris, I. M. Shoemaker and K. Tuominen, Phys. Rev. D **91**, no. 4, 043519 (2015) [arXiv:1411.3730 [hep-ph]].

[26] Y. Hochberg, E. Kuflik and H. Murayama, JHEP **1605**, 090 (2016) [arXiv:1512.07917 [hep-ph]].

[27] M. Hansen, K. Langæble and F. Sannino, Phys. Rev. D **92**, no. 7, 075036 (2015) [arXiv:1507.01590 [hep-ph]].

[28] D. Pappadopulo, J. T. Ruderman and G. Trevisan, Phys. Rev. D **94**, no. 3, 035005 (2016) [arXiv:1602.04219 [hep-ph]]; M. Farina, D. Pappadopulo, J. T. Ruderman and G. Trevisan, JHEP **1612**, 039 (2016) [arXiv:1607.03108 [hep-ph]]; J. A. Dror, E. Kuflik and W. H. Ng, Phys. Rev. Lett. **117**, no. 21, 211801 (2016) [arXiv:1607.03110 [hep-ph]].

[29] A. Berlin, D. Hooper and G. Krnjaic, Phys. Lett. B **760**, 106 (2016) [arXiv:1602.08490 [hep-ph]]; Phys. Rev. D **94**, no. 9, 095019 (2016) [arXiv:1609.02555 [hep-ph]].

[30] K. Griest and M. Kamionkowski, Phys. Rev. Lett. **64**, 615 (1990).

[31] S. Okawa, M. Tanabashi and M. Yamanaka, Phys. Rev. D **95**, no. 2, 023006 (2017) [arXiv:1607.08520 [hep-ph]].

[32] J. M. Pendlebury *et al.*, Phys. Rev. D **92**, no. 9, 092003 (2015) [arXiv:1509.04411 [hep-ex]].

[33] R. D. Peccei and H. R. Quinn, Phys. Rev. Lett. **38**, 1440 (1977); G. 't Hooft, Phys. Rev. Lett. **37**, 8 (1976); G. 't Hooft, Phys. Rev. D **14**, 3432 (1976) Erratum: [Phys. Rev. D **18**, 2199 (1978)].

[34] Y. Nambu and G. Jona-Lasinio, Phys. Rev. **122**, 345 (1961); Y. Nambu and G. Jona-Lasinio, Phys. Rev. **124**, 246 (1961).

[35] J. Goldstone, Nuovo Cim. **19**, 154 (1961); J. Goldstone, A. Salam and S. Weinberg, Phys. Rev. **127**, 965 (1962).

[36] P. W. Higgs, Phys. Rev. Lett. **13**, 508 (1964); F. Englert and R. Brout, Phys. Rev. Lett. **13**, 321 (1964).

[37] C. Patrignani *et al.* [Particle Data Group], Chin. Phys. C **40**, no. 10, 100001 (2016).

[38] R. H. Cyburt, B. D. Fields, K. A. Olive and T. H. Yeh, Rev. Mod. Phys. **88**, 015004 (2016) [arXiv:1505.01076 [astro-ph.CO]].

[39] G. Steigman, B. Dasgupta and J. F. Beacom, Phys. Rev. D **86**, 023506 (2012) [arXiv:1204.3622 [hep-ph]].

[40] S. Weinberg, Phys. Rev. D **13**, 974 (1976) Addendum: [Phys. Rev. D **19**, 1277 (1979)]; Phys. Lett. **82B**, 387 (1979); E. Gildener, Phys. Rev. D **14**, 1667 (1976); L. Susskind, Phys. Rev. D **20**, 2619 (1979).

[41] M. Srednicki, R. Watkins and K. A. Olive, Nucl. Phys. B **310**, 693 (1988).

[42] P. Gondolo and G. Gelmini, Nucl. Phys. B **360**, 145 (1991).

[43] E. W. Kolb and M. S. Turner, Front. Phys. **69**, 1 (1990).

[44] K. Harigaya, M. Ibe, K. Kaneta, W. Nakano and M. Suzuki, JHEP **1608**, 151 (2016) [arXiv:1606.00159 [hep-ph]].

[45] M. W. Goodman and E. Witten, Phys. Rev. D **31**, 3059 (1985).

[46] W. H. Press and D. N. Spergel, Astrophys. J. **296**, 679 (1985); K. Griest and D. Seckel, Nucl. Phys. B **283**, 681 (1987); Nucl. Phys. B **296**, 1034 (1988)]; M. Srednicki, K. A. Olive and J. Silk, Nucl. Phys. B **279**, 804 (1987); S. Ritz and D. Seckel, Nucl. Phys. B **304**, 877 (1988); M. Cirelli, N. Fornengo, T. Montaruli, I. A. Sokalski, A. Strumia and F. Vissani, Nucl. Phys. B **727**, 99 (2005) Erratum: [Nucl. Phys. B **790**, 338 (2008)] [hep-ph/0506298].

[47] E. Aprile *et al.* [XENON100 Collaboration], Phys. Rev. Lett. **109**, 181301 (2012) [arXiv:1207.5988 [astro-ph.CO]].

[48] M. Xiao *et al.* [PandaX Collaboration], Sci. China Phys. Mech. Astron. **57**, 2024 (2014) [arXiv:1408.5114 [hep-ex]].

[49] A. Cuoco, M. Krämer and M. Korsmeier, Phys. Rev. Lett. **118**, no. 19, 191102 (2017) [arXiv:1610.03071 [astro-ph.HE]]; M. Y. Cui, Q. Yuan, Y. L. S. Tsai and Y. Z. Fan, Phys. Rev. Lett. **118**, no. 19, 191101 (2017) [arXiv:1610.03840 [astro-ph.HE]].

[50] M. Cirelli *et al.*, JCAP **1103**, 051 (2011) Erratum: [JCAP **1210**, E01 (2012)] [arXiv:1012.4515 [hep-ph]].

[51] M. G. Ratti [ATLAS Collaboration], Nuovo Cim. C **39**, no. 1, 213 (2016); E. Tolley [ATLAS Collaboration], PoS DIS **2016**, 107 (2016); **CMS** Collaboration, C. Collaboration, "Search for dark matter in final states with an energetic jet, or a hadronically decaying W or Z boson using 12.9 fb^1 of data at $\sqrt{s} = 13$ TeV."; M. Aaboud *et al.* [ATLAS Collaboration], Phys. Rev. D **94**, no. 3, 032005 (2016) [arXiv:1604.07773 [hep-ex]].

[52] G. Aad *et al.* [ATLAS Collaboration], JHEP **1511**, 206 (2015) [arXiv:1509.00672 [hep-ex]].

[53] V. Khachatryan *et al.* [CMS Collaboration], JHEP **1702**, 135 (2017) [arXiv:1610.09218 [hep-ex]].

[54] LEP EWWG, http://lepewwg.web.cern.ch/LEPEWWG/lep2/.

[55] K. Griest and D. Seckel, Phys. Rev. D **43**, 3191 (1991).

[56] G. Aad *et al.* [ATLAS Collaboration], JHEP **1310**, 130 (2013) Erratum: [JHEP **1401**, 109 (2014)] [arXiv:1308.1841 [hep-ex]]; G. Aad *et al.* [ATLAS Collaboration], Eur. Phys. J. C **75**, no. 7, 299 (2015) Erratum: [Eur. Phys. J. C **75**, no. 9, 408 (2015)] [arXiv:1502.01518 [hep-ex]]; M. Aaboud *et al.* [ATLAS Collaboration], Phys. Rev. D **94**, no. 3, 032005 (2016) [arXiv:1604.07773 [hep-ex]].

[57] V. Silveira and A. Zee, Phys. Lett. **161B**, 136 (1985).

[58] S. Kanemura, S. Matsumoto, T. Nabeshima and N. Okada, Phys. Rev. D **82**, 055026 (2010) [arXiv:1005.5651 [hep-ph]]; A. Djouadi, O. Lebedev, Y. Mambrini and J. Quevillon, Phys. Lett. B **709**, 65 (2012) [arXiv:1112.3299 [hep-ph]]; A. Djouadi, A. Falkowski, Y. Mambrini and J. Quevillon, Eur. Phys. J. C **73**, no. 6, 2455 (2013) [arXiv:1205.3169 [hep-ph]].

[59] Y. G. Kim, K. Y. Lee and S. Shin, JHEP **0805**, 100 (2008) [arXiv:0803.2932 [hep-ph]; S. Baek, P. Ko and W. I. Park, JHEP **1202**, 047 (2012) [arXiv:1112.1847 [hep-ph]]; S. Baek, P. Ko, W. I. Park and E. Senaha, JHEP **1211**, 116 (2012) [arXiv:1209.4163 [hep-ph]].

[60] O. Lebedev, H. M. Lee and Y. Mambrini, Phys. Lett. B **707**, 570 (2012) [arXiv:1111.4482 [hep-ph]]; Y. Farzan and A. R. Akbarieh, JCAP **1210**, 026 (2012) [arXiv:1207.4272 [hep-ph]]. S. Baek, P. Ko, W. I. Park and E. Senaha, JHEP **1305**, 036 (2013) [arXiv:1212.2131 [hep-ph]].

[61] S. Bhattacharya, B. Melić and J. Wudka, JHEP **1402**, 115 (2014) [arXiv:1307.2647 [hep-ph]]; M. Holthausen, J. Kubo, K. S. Lim and M. Lindner, JHEP **1312**, 076 (2013) [arXiv:1310.4423 [hep-ph]]; O. Antipin, M. Redi and A. Strumia, JHEP **1501**, 157 (2015) [arXiv:1410.1817 [hep-ph]]; Y. Ametani, M. Aoki, H. Goto and J. Kubo, Phys. Rev. D **91**, no. 11, 115007 (2015) [arXiv:1505.00128 [hep-ph]].

[62] M. Escudero, A. Berlin, D. Hooper and M. X. Lin, JCAP **1612**, 029 (2016) [arXiv:1609.09079 [hep-ph]].

[63] G. Bélanger, F. Boudjema, A. Pukhov and A. Semenov, Comput. Phys. Commun. **192**, 322 (2015) [arXiv:1407.6129 [hep-ph]].

[64] S. Baek, P. Ko and W. I. Park, Phys. Rev. D **90**, no. 5, 055014 (2014) [arXiv:1405.3530 [hep-ph]]; S. Baek, P. Ko, M. Park, W. I. Park and C. Yu, Phys. Lett. B **756**, 289 (2016) [arXiv:1506.06556 [hep-ph]]; S. Baek, P. Ko and J. Li, Phys. Rev. D **95**, no. 7, 075011 (2017) [arXiv:1701.04131 [hep-ph]].

[65] T. Abe, Phys. Lett. B **771**, 125 (2017) [arXiv:1702.07236 [hep-ph]].

[66] D. S. Akerib *et al.* [LZ Collaboration], arXiv:1509.02910 [physics.ins-det].

[67] J. Aalbers *et al.* [DARWIN Collaboration], JCAP **1611**, 017 (2016) [arXiv:1606.07001 [astro-ph.IM]].

[68] A. Falkowski, J. Juknevich and J. Shelton, arXiv:0908.1790 [hep-ph]; P. Ko and Y. Tang, Phys. Lett. B **751**, 81 (2015) [arXiv:1508.02500 [hep-ph]]; B. Batell, T. Han, D. McKeen and B. Shams Es Haghi, arXiv:1709.07001 [hep-ph].

[69] A. Airapetian *et al.* [HERMES Collaboration], Phys. Rev. D **75**, 012007 (2007) [hep-ex/0609039].

[70] M. V. Polyakov, A. Schafer and O. V. Teryaev, Phys. Rev. D **60**, 051502 (1999) [hep-ph/9812393].

[71] P. Agrawal, Z. Chacko, C. Kilic and R. K. Mishra, arXiv:1003.1912 [hep-ph]; M. Cirelli, E. Del Nobile and P. Panci, JCAP **1310**, 019 (2013) [arXiv:1307.5955 [hep-ph]]; F. Bishara, J. Brod, B. Grinstein and J. Zupan, JHEP **1711**, 059 (2017) [arXiv:1707.06998 [hep-ph]].

[72] G. Belanger, F. Boudjema, A. Pukhov and A. Semenov, Comput. Phys. Commun. **180**, 747 (2009) [arXiv:0803.2360 [hep-ph]].